International Scientific-Theoretical and Production Journal

ADVANCES IN ELECTROMETALLURGY

1
2002

English translation of the quarterly «Problemy Spetsialnoj Electrometallurgii» journal published in Russian since January 1985

The National Academy of Sciences of Ukraine
The E.O. Paton Electric Welding Institute
International Association «Welding»

Quarterly

Editorial and advertising offices are located at PWI,
International Association «Welding»,
The E. O. Paton Electric
Welding Institute
of the NAS of Ukraine,
11, Bozhenko str., 03680,
Kyiv, Ukraine
Tel.: (38044) 227 67 57,
269 26 23,
Fax: (38044) 268 04 86
E-mail: journal@paton.kiev.ua
http://www.nas.gov.ua/pwj

Subscriptions:
$184, 4 issue per year,
postage and packaging included.
Back issue available

CONTENTS

ARC-SLAG REMELTING — STATE-OF-THE-ART AND PROSPECTS OF DEVELOPMENT

B.E. PATON*, V.Ya. SAENKO*, Yu.M. POMARIN*, L.B. MEDOVAR*, G.M. GRIGORENKO* and B.B. FEDOROVSKY*

Peculiarities and technological capabilities of the arc-slag remelting (ASR) method, developed at the E.O. Paton Electric Welding Institute, were considered. The results of experimental and industrial melting of steels and alloys are given. As compared with ESR the ASR method makes it possible to 1.5 times reduce the energy consumption, and also to decrease almost by 2 times the consumption of a synthetic flux per 1 t of metal during melting of ingots. As to the quality, the ASR metal is not inferior to the ESR metal. The main advantage of ASR is a feasibility to alloy metals with nitrogen from the gas phase, including that under pressure, at a complete elimination of expensive nitrogen-containing compounds, for example, silicon nitride, from the technological process of production of high-nitrogen steels and alloys. It is shown that the ASR is also effective in the production of titanium and its alloys and produces ingots with a good surface and high quality. The prospects of ASR further development are outlined.

Key words: *high-nitrogen steels and alloys, electric arc, slag pool, metal consumable electrode, copper water-cooled mould, arc-slag remelting, remelting under pressure*

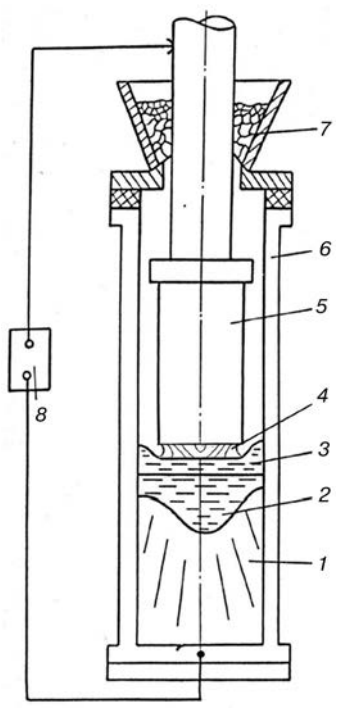

Figure 1. Diagram of ASR of the solid consumable electrode: *1* — ingot; *2* — metal pool; *3* — slag pool; *4* — electric arc; *5* — consumable electrode; *6* — water-cooled mould; *7* — flux seal; *8* — power source

At the beginning of the seventies a new method of remelting of a metal consumable electrode in a copper water-cooled mould using an electric arc, burning between the edge of the consumable electrode and surface of the molten slag pool, was developed at the E.O. Paton Electric Welding Institute of the National Academy of Sciences of Ukraine [1]. This method was named arc-slag remelting (ASR). A lot of the credit must go to the Prof. Boris I. Medovar in the creation of the ASR and substantiation of principal priority trends of its development and industrial implementation.

To realize the ASR process, it was necessary to provide the arc isolation from its contact with air and to create a controllable gas atmosphere in the zone of its burning. Two technological diagrams were tested, namely:

- ASR with the use of a flux seal, representing the simplest device, which is mounted directly on the upper edge of the mould (Figure 1);
- ASR in a chamber furnace (Figure 2).

In the latter case the available furnaces for the vacuum-arc remelting (VAR), in which a vacuum system was disconnected and also specially-designed chamber furnaces for the ASR, which could realize the ASR process in a controllable atmosphere, including that under the pressure, were used.

The arc-slag process combines the capability of treatment of the molten metal with an electric arc, which is burning in the controllable gas atmosphere, and a molten synthetic slag through which the current is passed during the consumable electrode remelting. In addition, a layer of the synthetic slag, covering a

*The E.O. Paton Electric Welding Institute, Kyiv, Ukraine.

metal pool, promotes the heat spreading in its section during the ASR process, thus reducing the metal pool depth, that makes it more shallow as compared with that in VAR and ESR. Moreover, the ASR ingots unlike the VAR ingots have a smooth lateral surface, due to formation of the slag skull, and do not require the obligatory mechanical treatment before the next processing.

The presence of the powerful electric arc in the zone of melting the consumable electrode during ASR in nitrogen creates the favourable conditions for the metal alloying with nitrogen directly from the gas phase, including those up to super-equilibrium its concentrations during ASR in nitrogen at a high pressure (ASRP). This is a main advantage of the arc-slag remelting, i.e. the full elimination of expensive nitrided high-alloyed additions (ferroalloys, silicon nitrides, etc.), which are usually used in other methods [2–3] in production of high-nitrogen steels and alloys. The ASR variants in a lined crucible [4] were tested, confirming the feasibility of metal nitriding during ASR in a crucible melting. The application of the arc-slag heating of metal melts with graphite electrodes proved to be effective [5], as it is characterized by a simplicity, reliability and does not require complicated expensive equipment for its realization. The undoubted advantage of this process is also the fact that it allows the metal melt to be treated with reactive gases, for example, metal nitriding from the gas phase.

The carried out investigations, including those under shop conditions [3] showed that ASR method, as compared with ESR, can decrease the energy consumption by 1.5 times and consumption of a synthetic flux per 1 t of metal by almost 2 times. As to the metal quality the ASR metal is not inferior to the ESR metal.

It should be noted that as far back as 1966 the Paton Institute has suggested a method of ESR of steels and alloys under the excessive pressure of nitrogen or its mixture with neutral gases over the slag pool to alloy metal with nitrogen [6]. The above-mentioned invention was patented in Great Britain, Belgium, Italy, Canada, France and India. It is also known that all the attempts of alloying the molten metal with nitrogen from the gas phase during ESR in a nitrogen-containing high-pressure atmosphere were not successful because of a low solubility of nitrogen in the slag pool [4]. Only after a dosed feeding of hard particles (granules, grains, shot) of nitrided ferroalloy or silicon nitride to the slag surface during the ESR in a special pressurized chamber furnace it was possible to provide the ingot metal alloying with nitrogen up to the super-equilibrium state [7]. However, a serious drawback remained which is typical of any diagram of remelting with an additional alloying with hard particles, namely chemical inhomogeneity of the ingot.

At the beginning of the 1990s a new impulse was given to the ASR for its development and industrial implementation, first of all, due to the arising interest

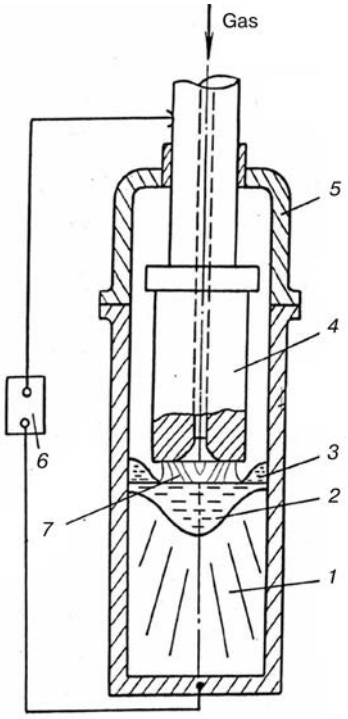

Figure 2. Diagram of ASR of hollow consumable electrode: *1* — ingot; *2* — metal pool; *3* — slag pool; *4* — hollow consumable electrode; *5* — water-cooled mould chamber; *6* — power source; *7* — electric arc

in the whole world to the high-nitrogen steels and alloys, and also to the methods of their production [8–11]. Theoretical fundamentals of processes of nitriding steels and alloys directly from the gas phase during pressurized ASR were created and the technology of production of ingots alloyed with nitrogen using the ASR method [12] was developed on the basis of research works, supervised by Prof. B. Medovar, which were carried out at the Paton Institute and at the factories.

The ASR process in a nitrogen-containing atmosphere combines three technological processes: arc melting of electrode, metal alloying with nitrogen directly from the gas phase and metal slag treatment with a formation of ingot in a slag skull. Depending on the parameters of the ASR process the arc can burn between the electrode edge and molten slag surface (see Figure 1); between the electrode and molten metal surface, partially bared from a slag due to arc column pressure (see Figure 2). In this case the slag covers only a periphery zone of the metal pool, thus forming a circular slag pool.

Both solid and hollow electrodes can be used for remelting. However, the application of hollow electrodes can influence the metal more effectively with gases by feeding the gas through the cavity directly to the arc-burning zone. Remelting with a metal pool (circular slag pool), partially covered with a slag, can be realized both in using hollow and solid electrodes.

In ASR with a complete slag pool (see Figure 1) the heat is generated at the end of electrode, in arc column, at the surface of the slag pool, in an electrode spot and also in a slag pool at the expense of current

passing through the slag. When the circular slag pool is used the heat is generated at the end of electrode, in arc column and in electrode spot, which is located directly at the molten pool surface. The presence of the molten slag pool, complete or circular, as in ESR, promotes heating of the periphery part (at the mould walls) of the metal pool. Due to this and the presence of a slag layer between the wall of mould and ingot a good formation of ingots of different section (round, square, rectangular) is provided. This is one of the important advantages of the ASR as compared with VAR.

The depth of the metal pool in melting ingots using ASR is smaller than that in ESR and the pool shape is shallower. This is explained by the fact that in ASR the pool surface is heated more uniformly because the most part of the heat is generated in the arc column. Heat is spread also in the pool due to the transfer of drops to the pool with several streams over the entire section of the electrode.

The use of a hollow electrode favours greatly the more uniform distribution of heat in the pool section (see Figure 2). In this case the drops are formed near the electrode lateral surface and enter the pool at the distance of not less than the half of its radius. The stream of the heated gas through the cavity, if the electrode is blown-through with a gas, is spreading over the pool surface and also promoting the more uniform heating of the entire surface. Moreover, the gas stream, passing through the axial channel contributes to the stabilization of the discharge into the arc space in the electrode axis. In this case the electrode spot (cathode or anode) is located at the inner surface of the hollow electrode.

In the ASR the electric arc is burning in the atmosphere of reactive (or protective) gas and slag vapours. The presence of slag vapours, which has chemical elements of a low potential of ionization, contributes to stabilizing of arc burning at atmospheric and high pressure. In ASR, unlike the VAR, there is no metal crown on the ingot. This is due to the fact that in ASR the metal spatters (fine drops) enter either the slag pool or the slag collar, which is formed around the slag pool perimeter. A thin layer of metal vapours can be condensed at the mould wall above the slag pool, but during ingot melting the molten heated slag melts the condensate and the crown is not formed. The gas feeding to the arc burning zone through the cavity in the consumable electrode or using another way promotes the removal of harmful gaseous impurities from the arc space. These can be gases (hydrogen, fluorine, etc.) or vapours of non-ferrous low-boiling metals (tin, lead and so on).

The ASR can be realized under the high-pressure conditions, because the electric arc burning is quite stable even at pressure measured by tens of atmospheres. The main thing is to select the electrical and technological condition parameters properly. Heat, required for proceeding the ASR process is generated mainly in electric arc, wherein current passes through the ionized discharge gap consisting of vapours or oxides of metal, vapours of slag and ionized gases. In ASR the surface of the molten slag (or metal) pool is one of electrodes. The slag pool represents a melt of an electrolyte with a large amount of complex and simple ions. Its temperature can reach 2000 °C. One of slag components at such temperatures can evaporate, other components are decomposed (dissociate) into separate ions and, having this form they can participate in the process of current transfer. However, as the temperature of the arc discharge is much higher than that of the slag pool, the processes of evaporation, dissociation and ionization are more clearly expressed.

The ASR can be performed both at direct and alternating current. And, here, the main advantages and drawbacks typical of VAR and ESR at DC and AC are preserved. In each concrete case of remelting of either alloy and steel it is necessary to select a type of current coming from definite conditions of melting.

Molten slag (ESR slags are used mainly) greatly influence the burning of arc discharge in the ASR process. The slags used include the following components: CaF_2, CaO, Al_2O_3, MgO, SiO_2, TiO_2, etc. In a molten state at the ASR process temperature different complex and simple ions, both positive and negative, can be formed from the mentioned components and can transfer to the arc column and participate in the current passing.

It should be noted that different components, included to the composition of ESR slags, influence differently the arc burning conditions. Alkali and alkali-earth metals, possessing a low potential of ionization, have a positive effect on the arc burning conditions. They are ionized easily, forming cations and free electrons, which will participate further in the charge transfer. For mixtures, whose composition includes different gases and vapours, that is typical of the ASR, the total potential of ionizing is determined by a component with a least potential of ionization and depends on its concentration. Thus, the potential of ionization of potassium, sodium and calcium is equal to 4.33, 5.11, 6.10 V, respectively, and that of nitrogen and argon is 14.5 and 15.7 V. Thus, the chemical composition of the fluxes used greatly influences the electrical characteristics of the process, such as stability of the arc burning, value of ignition peaks, presence of pauses in a current curve, open-circuit voltage of the power source, etc.

The presence of easily ionized elements in the slag, as was above-mentioned, reduces abruptly the voltage gradient in the arc column. The effect of elements of a low potential of ionizing becomes higher on the effective potential ionizing the gas mixture which tends to the potential of most easily-ionizing element in the arc atmosphere. Analysis of estimated and experimental data made it possible to conclude that the power source open-circuit voltage of 150–200 V is sufficient for the ASR process in nitrogen atmosphere at 1.5–3.0 MPa pressure [13].

Important parameter, which defines the process of consumable electrode melting in the ASR, is a supplied power, which is selected depending on the electrode section. As is seen from the Figure 3, which presents the results of different laboratory and industrial meltings, made by the ASR method, the required energy density to provide stable conditions is reduced

and less dependent on the diameter with an increase of the electrode diameter (more than 150 mm). Pluses denote meltings under non-steady conditions, they are located in region *A*. The values of energy density under steady conditions are located in region *B*.

The interaction of molten metal with nitrogen during the ASR process can be considered as a two-stage process, including the nitrogen absorption with a film of the molten metal at the electrode edge and surface of the metal pool, being covered completely with molten slag layer or opened partially directly under the action of the electric arc pressure (Figure 4). The rate of nitrogen absorption at the first stage will be determined by a value of its partial pressure in a gas phase, speed of electrode melting, its surface area, and also by the arc effect on the energy state of the gas particles.

In ASR the nitrogen can be fed easily through the axial cavity to the electrode, or in pipings, fixed at its external surface, directly to the zone of the electric arc burning. Therefore, during the ASR there is interaction of particles of nitrogen possessing an increased safety factor of intramolecular energy, with a film of molten metal that promotes the process of their absorption.

The investigations, including those performed in the industrial conditions, show that nitriding in the ASR is rather intensive in that case when a partial baring of the metal pool mirror from the slag is attained. In this case the process of nitriding from the gas phase occurs more completely both at the stage of film and drop and at the stage of the metal pool [14].

The ASR technology has been developed which makes it possible to alloy the molten metal with nitrogen from the gas phase at atmospheric and excessive pressures at a complete elimination of nitrogen-containing materials. Figure 5 presents the large-tonnage Kh18AG18 (Cr — 18.0; Mn — 18.0; V — 0.25; N — 0.25 wt.%) nitrogen-containing steel ingots of 560 × × 560 mm section and up to 3 t mass, produced in the EShP-5VG industrial furnace and ingots of 860 mm diameter and 8 t mass, melted in the ESR furnace of the «Consarc» Company.

Nitrogen and superhigh-nitrogen steels experience now the second youth. And the thing is not in appearance of new fields of application and widening on the basis of scales of production of these steels, but in revealing new remarkable properties which are attained due to a radical change in equipment and technology of the metallurgical production [15–17].

The scales of production of nitrided steels are increased, the dimensions (mass, volume) of ingots are enlarged. Here, an important drawback of ingots from steel alloyed with nitrogen, i.e. mircosegregation of this alloying element, was encountered, thus resembling in its pattern a chemical inhomogeneity of ingots in carbon, typical of large-tonnage steel ingots, well known to the metallurgists. The inhomogeneity of steel ingot by the content of nitrogen is, naturally, inherited the wrought metal, whether it be the rolled metal (sheets, rods, pipes), forgings or stampings. As it has turned out, the excellent characteristics of strength and toughness, their optimum ratio, stipu-

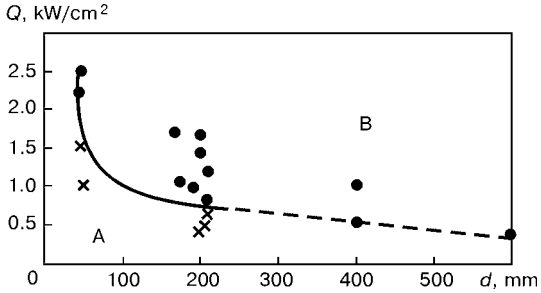

Figure 3. Regions of non-steady (*A*) and steady (*B*) remelting conditions using electrodes of different diameters

lated, first of all, by the given composition of steel or alloy, cannot be guaranteed not only in section of the ingot or forging, but also in length of the rolled metal or pipe.

In ASR two processes are combined: refining of metal from non-metallic inclusion, such as sulphur and other impurities, and steel alloying with nitrogen from the furnace atmosphere. This makes it possible to produce the extra-pure nitrogen-containing steels and to eliminate the use of expensive nitrogen-containing ferroalloys from the metallurgical production. In addition, the ASR metal will be more pure as to the content of harmful impurities, which enter inevitably the melt during alloying with nitrogen-containing ferroalloys. Undoubtedly, that the ASR will minimize noticeably the nitrogen inhomogeneity of the ingots, and also the wrought metal that is especially important in production of cryogenic steels for the thermonuclear power engineering [18].

It is also shown [19] that the ASR in nitrogen-containing atmosphere, including that under the pressure, which is used in production of high-nitrogen stainless duplex-steels, allows introduction of a preset amount of nitrogen from the gas phase to the molten metal and, thus, provides a high chemical homogeneity and structural stability of the ASR ingot metal.

Another promising application of the ASR is the producing nitrogen-microalloyed steels. The basic fields of their practical use: sheet, pipes and sections.

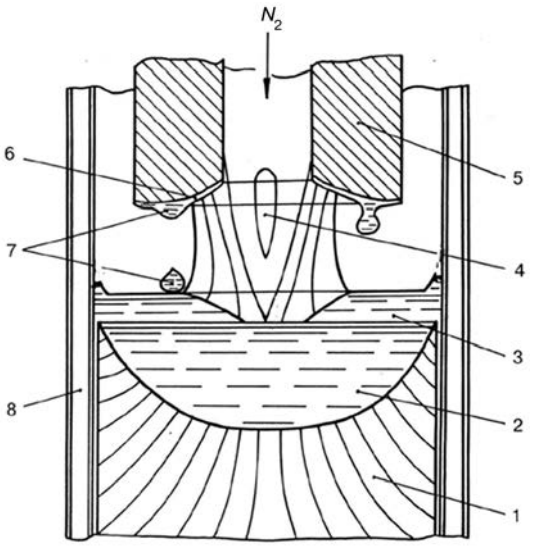

Figure 4. Diagram of nitrogen absorption in ASR: *1* — ingot; *2* — metal pool; *3* — slag pool; *4* — electrical arc; *5* — consumable electrode; *6* — thin metal film; *7* — drops; *8* — mould

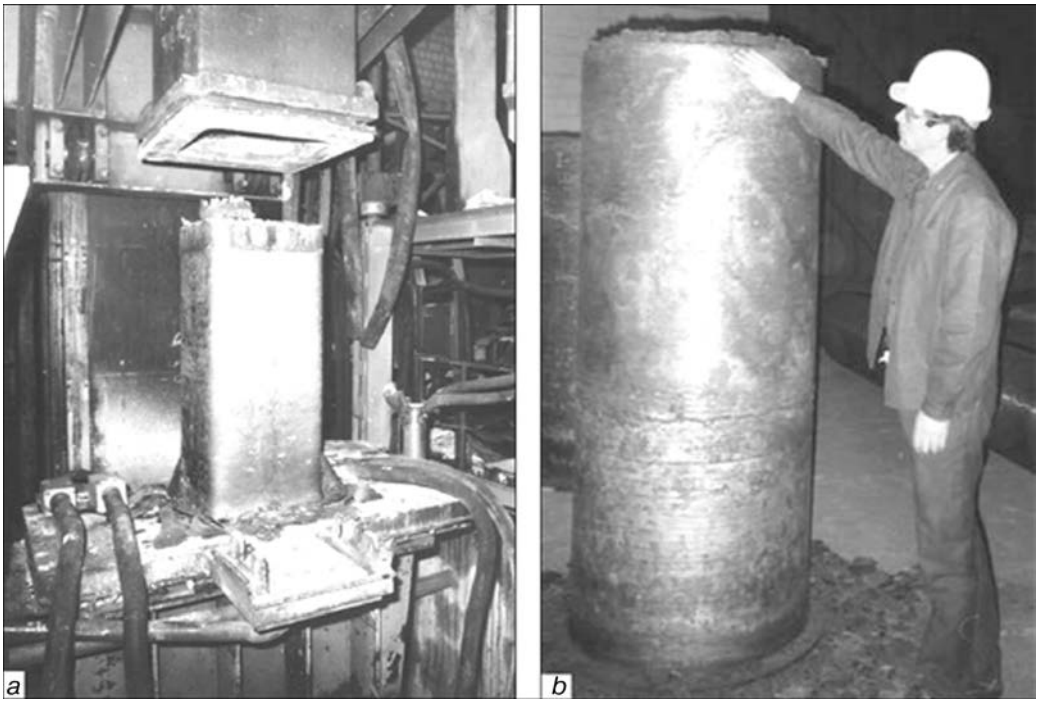

Figure 5. Appearance of ASR ingots of steel Kh18AG18: 560 × 560 mm section, 3 t mass (*a*) and 860 mm diameter, 1900 mm height, 8 t mass (*b*)

Low- and medium-alloyed sheet steels, alloyed with nitrogen (0.015–0.030 %), the so-called steels with a carbonitride strengthening, found a wide application [20]. At the same time, these steels of open methods of melting are characterized by defects of metallurgical origin (liquation banding, line non-metallic inclusions, slip microcracks) which cause the anisotropy of mechanical properties, reduce the ductility, in rolled metal across thickness in particular, and, as a consequence, provoke the tendency of steel to the formation of laminar cracks in fillet and T-joints during welding. The microalloying with nitrogen in the ASR provides a uniform distribution of fine-dispersed carbonitride phase in the sheet thickness.

The high chemical homogeneity and low content of harmful elements, typical of the ASR steels, stipulate the isotropy of mechanical properties of the rolled metal and resistance against cold laminar cracking during welding.

Alongside with a rising interest to the high-nitrogen steels, titanium, the former aerospace structural metal, becomes before our eyes a metal of the civil application. The fact that titanium acquires a quite civil use makes it possible to consider anew all the structure of the titanium industry.

Strict requirements specified to the titanium by the creators of the aerospace engineering, military ship-building, armament, ammunition and other military products, are also justified completely now. However, they can somewhat be softened, if titanium finds its main application for the manufacture of objects of home appliances, different kinds of civil constructions, bicycles, motor cars and other peaceful products. Coming from these considerations, all efforts should be applied for making titanium and its alloys cheaper, to make them quite competitive relative to stainless nickel-containing steels and alloys. In the solution of this problem the ASR process will have a challenging future [21–22]. With undoubted advantages, such as an excellent surface of ingots, feasibility of producing large-tonnage ingots of rectangular section (Figure 6) for direct rolling of sheet, feasibility of realizing the single-stage remelting of spongy pressed electrode with a producing of ingot or slab, being ready for processing, it can reduce considerably the metal losses in production of rolled metal, thus leading to the reduction of cost of the titanium products.

New opportunities for producing defect-free titanium ingots using the method of ASR are opened up as a result of creation of the new technological process developed on the basis of use in the ASR of a current-carrying mould in combination with reactive slags, containing a metallic calcium, thus allowing more complete dissolution of hard high-nitrogen inclusions during remelting, if they occurred occasionally in the consumable electrodes. However, this active technological process of the ASR, as shown in [23] can be realized only in a chamber furnace with a controllable atmosphere.

Over the recent years some new promising fields of the ASR application were defined. Thus, research works were carried out by the suggestion of Prof. B. Medovar and due to the problems of utilization of military engineering objects.* They were aimed at the assessment of efficiency of application of the ASR

*The research works were carried out in 1996–1998 under the supervision of Prof. B. Medovar in accordance with STCU projects No.315 and 316, fulfilled by R&D EST Center of the E.O. Paton Electric Welding Institute.

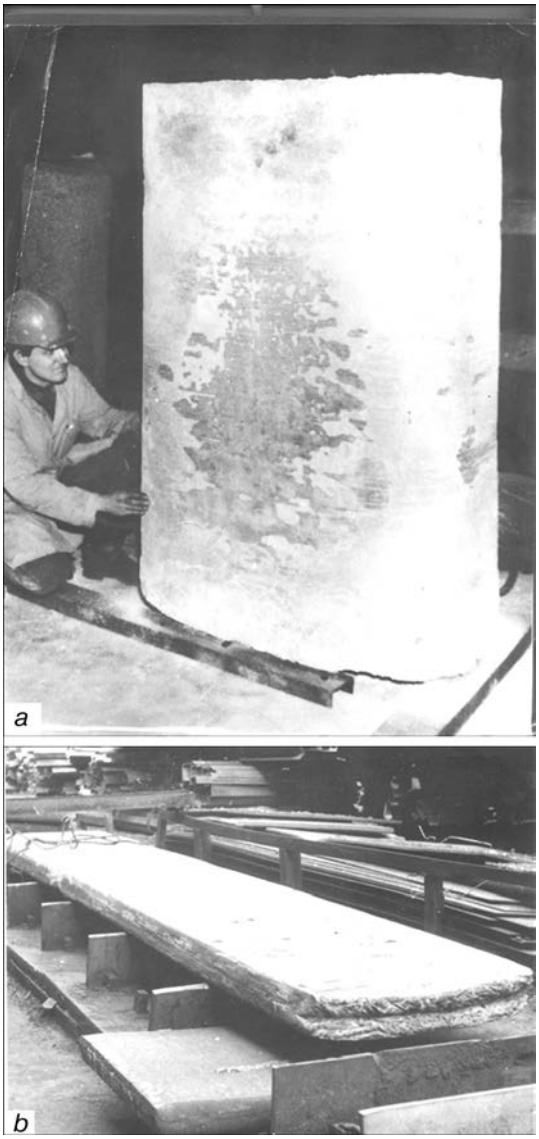

Figure 6. Appearance of ASR slag ingot of titanium VT1-0: 650 × × 1150 mm section, 1700 mm height, 5 t mass (*a*) and 115 mm thick plate, rolled from it (*b*)

method in remelting of artillery barrels of tank guns made from steel 38KhN3MFA (C — 0.38; Cr — 1.0; Ni — 3.0; Mo — 0.6; V — 0.6 wt.%) with a simultaneous alloying of ingot metal with nitrogen directly from the gas phase [24]. Here, it was assumed that the most effective technological scheme can be realized in the process of the ASR of the artillery barrels, according to which the nitrogen is supplied directly to the zone of arc burning through the barrel channel (see Figure 2).

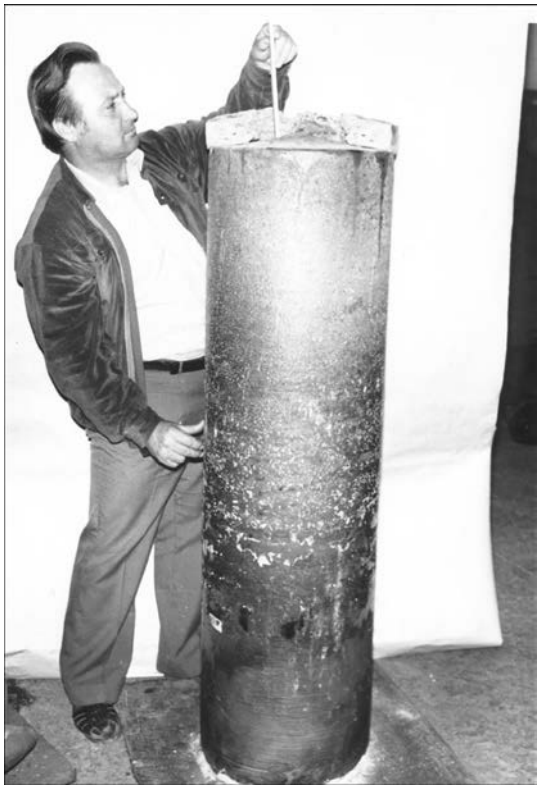

Figure 7. Appearance of ASR ingot of steel 38KhN3MFA: 400 mm diameter and 1500 mm height

The ASR was performed in furnace R951 using a stationary 400 mm diameter mould with a flux seal. After removal of the slag skull all the ingots had a good surface. The appearance of the stationary 400 mm diameter mould and one of the ASR ingots are given in Figure 7.

As seen from the Table, the content of nitrogen in ingots of steel 38KhN3MFA after the ASR was 0.023–0.031 %, i.e. it was 2–3 times increased as compared with its initial content (0.009–0.013 %). Moreover, the increase in consumption of nitrogen, supplied to the consumable electrode channel, to 70 l/min (melting No.2) allowed the nitrogen content in the ASR ingots to be increased by 14 % as compared with melting No.1. The further increase in nitrogen consumption to 80 l/min (melting No.3) did not cause any increase in nitrogen content in the ASR ingot metal. It should be noted that the equilibrium content of nitrogen calculated according to [12] for a definite chemical composition of steel 38KhN3MFA used for production of a pilot batch of the ASR ingots is 0.048 %.

Using the technological conditions, mentioned in the Table, we reach, in principle, about 64 % of nitrogen in ingot from its equilibrium concentration at

Technological parameters of ASR with the flux seal of steel 38KhN3MFA in 400 mm diameter mould

No. of melting	Electrode diameter, mm		Electrical condition		Slag pool height, mm	Gas consumption, l/min	Nitrogen content, %	
	OD	ID	*I*, kA	*U*, V			in electrode	in ingot
1	215	115	3.0	92	30	50	0.013	0.023
2	215	115	4.0	98	30	70	0.009	0.031
3	180	115	2.5	100	50	80	0.010	0.029

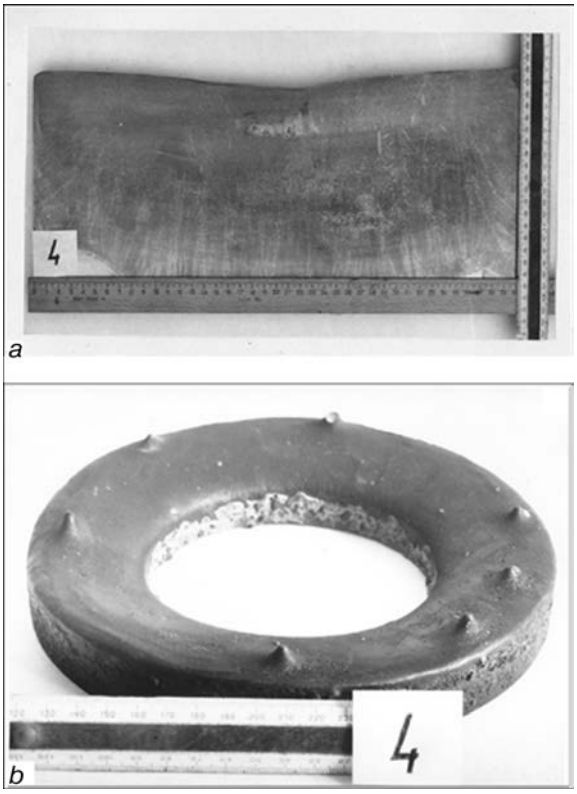

Figure 8. Fragment of macrostructure of top part of longitudinal section of ASR 400 mm diameter ingot of 38KhN3MFA steel with 0.031 % nitrogen content (*a*) and external end of hollow electrode after ASR (*b*)

the nitrogen atmospheric pressure. This is explained by the fact that process of nitriding during the ASR is proceeding in a kinetic condition. Therefore, to produce higher nitrogen concentrations in ingot it is necessary to perform the ASR process under the excessive pressure of nitrogen. This is possible to realize only in the chamber furnaces.

Figure 8 shows a fragment of a longitudinal macrosection of the top part of the ASR ingot melted in accordance with technological conditions of melting No.2 and the appearance of the consumable electrode end after the melting completion. It is seen from the Figure that the macrostructure of ingot is compact, and the electrode melting is characterized by a clearly expressed uniform drop formation of metal over the entire electrode section.

The ASR process can be also used efficiently for the utilization of the artillery barrels and without the additional alloying of metal with nitrogen. The existing ESR furnaces can be used for this purpose. As compared with ESR, as was above-mentioned, the consumption of energy and flux is greatly decreased in the ASR. Thus, the ASR can find the widest and efficient application in industry for the utilization of the artillery barrels.

In the forthcoming years a great deal can be and should be done to make the arc-slag remelting challenging in the metallurgical industry.

1. Paton, B.E., Medovar, B.I., Lakomsky, V.I. *et al*. Method of consumable electrode remelting. USSR author's certificate 520784. Filed 09.08.74. *Bull. of Inv*., 1982, 20.
2. Paton, B.E., Medovar, B.I., Saenko, V.Ya. *et al*. (1990) The place of the electroslag technology in production of superhigh-nitrogen steels. *Problemy Spets. Elektrometallurgii*, **3**, 4–13.
3. Paton, B.E., Medovar, B.I., Saenko, V.Ya. *et al*. (1990) Steel alloying with nitrogen in electroslag processes. High-nitrogen steels. In: *Proc. of 1st All-Union Conf*., Kyiv, Apr. 18–20. Kyiv: Institute of Metal Physics.
4. Bojko, G.A., Ignatov, A.P., Chernets, A.V. *et al*. (1991) Evaluation of feasibilty of metal nitriding in the process of a crucible melting. *Problemy Spets. Elektrometallurgii*, **3**, 17–19.
5. Paton, B.E., Grigorenko, G.M., Medovar, B.I. *et al*. (1995) About new potentialities of the arc-slag remelting. *Ibid*., **4**, 3–6.
6. Medovar, B.I., Latash, Yu.V., Stupak, L.M. *et al*. Method of electroslag remelting in high-pressure nitrogen atmosphere. USSR author's certificate 196066. Filed 22.01.66. Patented in Great Britain (Pat. 1209229), Belgium (Pat. 715710), Italy (Pat. 834428), Canada (Pat. 820527), France (Pat. 1575856), India (Pat. 116218). *Bull. of Inv*., 1967, 11.
7. Kubish, Kh., Holtsgruber, V. (1973) Results, obtained in pressurized ESR method developed by the «Bohler» Company. In: *Proc. of 3rd Int. Symp. on ESR Technology*, Pittsburgh, USA, Apr. 8–10. Kyiv: Naukova Dumka.
8. Foct, J. (1993) Role of nitrogen alloying on mechanical behaviour. In: *Proc. of 3rd Int. Conf. on High Nitrogen Steels*, Kyiv, Sept. 14–16.
9. Stein, G., Lueg, J. (1993) High nitrogen steels — applications, present and future. *Ibid*.
10. Feichtinger, H.K. (1993) Concepts of nitrogen solubility. *Ibid*.
11. Pomarin, Yu.M., Grigorenko, G.M., Saenko, V.Ya. *et al*. (1993) A modern conception of nitrogen alloying of metals from gas atmosphere under pressure during arc-slag remelting. *Ibid*.
12. Medovar, B.I., Saenko, V.Ya., Grigorenko, G.M. *et al*. (1996) *Arc-slag remelting of steels and alloys*. Cambridge Int. Sci. Publ.
13. Grigorenko, G.M. (1990) About arc voltage in nitrogen arc-slag remelting. *Problemy Spets. Elektrometallurgii*, **3**, 19–20.
14. Paton, B.E., Medovar, B.I., Grigorenko, G.M. *et al*. (1991) Nitriding processes in arc-slag remelting. *Ibid*., **3**, 14–16.
15. Feichtinger, H.K, Stein, G. (1998) Melting of high nitrogen steels. In: *Proc. of 5th Int. Conf. on High Nitrogen Steels*, Espoo, Finland, May 24–26; Stockholm, Sweden, May 27–28. Helsinki Univ. of Techn. and Swedish Inst. for Metals Research.
16. Medovar, B.I., Medovar, L.B., Saenko, V.Ya. *et al*. (1998) Influence of the flux composition and state of the gas atmosphere over the kinetics of nitrogen absorption by steel and alloys at the arc-slag remelting. *Ibid*.
17. Gavrilyuk, V.G., Berns, H. (1999) *High nitrogen steels. Structure, properties, manufacture, applications*. Springer.
18. Paton, B.E., Medovar, B.I., Saenko, V.Ya. (1992) Advanced processes of production of high-nitrogen steels and alloys and prospects of application of pressurized arc-slag remelting for their producing. *Problemy Spets. Elektrometallurgii*, **2**, 9–13.
19. Saenko, V.Ya., Pomarin, Yu.M., Us, V.I. (2000) High-nitrogen stainless duplex steels. *Ibid*., **3**, 10–16.
20. Medovar, L.B., Saenko, V.Ya., Nagaevsky, I.D. *et al*. (1984) *Electroslag technology in machine-building*. Ed. by B.E. Paton. Kyiv: Tekhnika.
21. Paton, B.E., Medovar, B.I., Saenko, V.Ya. *et al*. (1992) Arc-slag remelting of titanium and its alloys. In: *Proc. of 7th World Titanium'92 Conf. on Titanium: Sci. and Techn*., San Diego, Calif., June 29–July 2.
22. Medovar, B.I., Shepelev, V.V., Saenko, V.Ya. *et al*. (1992) Arc-slag remelting of titanium and its alloys. *Problemy Spets. Elektrometallurgii*, **2**, 13–16.
23. Medovar, L.B., Saenko, V.Ya., Pomarin, Yu.M. *et al*. (2000) Prospects of application of metallic calcium and REM in ESR. *Ibid*., **4**, 18–29.
24. Paton, B.E., Medovar, B.I., Saenko, V.Ya. *et al*. (2000) Utilization of artillery barrels using ASR with a simultaneous metal alloying with nitrogen. *Ibid*., **1**, 13–18.

ABOUT DETERMINATION OF CHEMICAL COMPOSITION OF METAL OF ELECTROSLAG REMELTING

I.V. KAPUSTIN*, V.P. AKULOV*, A.A. GALUSHKA* and N.A. STOVBUN*

Statement of GOST 7565–81, concerning the determination of chemical composition of metal of the electroslag remelting, is considered. It is shown that the composition of metal, sampled from the bottom part of the ESR ingot can differ, according to the recommendations of this GOST, from the metal of the rest part of the ingot in carbon, sulphur, silicon and other easily-oxidizing elements. The sampling is suggested to be made from the top part of the ingot.

Key words: *electroslag remelting, ingot, flux, solubility, slag pool, consumable electrode, chemical composition*

In accordance with GOST 7565–81, item 3.3, the determination of the chemical composition of the ESR metal is performed using a sample taken from a bottom part of the ingot, the appropriate part of a billet or a ready rolled stock. From data of [1, 2], the chemical composition of metal of the ESR ingots is determined usually before and after the electroslag remelting without indicating the sampling place in the ingot.

The experience of production of large-tonnage ESR ingots using multielectrode diagrams at a liquid start was not described in this GOST. The chemical composition of the metal sample from the bottom part of the ESR ingot can differ both from the initial metal and also from the metal of the rest part of the ingot. There exist the following reasons of such discrepancy in main elements of the steel being remelted.

In carbon. Flux for the liquid start is melted usually in a flux melting furnace with a graphite lining and the carbon is dissolved partially in it. The carbon solubility in flux ANF-6 (SiO_2 — up to 2.5; CaO — up to 8; Al_2O_3 — 25–31 wt.%; CaF_2 — balance) is 0.89 % [3]. At the initial period of the electroslag remelting the carbon from the flux is transferred partially into the metal of the ingot bottom part, in particular in remelting low-carbon steels, thus reaching, in separate cases, concentrations exceeding the upper limit for the given steel grade. Commonly, this increased concentration of carbon is not spread higher of the ingot bottom crop ends and the carbon content in the rest its part corresponds to the content in the initial metal. Table 1 shows the averaged statistic data about the carbon concentration in slab ESR ingots of 14–20 t mass, produced by OJSC «MK Azovstal»

Consequently, as to the carbon concentration, only metal sampling from the ingot top part may be representative.

In sulphur. The sulphur concentration in height of the ESR ingot is increased from minimum values in the bottom its part and to maximum values in the top part because of reducing the refining ability of the slag pool due to accumulation of iron and silicon oxides in it and decrease in its basicity. In this case, the sampling from the top part of the ESR ingot is representative for ESR metal in sulphur (Table 2). When the slag pool is deoxidized with aluminium during remelting the difference between the sulphur concentration in the bottom and top parts of the ingot is almost disappeared.

In phosphorous. The phosphorous content in metal of the ESR is usually close to the initial content, differing negligibly within the ranges of 0.001–0.002 % in the ingot height.

Table 1. Change of carbon concentration in ingot height at ESR using an oxyfluoride flux

Number of determinations	Steel grade	Carbon concentration, %			Exceeding in carbon content in bottom part of ingot as compared with initial content, %
		Initial metal	Bottom part of ingot	Top part of ingot	
150	09G2SSh	0.08	0.15	0.09	87.5
100	20YuChSh	0.20	0.24	0.20	20.0
20	14G2AFSh	0.14	0.17	0.14	21.4

*OJSC «MK Azovstal», Mariupol, Ukraine.

Table 2. Change of sulphur concentration in ingot height during ESR without deoxidation of the slag pool in the remelting process

Number of determinations	Steel grade	Sulphur concentration, %		
		Initial metal	Bottom part of ingot	Top part of ingot
150	09G2S	0.018	0.005	0.011
		0.015	0.004	0.009
		0.010	0.004	0.007

In manganese, silicon, aluminium and titanium. During the electroslag remelting the oxidizing potential of the slag pool is increased due to its contact with the air atmosphere and growth of scale at the surface of consumable electrodes. This results in change of content of those elements in the height of ingots which possess the highest affinity to oxygen: titanium, aluminium, silicon. Moreover, their maximum losses are observed in the top part of the ingot. Manganese is most close to the initial concentration, however, it is also oxidized by 0.01–0.03 % in the ingot top part.

However, there are technological measures (deoxidation of slag pool during the ESR, ESR in inert gas, etc.), which make it possible to preserve the content of elements at the level of the initial metal.

Taking into account the above-mentioned, we consider that the sampling from the top (head) part of the ingot or corresponding part of the billet or ready rolled stock is more representative for determination of the chemical composition of the electroslag remelting metal.

1. (1987) *Electroslag metal*. Ed. by B.E. Paton, B.I. Medovar. Kyiv: Naukova Dumka.
2. Latash, Yu.V., Medovar, B.I. (1970) *Electroslag remelting*. Moscow: Metallurgia.
3. Ponomarenko, A.G., Kozlov, Yu.E. (1974) About solubility of carbon in slags. *Izv. AN SSSR, Metally*, **5**, 73–80.

ELECTROSLAG CRUCIBLE BIFILAR FURNACE ETPB-2.5 WITH A CONSUMABLE ELECTRODE AND A BLOCK OF NON-CONSUMABLE ELECTRODES

V.I. ZAKHARCHENKO[*], S.V. SKRIPNIK[**], D.F. CHERNEGA[***], V.P. SKRIPNIK[**], A.N. SEMENOV[**] and L.R. DUDETSKAYA[****]

The design diagram of the electroslag crucible furnace for utilization of metal rejections, in particular large dies, has been suggested. The technological variants of remelting composite consumable electrodes from metal rejections of large sections using the water-cooled non-consumable electrodes were developed. The installation can produce liquid metal of up to 2.5 t mass of the required composition under the conditions of machine-building enterprise with use of their own metal rejections.

Key words: *electroslag remelting, non-consumable electrode, bifilar current supply, metal rejections, control parameters of process*

In the present economical conditions the use of carbon and alloyed steel rejections of own production acquires especial significance for many machine-building enterprises. The electroslag crucible furnace can be used not only for the utilization of the metal rejections, but also for producing anew the billets of various mass and configurations. This saves the time and money and improves the production flexibility. The existing electroslag crucible furnaces can remelt small lumpy wastes [1] or composite consumable electrodes of a relatively small section [2–4].

Thus, at some machine-building enterprises the comparatively small (up to 0.3–0.4 t) rejected dies are reforged into elements of the consumable electrodes which are joined by the electroslag or arc welding for their next remelting. The reforging is an expensive operation.

The large rejected dies of 0.5–6.0 t mass sometimes cannot be subjected to this operation and they are

[*]PO «BelAvtoMaz», Minsk, Belarus.
[**]NPF «Titan», Kyiv, Ukraine.
[***]National Technical University of Ukraine «KPI», Kyiv, Ukraine.
[****]Physical-Technical Institute of NAS of Belarus, Minsk, Belarus.

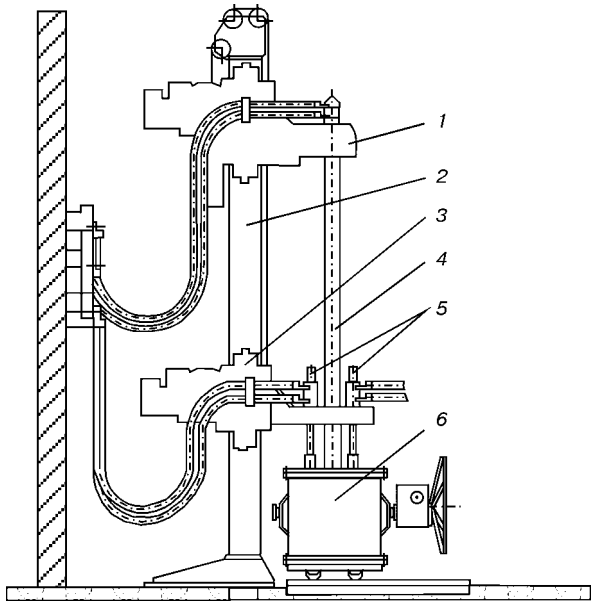

Figure 1. Electroslag crucible bifilar furnace ETPB-2.5 with a consumable electrode and a block of non-consumable electrodes: *1* — upper carriage; *2* — column; *3* — lower carriage; *4* — consumable electrode; *5* — block of non-consumable electrodes; *6* — crucible-ladle with a hand drive

used as a metal scrap. To eliminate the expensive processing and irrevocable losses of large-sized rejected dies the technology of producing new cast dies was suggested.

At the machine-building plants there is often feasibility to produce the elements of composite electrodes of 200–400 mm thickness from the rejected dies using the oxygen cutting. These elements can be joined by the electroslag welding. The manufactured electrodes can differ, depending on the configuration of the dies being cut, both in geometric shape and in section in areas of different length by 10–50 %. It is impossible to remelt them directly into a water-cooled mould due to an inevitable formation of ripples at the ingot surface.

However, these composite electrodes can be remelted, and if necessary, alloyed additionally in the electroslag bifilar crucible furnace furnished with non-consumable electrodes. The furnace ETPB-2.5 (Figure 1) was designed by modification of the serial furnace EShP-2.5. This furnace consists of a load-carrying column and two moving carriages along it, upper and lower carriages. A consumable electrode of irregular geometric shape is fixed to the upper carriage, while a block of non-consumable electrodes — to the lower carriage (Figure 2). A lined crucible-ladle for the liquid metal is mounted on a wheeled-out carriage, moving along the rail track.

The electroslag bifilar crucible furnace is operating mainly on a liquid start. A portion of 50–60 kg of molten flux is melted in a separate crucible-ladle and, then, poured into a crucible-ladle for the liquid metal.

The ESR process control is provided both in manual and automatic conditions (for example, by current). Here, the movement of upper and lower carriages is performed in opposite direction autonomously. The diagram of connection of recording instruments provides a simultaneous control of several electrical circuits (Figure 3).

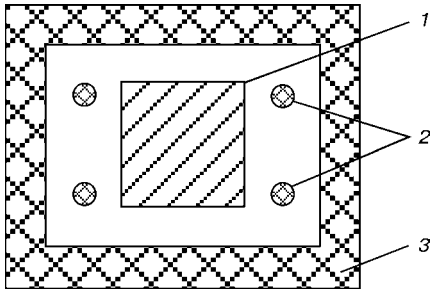

Figure 2. Scheme of melting space with a consumable electrode and a block of non-consumable electrodes arranged in it: *1* — consumable electrode; *2* — non-consumable electrodes; *3* — lined crucible-ladle

For automatic control of the remelting process a standard controller of ARShMT type, including thyristor control devices of the BTU-3601 type, is used. The diagram of device control (Figure 3) is designed on the principle of two-circuit system of governed adjustment of parameters using PI-controllers of current and speed of motor, moving the carriage.

Technical data of furnace

Type of furnace	Bifilar
Mass of portion of liquid metal, t	<2.5
Maximum section of electrode remelted, mm	<500
Maximum length of consumable electrodes, mm	4000
Number of non-consumable electrodes, pcs	2–8
Range of movement speeds of upper and lower carriages, m/min	0.001–0.6
Travel of wheeled-out carriage, mm	1500
Temperature of water, °C:	
at inlet	5–30
at outlet	60
Water pressure at inlet, MPa	0.3–0.4
Efficiency of furnace, t/h	0.4–0.8
Power source	Single-phase transformer EODTsN 4800/10
Maximum current, kA	28
Open-circuit voltage, V	49.5–122.0
Rated power, kV·A	2500
Number of stages of voltage adjustment	49
Dimensions of furnace, mm:	
length	7885
width	4100
height	9150
Mass of furnace, t	60

During operation the preset current of remelting is compared with the measured current. In case of a disbalance the controller energizes the control action supplied to the thyristor device in which the voltage is formed to supply the DC reverse motor of PBST type, moving the upper carriage with a consumable electrode. A tachogenerator, realizing the feedback in the speed of motor rotation with a thyristor device, is mounted on the motor shaft.

The control of the lower carriage with the non-consumable electrodes is similar. This carriage is also moved with the help of the motor PBST type opposite the consumable electrode as the metal accumulates in the crucible.

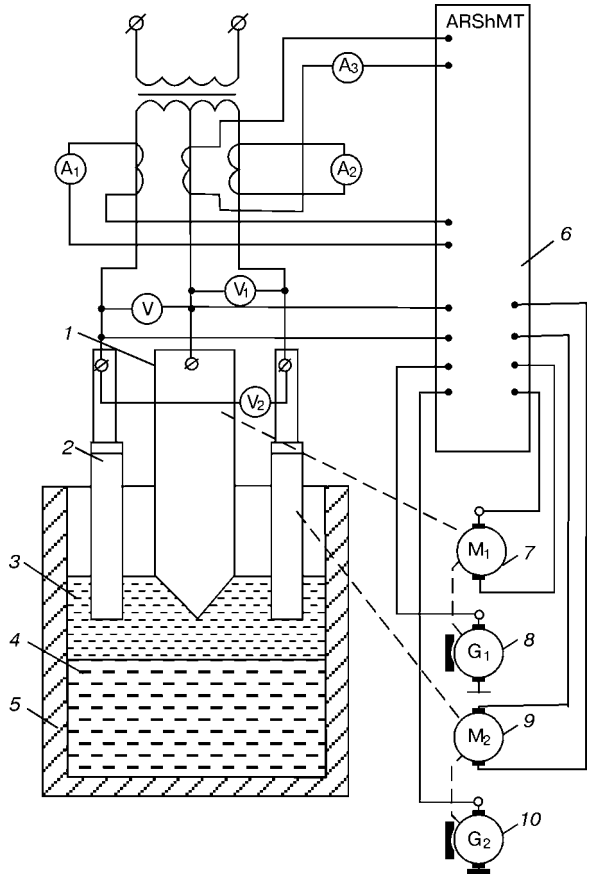

Figure 3. Diagram of connection of consumable and non-consumable electrodes: *1* — consumable electrode; *2* — non-consumable electrodes; *3* — slag pool; *4* — metal pool; *5* — lined crucible-ladle; *6* — controller ARShMT; *7* — motor of movement of upper carriage with a consumable electrode; *8* — tachogenerator of the upper carriage; *9* — motor of movement of lower carriage with non-consumable electrodes; *10* — tachogenerator of the lower carriage

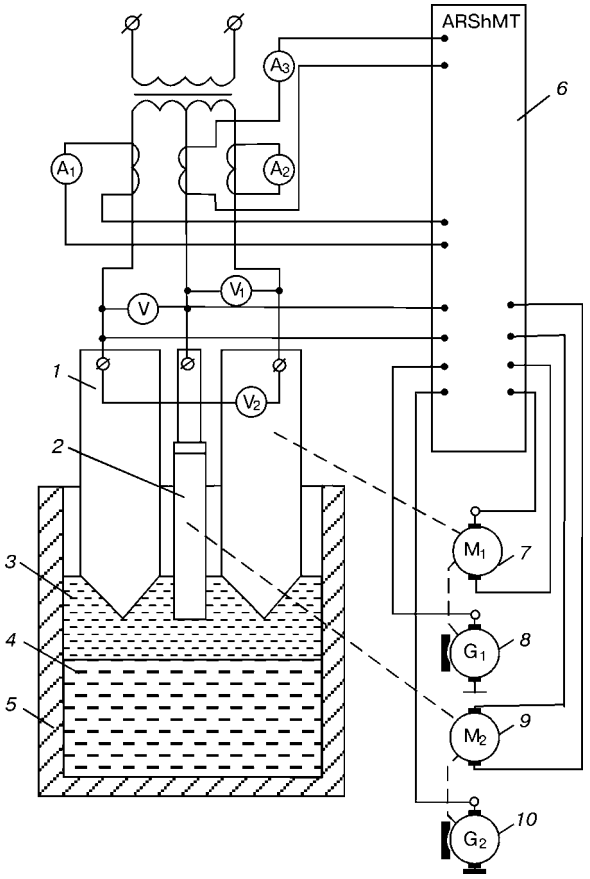

Figure 4. Diagram of connection of consumable and non-consumable electrodes: *1* — consumable electrodes; *2* — non-consumable electrode; *3* — slag pool; *4* — metal pool; *5* — lined crucible-ladle; *6* — controller ARShMT; *7* — motor of movement of the upper carriage with consumable electrodes; *8* — tachogenerator of the upper carriage; *9* — motor of movement of the lower carriage with non-consumable electrode; *10* — tachogenerator of the lower carriage

Other variants with consumable and non-consumable electrodes are possible. For example, two consumable electrodes are fastened on the upper carriage using the bifilar diagram connection, while one non-consumable electrode is fixed on the lower carriage. The diagram of the automatic control is similar (Figure 4).

This furnace can accumulate a portion of 2.5 t of pure electroslag metal in a crucible-ladle and perform its pouring into several forms located in a furnace bay, without use of an intermediate pouring ladle. The absence of a hearth electrode increases the reliability of the furnace, as the feasibility of leakage of the molten metal through the crucible bottom part is eliminated. Simultaneously, the service life of the bottom part lining and, consequently, of the crucible, as a whole, is increased.

Using the above-described crucible furnace it is possible to produce the liquid metal of almost any chemical composition. The furnace ETPB-2.5 makes it possible to create a closed cycle of metal use at one machine-building enterprise. In addition, the enterprise saves funds for purchase of metal, transport expenses, as in this case only the delivery of ferroalloys containing separate lacking elements for producing alloyed steels and alloys is necessary.

1. Skripnik, S.V., Chernega, D.F., Sushkevich, N.N. (2000) Design peculiarities of electroslag crucible bifilar furnace ETPB-0.5. *Problemy Spets. Elektrometallurgii*, **4**, 15–17.
2. Paton, B.E., Medovar, B.I., Marinsky, G.S. *et al.* (1988) State-of-the-art and prospects of development of electroslag crucible melting and pouring of metal. In: *Electroslag technology*. Kyiv: Naukova Dumka.
3. Medovar, B.I., Shevtsov, V.L., Martyn, V.I. *et al.* (1998) *Electroslag crucible melting and pouring of metal*. Kyiv: Naukova Dumka.
4. Chernets, A.V. (1998) Electroslag crucible melting as a method of production of liquid metal for the new generation of electroslag technologies without consumable electrodes. *Problemy Spets. Elektrometallurgii*, **3**, 5–8.

EFFECT OF INITIAL COOLING RATES IN SOLIDIFICATION ON STRUCTURE OF HEAT-RESISTANT NICKEL ALLOYS

B.E. PATON*, G.V. ZHUK* and N.P. TRIGUB*

Suggested is the method of electron beam hot spraying for producing structural materials out of a dispersed melt. The method combines advantages of granulating and casting technologies. The mathematical model of thermal processes of solidification of a dispersed melt has been developed. The initial rate of cooling of a heat-resistant nickel alloy in solidification has been determined, and effect of a high cooling rate on structure of the alloy has been studied.

Key words: *heat-resistant nickel alloy, electron beam, dispersed melt, cooling rate, structure, mathematical model*

Multicomponent heat-resistant Ni-base superalloys are widely applied for manufacture of turbine units and jet engines. One of the key problems of their technology is producing a homogeneous, fine-grained structure of metal at the stage of ingot or casting. This structure can be achieved by multistage thermomechanical treatment (in this case losses of metal amount to 70 %) or using technologies which provide a high rate of cooling of the melt at the stage of solidification.

The mechanism of dependence of structure of a material upon the cooling rate can be traced from the chain cooling rate–overcooling–rate of nucleation–quantity of solidification centres–structure [1]. An increase in the rate of cooling of the melt at the stage of solidification is accompanied by an increase in the number of nuclei of crystalline grains. This leads to refining of structure of an ingot and a more uniform distribution of alloying elements and phases. In heat-resistant nickel alloys, in particular, this shows up as a decrease in sizes of dendrites, decrease in liquation, refining and improvement of configuration of the strengthening γ'-phase and other phase components of a microstructure.

Experiment. The E.O. Paton Electric Welding Institute developed a new electron beam hot spraying (EBHS) method for producing structural materials from dispersed melts [2]. The method comprises electron beam melting of a consumable billet, formation of a directed flow of dispersed droplets of the melt under the effect of centrifugal forces and deposition of this flow on a shaping surface (substrate) to produce an ingot, billet of a part or coating. Owing to a high velocity of the droplets in the flow (about 10 m/s), upon colliding with the substrate they spread over the surface to a thickness of 100–200 μm, thus providing a high cooling rate during solidification. The process is carried out in a shielding environment of vacuum. Therefore, the spread droplets solidify to form a dense layer of a material with no oxidized interfaces. Therefore, the method combines advantages of casting and granulating technologies.

The EBHS process was employed to produce a heat-resistant nickel alloy whose composition is given in the Table. An initial billet was produced by the electron beam cold-hearth (EBCH) remelting method [3]. During the EBHS process the alloy was deposited on a steel substrate preheated by the electron beam. Temperature of the substrate during the experiment was fixed using three tungsten-rhenium thermocouples. Mass of the deposited material was determined by weighing the samples before and after the experiment. After EBHS the heat-resistant alloy was subjected to standard heat treatment (quenching + ageing).

Mathematical model. The mathematical model describing the EBHS process was developed for numerical calculation of thermal-physical parameters of solidification of the melt. The melt was deposited on a substrate by a continuous jet or flow of droplets, configuration and consumption of the material being kept constant. The deposition was performed layer

Chemical composition of heat-resistant nickel alloy after different types of remelting

Type of process	Content of elements, wt.%						
	Cr	Ni	Al	Ti	Mo	Co	Fe
EBCH	16.0	Base	2.6	4.1	3.3	13.0	1.3
EBHS	15.5	Base	2.4	4.0	3.2	13.0	1.5

*The E.O. Paton Electric Welding Institute, Kyiv, Ukraine.

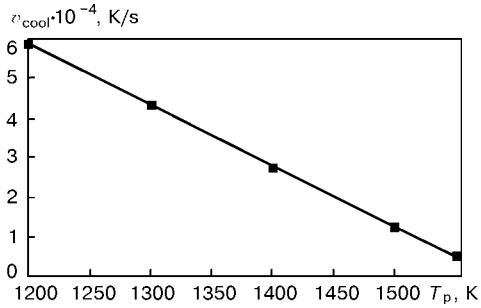

Figure 1. Dependence of the rate of cooling of the melt in solidification upon the temperature of preheating of the substrate

by layer. In addition, it was accompanied by heating of the deposition zone with a surface-action energy source, such as electron beam. Conditions of heat exchange with an environment, determined by vacuum, are limited by radiation in accordance with the Kirchhoff's law.

The basic thermal-physical processes are described by the equation of heat transfer into the regions of solid and liquid phases. In the solid phase the temperature field obeys the Fourier equation of thermal conductivity

$$c\rho \frac{dT}{dt} = \mathrm{div}(\lambda \cdot T_{\mathrm{grad}}) + f,$$

where T is the temperature; c is the specific heat; ρ is the material density; f is the power of the volumetric heat sources and λ is the thermal conductivity. In a region of the liquid phase the hydrodynamic aspects are ignored. This is associated with specific conditions of the method: thin layers of a solidifying material determine direction of the temperature gradient normal to the substrate and laminar ($\mathrm{Re} \approx 1$) flows of the liquid metal directed parallel to the substrate surface. The effect of release of latent solidification heat is allowed for in the form of addition of certain function $\varphi(T)$ to heat capacity, this function being continuous within the solidus–liquidus range $[T_S, T_L]$: $\int_{T_S}^{T_L} \varphi(T) = L$ (L is the latent heat of phase transition) and $\varphi(T) = 0$ within a range of $(T < T_S) \cup (T > T_L)$.

Radiant heat exchange with the environment occurs on the surface of the deposited layer. This surface is heated by an energy source with specific power $W(t)$.

Boundary condition has the following form:

$$\lambda(T) \frac{\partial T}{\partial x} = W(t) - \varepsilon\psi (T^4 - T_{\mathrm{en}}^4),$$

where ψ is the Stefan–Boltzmann constant; ε is the surface emissivity factor and T_{en} is the environment temperature. Allowance for release of latent solidification heat makes it possible to solve the problem by the shock-capturing method without explicit separation of the phase transition boundary.

Calculation results and investigation of samples. Calculations were made within the frames of the model for the steel substrate and deposited heat resistant alloy (T_S = 1550 K). The calculations resulted in the evolving temperature fields in the system material–substrate. Analysis of the temperature fields made it possible to derive dependence of the rate of cooling of the melt, v_{cool}, upon the temperature of preheating of the substrate, T_p (Figure 1). The order of magnitude of the cooling rates, characteristic of the method under consideration, is 10^4 K/s, which is much higher than that of traditional types of remelting, i.e. below 1 K/s.

Structure of the produced samples was studied using the optical microscope «Neophot». High cooling rates lead to refining of the dendritic structure (Figure 2) of the alloy after EBHS, as compared with the initial billet. The empirical dependence [4] allowed estimation of the cooling rates during solidification for the initial metal (0.8 K/s) and resulting samples ($(1–5)\cdot10^4$ K/s) on the base of the distance between the secondary dendrite branches, which coincide with the calculated data.

Investigation of distribution of elements in dendrite branches and dendrite spacings conducted using the «Camebax» microanalyser showed that liquation of basic alloying elements was not in excess of 4 %.

Microstructure of the heat-treated samples (Figure 3) was studied using the transmission electron microscope. The analytic electron microscope and the «Superprob» analyser were used to identify phases. Particles of the γ'-phase were 10–30 μm in size, and the γ-phase had a favourable configuration. Carbides were not in excess of 5 μm in size, and they were

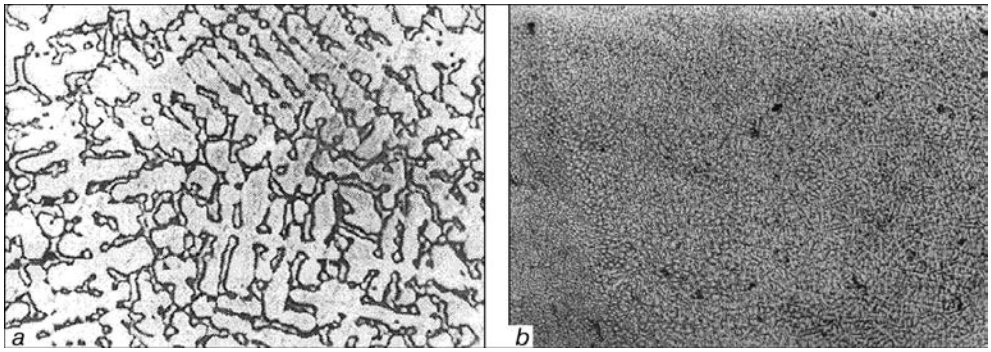

Figure 2. Structure of heat-resistant nickel alloy after EBCH (*a*) (×100) and EBHS (*b*) (×300)

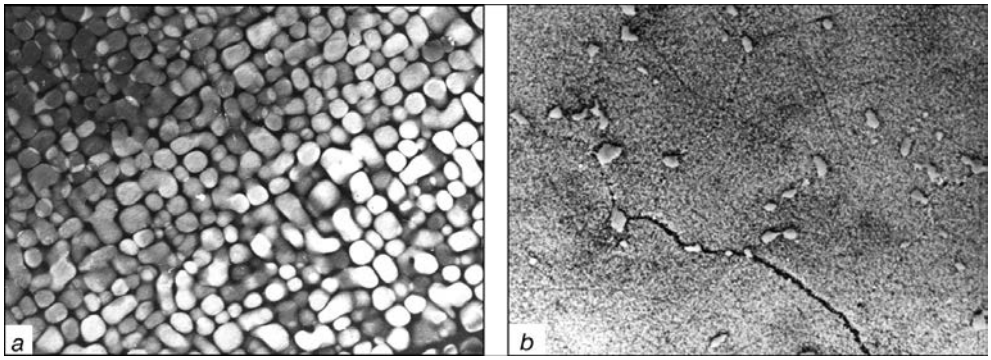

Figure 3. Microstructure of heat-resistant nickel alloy after heat treatment: *a* — γ-phase (×10000); *b* — carbides (×1000)

dissipated in the bulk of grain, rather than concentrated along its boundaries.

CONCLUSIONS

1. An increase in the cooling rate at a stage of solidification of heat-resistant nickel alloys leads to refining of the dendritic structure, uniform distribution of alloying elements, decrease in size and improvement of configuration of the phase components.

2. The EBHS method provides cooling rates of 10^4 K/s. The distance between the secondary dendrite branches in the EBHS heat-resistant alloys is decreased 20 times, the degree of liquation of alloying elements is reduced and refining of the strengthening γ-phase occurs.

1. (1987) *Physical metals science*. Ed. by R.U. Kan and P. Haazen. Moscow: Metallurgia.
2. Tikhonovsky, A.L., Pap, P.A., Kozlitin, D.A. *et al*. (1993) Method of electron beam casting from a dispersed melt. *Problemy Spets. Elektrometallurgii*, **3**, 35–39.
3. Paton, B.E., Trigub, N.P., Kozlitin, D.A. *et al*. (1997) *Electron beam melting*. Kyiv: Naukova Dumka.
4. Brody, H.D. (1973) Grains, dendrites and liquation in cast alloys. In: *Vacuum metallurgy*. Moscow: Metallurgia.

FAILURE OF A PROTECTIVE COATING ON NIOBIUM AT HIGH-TEMPERATURE OXIDATION

A.V. DEMCHISHIN*, Yu.A. KURAPOV*, E.P. POLISHCHUK* and E.G. TERNOVOJ*

The paper proposes a more stringent procedure of testing high-temperature resistant protective coatings on refractory metals and alloys in a dynamic gaseous medium with addition of an oxidiser. Studied was the mode of breaking up of a four-layer protective coating, applied on flat tensile testing specimens of niobium by the method of vacuum electron beam deposition from the vapour phase.

Key words: *protective coatings, refractory metals, high-temperature resistance, high-temperature oxidation, molybdenum disilicide, multilayer coating, procedure, dynamic gaseous medium, oxidiser, temperature field, tensile testing specimens, fracture mode*

Refractory metals and alloys on their base are finding ever wider application in modern engineering due to their excellent high-temperature strength. Niobium is of special interest among them, being characterised by a high ductility and satisfactory weldability. It lends itself readily to mechanical treatment by forging, stamping, broaching, drawing, etc. Alloys with high values of mechanical strength were produced on niobium base [1]. The main disadvantage, limiting a broad introduction of niobium alloys into high-temperature engineering, is their low high-temperature strength. One of the ways to solve this problem is development of protective coatings that lower the activity of oxidation processes, occurring both inside the metal matrix, and on the metal–gaseous medium interface.

Increase of high-temperature strength of niobium alloys is possible by applying one- and multicomponent diffusion coatings [2–4]. The protective effect of such coatings, however, decreases at temperatures above 1000 °C through development of diffusion pro-

*The E.O. Paton Electric Welding Institute, Kyiv, Ukraine.

cesses on the coating–substrate interface. Silicide coatings are used, for instance, for protection of niobium alloys from oxidation [5]. However, niobium disilicide at temperatures above 1000 °C has a low high-temperature resistance as a result of formation of a loose oxide film, consisting of Nb_2O_3 and SiO_2 that slightly slows down oxygen diffusion into the matrix, and easily separates from the metal substrate during oxidation.

Over the recent years the researchers' attention has been attracted by coatings, based on refractory compounds, more stable in high-temperature gas flows, for instance, molybdenum disilicide, that features an excellent high-temperature resistance and value of thermal coefficient of linear expansion (TCLE), close to that of niobium [6–9].

Promising approaches to refractory metal protection from oxidation are creation by various methods, of compositions, consisting of several layers, each of which has a certain function [10]. A multilayer coating has a longer service life and limited susceptibility to overheating, thus allowing the temperature mode of the item service to be increased.

This study consisted in investigation of the features of breaking up of a four-layer protective coating on niobium alloy 5VMTs (W — 5.5; Mo — 2.2; Zr — 1.15 wt.%; Nb — base) under the conditions of high-temperature oxidation. The multilayer coating was applied on specimens by the method of vacuum electron beam vapour phase deposition [11].

Pure molybdenum of 5 μm thickness was applied as the first diffusion barrier, that, on the one hand, should prevent direct interaction of the scale-resistant coating layer of $MoSi_2$ with the base, and, on the other hand, promote relaxation of stresses in the coating and improvement of adhesion.

The second scale-resistant layer of $MoSi_2$ ~50 μm thick was produced by simultaneous deposition of molybdenum and silicon from two sources under vacuum. Oxidation resistance of the scale-resistant layer can be further improved by applying on its surface a composition, where the components have a high melting temperature, low degree of dissociation, high density and continuity. In addition, they should not form any low-melting and volatile compounds with the elements, present either in the oxidising medium or in the diffusion coating, and the oppositely-directed diffusion of atoms (ions) of the metal and non-metal in them should be minimal.

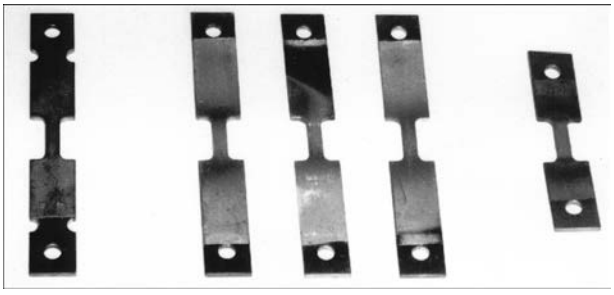

Figure 1. Flat tensile testing specimens of 5VMTs alloy with a four-layer protective coating

Therefore, a layer of mullite (Al_2O_3 + SiO_2), ~20 μm thick, was applied as the third barrier layer. And, finally, applied as the fourth heat-reflecting layer was a ZrB_2 layer ~10 μm thick with a high oxidation resistance at elevated temperatures and emission coefficient of 0.89–0.91. This four-layer composition, probably, should have had a good resistance to thermal loads, as the TCLE of its components is the closest to that of the niobium alloys.

The known procedure of testing high-temperature coatings for high-temperature resistance [12], according to which the coatings are applied on cylindrical specimens with a semi-spherical crown and placed into the resistance furnace with a static air atmosphere at a specified temperature, does not always reproduce the actual pattern of the item operation. In reality the item often operates under the conditions of a gas or air flow, a certain temperature gradient is in place on the surface of various parts of the item, as well as stress raisers (edges, angles, mating regions, etc.) resulting from the item design features. All this is the cause for premature failure of the item, because of faster breaking up of the protective coating in the critical zones. Therefore, after high-temperature resistance testing of the four-layer coating by the traditional method in a resistance furnace, without any noticeable changes in the coating at temperature T = = 1200 K and soaking for τ = 200 h, it was decided to test the coating high-temperature resistance under the conditions, close to the actual conditions, i.e. purposefully make the tests more severe by introducing factors, detrimental for the coating fatigue life, namely replace the static air atmosphere of the resistance furnace by a dynamic gaseous medium; increase the amount of the oxidiser in the test atmosphere; add the element of a non-isothermal temperature field; add structural elements, that are stress raisers and concentrators of possible coating defects.

This was the basis for applying a more stringent procedure for high-temperature resistance testing, namely oxidation in the acetylene-gas torch flame with addition of oxygen (~20 %). Flat tensile testing specimens were used, whose grip ends were not protected by the coating (Figure 1). Torch flame was aimed at the test part of the tensile testing specimen (Figure 2). The test zone cross-section being smaller, than that of the rest of the specimen, just the specimen test part was heated up to a high temperature, being practically in an isothermal temperature field. The rest of the specimen right up to the ends of the grip was exposed to a non-isothermal temperature field. Temperature mode was controlled by an optical pyrometer. Edges, angles and mated regions of the flat specimen were stress raisers and regions of possible coating defects.

Four specimens were tested simultaneously, which were fastened in a special rotating grip at 90° angle to each other. After 20 h one specimen was taken off, and the others were tested further with their subsequent removal after 50, 100 and 200 h. Testing

program included three modes with temperatures of 1000, 1200 and 1450 K. Change of specimen weight Δm was determined by weighing it before and after testing and visual inspection was performed. Testing results are given in the Table.

Visual examination of the specimens (No.1, 5, 9), removed after 20 h of soaking at all the temperatures showed, that the four-layer coating starts breaking up because of spallation of the upper layers of $Al_2O_3(SiO_2)$ and ZrB_2 in the HAZ between the specimen test part, where the temperature is maximal, and the zone of temper colours at the end of the specimen, where the temperature is minimal. On the specimen test part, however, the coating did not break up in any of the temperature modes.

Extension of specimen soaking time up to 50 h did not lead to any essential change of the morphology of the specimen oxidised surface. Upper layers of $Al_2O_3(SiO_2)$ and ZrB_2 did come off the test part in specimen No.2 at 1000 K. In specimens No.6 and 10, oxidised at 1200 and 1450 K, just the area of spallation of the two upper layers in the HAZ increased slightly, while all the layers were preserved on the test part.

Further increase of the specimen soaking time up to 100 h has a greater effect on the morphology of the specimen oxidised surface. In specimen No.3, oxidised at 1000 K, upper layers of $Al_2O_3(SiO_2)$ and ZrB_2 delaminated practically over the entire surface, although the upper layers were preserved on one side of the test part, in the maximal temperature zone. In specimen No.7 right after testing at 1200 K, the upper layers are absent on the test part and a whitish powder-like deposit is visible. The specimen failed in the middle of the test part, when being removed from the rig. A specimen, oxidised at 1450 K (No.11), was removed from testing after τ = 90 h for the reason of breaking up of the specimen test part. The coating upper layers were absent in the specimen test part.

And, finally, not all the specimens withstood further extension of the testing time. Specimen No.4 after oxidation for 200 h at 1000 K stood all testing without failure. However, the specimen test part became changed, namely the edges rounded off and the cross-sectional area was reduced. Specimen No.8, oxidised at 1200 K, was removed from testing for the reason of the test part failing at the neck end after τ = 145 h. The four-layer coating was preserved in the remaining part of the specimen. Specimen No.12, oxidised at 1450 K, withstood 170 h before failure of the test part. Upper layers of $Al_2O_3(SiO_2)$ and ZrB_2 coating were absent on the specimen test part, while a whitish powder-like deposit was observed in the zone of failure and oxidation of the adjacent parts of the specimen.

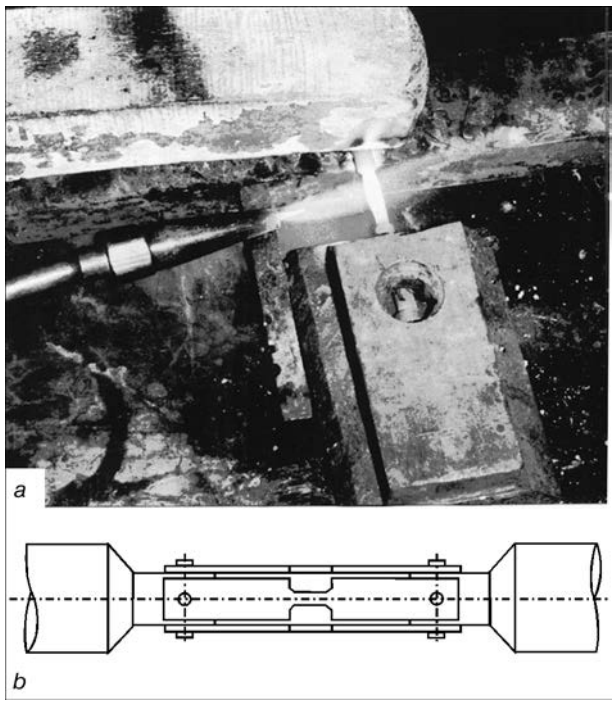

Figure 2. High-temperature resistance testing in the flame of the acetylene-gas torch with addition of oxygen (~20 %): *a* — oxidation of one specimen; *b* — rotating grip with simultaneous attachment of 4 specimens at the angle of 90° to each other

According to the procedure used by us, high-temperature resistance testing of the coating on the specimen test part in an isothermal temperature field was complemented by testing the coating in a non-isothermal field, this introducing certain special features into the performance of the metal — four-layer coating system under the conditions of a high temperature gradient. In this case the information on coating behaviour in the gradient temperature field is of primary interest.

Proceeding from the general appearance of the oxidised specimen surface, the gradient temperature field can be divided into the following 4 zones (Figure 3): *I* — specimen surface zone ~15 mm long, where specimen ends, not protected by the coating, are located. This zone is characterised by temperature gradient of 80–150 °C; *II* — initial oxidation zone 15–20 mm long, where temper colours (interference colours) are observed. It is characterised by tempera-

Specimen No.	1000 K		Specimen No.	1200 K		Specimen No.	1450 K	
	τ, h	Δm, g		τ, h	Δm, g		τ, h	Δm, g
1	20	0.94	5	20	0.85	9	20	0.60
2	50	1.44	6	50	1.46	10	50	1.41
3	100	1.64	7	100	1.88	11	90	1.45
4	200	3.03	8	145	2.61	12	170	2.48

Note. Specimen No.7 failed when being removed, specimens No.8, 11 and 12 were removed from testing because of fracture in the test part.

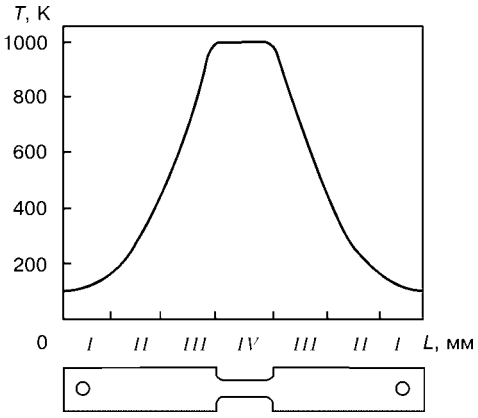

Figure 3. Gradient temperature field along length *L* of the specimen: *I, II, III, IV* — zones

ture gradient of 150–450 °C; *III* — heat-affected zone 15–20 mm long, where intensive breaking up (spallation) of the coating is observed. This zone is characterized by the highest temperature gradient of 450–730 (1180) °C; *IV* — working temperature zone 20 mm long, that is continuously exposed to the impact of the oxidising flame of the gas torch. In this zone the temperature gradient is practically absent, as the specimen thinner part is rather uniformly heated by the gas torch flame.

Zone *I* is characterised by the absence of visible traces of oxidation of unprotected niobium, as the temperature of its heating is quite low. If the oxidation process is going on here, this occurs at the expense of formation of stable NbO and NbO_2 oxides.

In zone *II* the coating remained practically on all the specimens, except for several of them. Interference effects can be created by oxide films in this temperature range, for instance, NbO, NbO2 films, since niobium diffuses into the coating.

Zone *III* is the most critical. Apparently, such a high temperature gradient, to which the metal–coating system is exposed, induces here an extremely complex stress pattern, because of the difference in the TCLE of the substrates and the coating, as well as the multilayer coating components. It is this complex stressed state of the metal–coating system in the zone of a considerable temperature gradient, that is the primary reason for failure.

Zone *IV* is exposed to the impact of maximal temperatures in the oxidising flame of the gas torch. However, a complex stressed state of the metal–coating system due to the temperature gradient, is absent here. Therefore, the coating is preserved after soaking for 20 and 50 h. At longer soaking, the specimen test part breaking up is initiated by the processes of failure of the coating in the adjacent zone *III*.

Therefore, the breaking up pattern of the four-layer (Mo + $MoSi_2$ + $Al_2O_3(SiO_2)$ + ZrB_2) coating on niobium alloy 5VMTs in an oxidising medium of the gas torch can be presented as follows.

The complex stressed state of the metal–coating system and the four-layer coating proper in the zone of a considerable temperature gradient (zone *III*) causes delamination of two upper coating layers ($Al_2O_3(SiO_2)$ + ZrB_2). This results in exposure of molybdenum disilicide layer surface. At high temperatures disilicides feature an excellent oxidation resistance that is due to formation of a protective glass-like layer, consisting chiefly of SiO_2. Formation of the glass-like layer is followed by predominant oxidation of silicon. The reaction rate is determined by solid-phase diffusion through scale. Since oxygen is a reagent that diffuses in the oxide at the highest rate, SiO_2 layer grows on the inner interphase. Glass-like oxide scale, formed at high temperatures, has the best protective properties. Therefore, it is probably beneficial to oxidise $MoSi_2$ coatings at 1700–1800 K, before using coated metal at lower temperatures.

At 750–900 K temperatures, however, $MoSi_2$ oxidation leads to the most unexpected result, consisting in that all the material completely dissolves quickly, turning into loose powder with a high specific volume. This phenomenon is called silicide «pest». It is a certain form of intercrystalline oxidation of $MoSi_2$, at which each $MoSi_2$ grain is ultimately encircled by the oxidation reaction products. It is believed that «pest» attack is due to predominantly intergranular diffusion of the reacting gas in combination with ageing that is dependent on temperature.

This is exactly the process that is observed in the third temperature zone, where the whitish powder-like deposit is found. Loosening the remaining coating layer, it allows oxygen to penetrate to the niobium alloy, that is oxidised in its turn, and moving towards the high-temperature zone, disrupts the four-layer coating from the inside, leading to its delamination and breaking up. After that the niobium alloy «burns» in the specimen test zone and breaks up.

The initial process of breaking up is also caused by coating defects, present on the sharp edges of the specimens, in the mating regions, as well as the local coating spallation areas.

Analysis of the results of studying the high-temperature resistance of the four-layer protective coating on niobium alloy 5VMTs, produced by vacuum electron beam vapour phase deposition shows that the proposed composition provides good protection of niobium from high-temperature oxidation in an isothermal temperature field. This is demonstrated by the results of high-temperature resistance testing by the traditional method in a resistance furnace (T = = 1200 K, τ = 200 h), as well as partial preservation of the four-layer coating on the specimen test part (No.6, 8, 10) in testing under more stringent conditions. In the presence of a non-isothermal temperature field, the unprotected and particularly not subjected to high-temperature oxidation layer of $MoSi_2$ decomposes at low temperatures, disrupts and destroys the protective coating.

Thus, in order to evaluate the high-temperature resistance of especially complex multilayer coatings, having a long enough service life, it is rational to apply a stringent testing procedure by introducing additional factors, acting on the metal–coating sys-

tem. This, on the one hand, allows bringing the testing as close as possible to the actual conditions of the item service, and, on the other hand, studying the nature, cause and, possibly, also the mechanism of the coating failure.

1. Baron, V.V. (1981) *High-temperature niobium alloys. Physical chemistry of rare metal alloys*. Moscow: Nauka.
2. Maksimovich, G.G., Pavlina, V.S., Stakhnyak, B.N. *et al.* (1980) High-temperature strength of multicomponent coatings on niobium alloys. *Fiz.-khim. Mekhanika Materialov*, **6**, 27–30.
3. Shatinsky, V.F., Rybakov, S.V., Gojkhman, M.S. *et al.* (1980) Diffusion coatings for improvement of high-temperature strength of niobium alloys. *Zashchitn. Pokrytiya na Metallakh*, **14**, 58–61.
4. Maksimovich, G.G., Pavlina, V.S., Zbozhnaja, O.M. *et al.* (1980) Production of multicomponent diffusion coatings on niobium alloy 5VMTs in liquid-metal solution medium. *Ibid.*, 61–64.
5. Tsirlin, M.S., Kasatkin, A.V., Byalobzhesky, A.V. (1975) Oxidation of silicide coatings on niobium and its alloys VN-2 and VN-3. *Zashchita Metallov*, **5**, 592–596.
6. Tsirlin, M.S., Kasatkin, A.V., Byalobzhesky, A.V. (1978) Silicide type high-temperature coating for niobium alloys. *Poroshk. Metallurgia*, **12**, 31–34.
7. Lazarev, E.M., Monakhova, L.A., Romavonich, I.V. *et al.* (1981) Molybdenum-boron-silicon coating on a niobium alloy VN-3. *Fiz. i Khim. Obrab. Materialov*, **3**, 68–72.
8. Cadd, J.D. (1970) *Columbium. High-temperature oxidation-resistant coatings*. N.Y.
9. Lorenz, R.H., Michael, A.B. (1961) Oxidation-resistant silicide coatings for columbium and tantalum alloys by vapor phase reaction. *J. Electrochem. Soc.*, **9**, 123–126.
10. Dzyadykevich, Yu.V. (1994) Improvement of high-temperature resistance of refractory metals. *Neorganich. Materialy*, **11**, 1405–1408.
11. Movchan, B.A., Demchishin, A.V., Chursanov, N.A. *et al.* (1979) Structure and properties of refractory joints produced by electron beam evaporation. In: *Problems of special electrometallurgy*. Kyiv: Naukova Dumka.
12. Kofstad, P. (1969) *High-temperature oxidation of metals*. Moscow: Mir.

MODELLING OF CONDITIONS OF REMOVAL OF SHRINKAGE PIPE FROM CYLINDRICAL EBCH INGOTS

G.V. ZHUK*, A.N. KALINYUK* and N.P. TRIGUB*

Methods of mathematical modelling were used to study the process of removal of a shrinkage pipe (porosity) from cylindrical ingots of titanium alloy Ti–6Al–4V. The three-stage process of electron beam cold-hearth (EBCH) remelting is considered. Technological parameters are recommended, providing ingots free from defects in the head part.

Key words: *electron beam remelting, mathematical modelling, thermal processes, shrinkage pipe*

One of the topical problems of production of ingots by the special electrometallurgy methods is formation of shrinkage pipes (porosity) at the final stage of ingot melting [1]. This problem is characteristic, in particular, of production of cylindrical ingots of titanium alloys by the EBCH remelting method. The cause of formation of a shrinkage pipe in a solidifying ingot is the presence of a developed molten metal pool at the main stage of ingot melting. Formation of the shrinkage pipe can be avoided by decreasing depth of the molten pool through reducing the rate of remelting. Nevertheless, this is not always possible, based on the established flow diagram of EBCH remelting of multicomponent titanium alloys [2]. Another way of avoiding formation of the above defects in the head part of the ingots consists in providing such conditions of heating of the ingot surface in a mould at the final stage of melting, under which the depth of the molten pool would be gradually decreased to a zero value without formation of a hard crust at the ingot tip. Development of such conditions is a difficult problem which is handled using mathematical modelling methods.

The authors studied conditions of removal of a shrinkage pipe in the Ti-6Al-4V ingots, based on the earlier developed software for calculation of thermal fields in cylindrical EBCH ingots [3].

Statement of the problem. The following problems were solved during performance of the work:

- identification of optimal technological parameters at the stage of melting of an ingot under quasi-

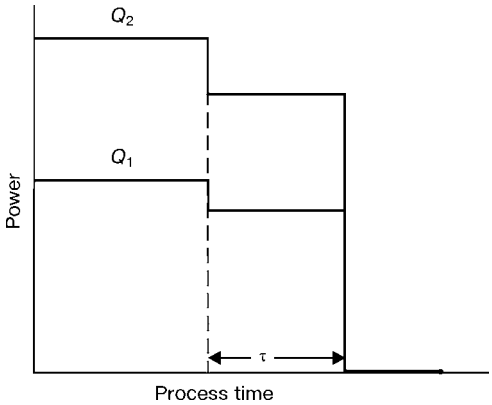

Figure 1. Schematic of variations in power of electron beam heating of the ingot surface

*The E.O. Paton Electric Welding Institute, Kyiv, Ukraine.

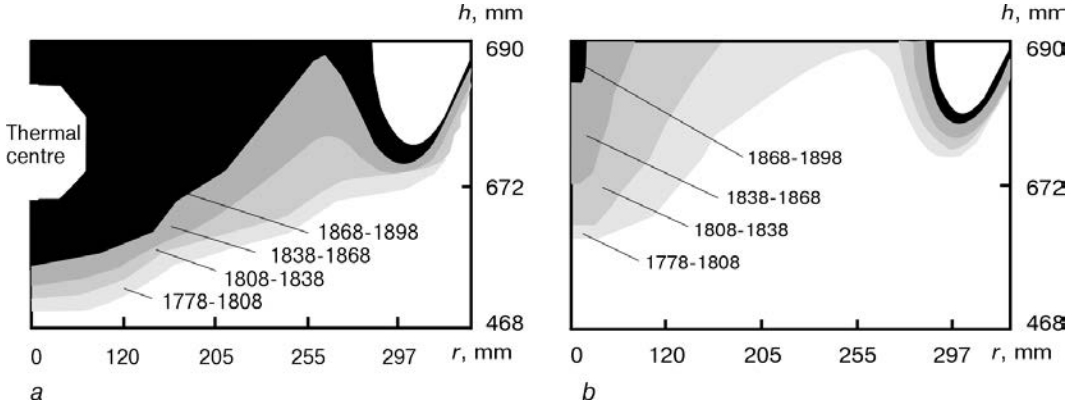

Figure 2. Temperature fields, K, in height h and radius r of the ingot with a diameter of 630 mm at the stage of melting (*a*) and after removal of a shrinkage pipe (*b*)

stationary conditions within the frames of the mathematical model of electron beam melting of cylindrical ingots;

• determination of a permissible range of variations in technological parameters at the stage of removal of a shrinkage pipe;

• calculation of optimal technological parameters of removal of a shrinkage pipe in ingots of different diameters. This was done by considering technological parameters of melting of ingots with a diameter of 200, 310, 400 and 630 mm.

Choice of optimal technological parameters of melting was based on the following considerations. A minimum value of the depth of the molten pool corresponds to a minimum size of solidification structures of an ingot and provides a uniform distribution of structural components and alloying elements. In this case the molten pool should cover the entire surface of the ingot, thus preventing formation of defects of the type of lack of fusion and porosity on the surface and in the bulk of the ingot. One should especially note the importance of formation of a liquid ring at the ingot and mould interface, which is an imperative requirement for producing a smooth and defect-free surface of the ingot. Limitations on the surface temperature were also taken into account.

Identification of the optimal technological parameters of melting was followed by estimation of values of power of electron beam heating of the head part of the ingot at a stage of removal of a shrinkage pipe. The following fact was assumed to be a criterion of absence of a shrinkage pipe (porosity) in a finished ingot: prior to complete solidification the last region of the molten pool along the axis of the ingot should be located on its surface.

Ingot diameter, mm	Power at the ingot melting stage, kW		Power after pouring of the last portion, kW		Time of the intermediate stage, s
	Q_1	Q_2	Q_1	Q_2	
200	9	15	8	8	225
310	30	35	25	25	320
400	54	56	50	50	890
630	145	70	125	65	1100

Parameters of a linear variation in power of electron beam guns were used as the basis for mathematical calculations. That is, power was assumed to be constant in time at the main stages of melting, and in mathematical modelling of transition to the next stage it changed in an infinitely short time. The entire melting process was broken in time into three stages (Figure 1).

1. Initial stage (melting of an ingot), at which metal is periodically poured in portions into the mould at a constant frequency. Part of the power of heating of the ingot surface, Q_1, is uniformly distributed in the central region of the ingot, while the other part Q_2 is distributed on the periphery following a law which allows smoothness and continuity of heating of a portion of metal in transition from the central region of the ingot to its periphery.

2. Intermediate stage, at which heating of the metal surface in the mould occurs without pouring of new portions. The time of the intermediate stage, τ, is a key parameter of calculations and characterizes the moment of the technological process where the liquid-solid phase at the ingot axis is fully transformed into the solid phase.

3. Final stage of melting, at which the guns are switched off and metal cools down in the solid phase.

Power of the electron beam guns in transition from the initial to intermediate and then from intermediate to final stage changes in a extremely short time in a stepwise manner and then remains constant up to the end of a stage.

Choice of power of a gun was based on the following technological requirements. Temperature of metal at any point of the ingot surface during the first stage should correspond to temperature of metal in the liquid phase. To save electric power and avoid losses of alloying elements, overheating of metal by more than 100 K is not permitted. In this connection, the power range selected for preliminary estimation of temperature was limited to an upper value, which was 50 kW for the ingot with a diameter of 200 mm, 120 kW for the ingot with a diameter of 310 mm, 210 kW for the ingot with a diameter of 400 mm and 450 kW for the ingot with a diameter of 630 mm.

The temperature gradient of metal during the intermediate stage should not be directed from the surface deep into the ingot, so that no shrinkage pipe is formed during the cooling process at the final stage. Therefore, chosen was the lower limit of the range of search for the optimal power of the guns. Values of this power were finally determined by successive iterations.

Calculation results. Numerical calculations resulted in determination of temperature fields inside ingots of different diameters at the stage of melting with an interval of 100–400 s and at the stage of removal of a shrinkage pipe with an interval of 10–60 s. The fields were processed using *Microsoft Excel* and represented in a graphical form. Typical diagrams of temperature fields (for an ingot with a diameter of 630 mm) at the stage of melting and after removal of a shrinkage pipe are shown in Figures 2, *a*, *b*. It can be seen from the Figures that at the stage of melting of an ingot its head part contains a developed molten pool, the thermal centre (point at the axis of the ingot having the highest temperature) being located not on the surface. In removal of a shrinkage pipe the depth of the pool, while gradually decreasing, reaches a zero value. In this case, the thermal centre moves from the depth to the surface of the ingot, and no closed liquid cavities are formed at its head part. The optimal technological parameters of melting (Table) were recommended as a result of analysis of the diagrams plotted.

The employed mathematical modelling methods and calculated technological parameters of melting and removal of a shrinkage pipe can be used not only for electron beam remelting, but also for other vacuum technologies.

1. Chalmers, B. (1968) *Theory of solidification*. Moscow: Metallurgia.
2. Paton, B.E., Trigub, N.P., Akhonin, S.V. *et al*. (2000) Development of the technology of electron beam melting of titanium. *Problemy Spets. Elektrometallurgii*, **2**, 34–40.
3. Zhuk, G.V., Akhonina, L.V., Trigub, N.P. (1998) Mathematical modelling of processes of solidification of titanium alloy Ti–6Al–4V in EBCH. *Ibid*., **2**, 21–25.

CERTAIN POSSIBILITIES FOR STEEL TREATMENT IN THE ARC AND PLASMA LADLE-FURNACES

G.A. MELNIK*, O.S. ZABARILO*, M.L. ZHADKEVICH*, A.A. ZHDANOVSKY*, M.S. PRIKHODKO* and A.A. POBOL*

Technological possibilities for melting of steels in the arc steel-melting furnaces (ASMF) by the conventional method and by the duplex-process (melting in the ASMF–ladle treatment of steel) are considered. Basic power indices of the steel melting are analyzed. It is shown that the ladle treatment of steel in the arc ladle-furnaces and especially in plasma ladle-furnaces permits improving the steel quality, increasing efficiency of the ASMF, decreasing the power consumption and expanding technological and metallurgical potentialities of the process. Steels after plasma ladle treatment in argon, nitrogen or their mixture are on par in quality with steels produced by the methods of special electrometallurgy, and meet the requirements of the international standards.

Key words: *ladle treatment of steel, arc and plasma ladle-furnaces, power-saving technological systems, plasma-arc heating complex, parameters of the power regime, steel, slag, gas, steel heating rate*

A concept of high technology was long ago formed in steel production of industrially developed countries. This was conditioned by the favorable market situation and requirements to drastically change technology of steel melting and a design of the arc steel-melting furnaces (ASMF), thus providing the efficiency increase and power consumption optimization. The essence of the process implies production of steel by a duplex-process: melting in the ASMF–ladle treatment (LT) of steel. The process suggests the use of ASMF as a high-productive melting unit maximally providing its operational conditions for acceleration of the melting of metal scrap, cast iron and slag. Removal of phosphorus from the melt is the only element of the metallurgical technology performed along with the melting of charge. All other operations are performed by the steel LT, namely:

- steel refining for chemical composition and temperature;
- removal of harmful impurities, gases and non-metallic inclusions;
- microalloying and modifying of metal, control of non-metallic inclusions morphology;
- improvement of the technical and economical indices of the metal production both in the steel melting process and during the whole production chain.

The units of arc ladle-furnace (ALF) or plasma ladle-furnace (PLF) type are the most advanced machines for steel LT. They provide heating of the liquid steel, its mixing and addition of lumpy and injection of powder materials. Let us analyze the main power indices of the steel melting by the duplex-process and in the ASMF. Under conventional ASMF technology when all operations are performed in the furnace, the duration of the steel refining 2–3 times exceeds the time of its melting. Under refining less than 20–70 % of the set power is used. The higher the requirements to steel quality, the worse the charge, the higher the set power, the lower the active power of the transformer used. [1]. Under melting of electric steel at the Stock-Holding Company «Bummash» (Izhevsk, Russia) the specific consumption of the electric power for 25 t ASMF is 690–850 kW·h/t. Specific energy consumption for melting in this furnace is 435 kW·h/t [2].

Thus, steel refening in ASMF requires 255–415 kW·h/t. Under steel LT in arc and plasma ladle-furnases a specific consumption of electric power is only 30–60 kW·h/t [3, 4], which is 4.2–13.9 times less than under refining steel in ASMF and 1.4–1.7 times less than under duplex-process (ASMF + ALF). Power consumption in ALF or PLF includes also energy necessary to heat the ladles or to maintain a preset temperature level after tapping the previous portion of metal and up to pouring the next portion. The use of ALF together with ASMF of normal power increases furnace efficiency by 30–50 %. The use of ASMF with increased power permits increasing the duplex-process efficiency by 50–80 % [5].

The duplex-process is much better than the multistage steel melting in ASMF in terms of steel quality

*The E.O. Paton Electric Welding Institute, Kyiv, Ukraine.

Table 1. Assimilation degree of alloy additions

Unit	Alloy additions, wt.%								Reference
	C	Si	Mn	Cr	Al	Ni	Mo	V	
ASMF	–	0.7	0.75	0.85	0.4	0.9	–	–	[6]
ALF	–	0.9	0.95	0.95	0.5	1.0	–	–	[6]
ALF	0.98	0.9	0.98	1.0	–	1.0	1.0	–	[3]
ALF	0.96	–	0.94	–	–	–	–	0.98	[4]
PLF	1.0	1.0	1.0	1.0	–	1.0	–	–	[7]

increase and saving of alloying elements. The use of ALF in steel-making plants allows increasing range of the grades of produced steel, including conventional electric steel grades. The use of ALF allows producing carbon, low-alloy, high-alloyed steels including bearing, rail, boiler, spring, tool, stainless steels, steels of deep drawing and others. Metallurgy of steel production improves as a result of using steel LT in ALF or PLF. It is recognized that introduction of 1 % of alloying elements decreases the steel temperature in ALF by about 25 °C. Addition of alloying elements in considerable amounts requires to prolong the heating. Heating in 100 t ALF lasts 3–4 h if 13 % of alloy additions are put to the metal [4]. There is a case when the whole process of refining and alloying of the alloyed steel with the content of alloy additions of up to 8 % was performed in ALF [5]. The assimilation degree of the alloy additions in ALF [6] and especially in PLF [7] increases as against ASMF (Table 1).

It is agreed that the steel LT in ALF permits increasing a utilization degree of alloy additions by 5 % of the metal charge [8]. For PLF this index must be even higher. Steel LT in ALF allows increasing the homogeneity of melt by temperature and chemical composition, thus lowering composition variations of the produced steels [9] (Table 2).

Accuracy in determining temperature at the end of steel LT in ALF is 4–5 °C [3, 8]. The results of steel LT in the 60 t ALF have shown that the content of sulfur and gases in liquid steel may be decreased within the following range: S — 0.023–0.014 wt.%; O_2 — 40–20 ppm; H_2 — 4.7–2.0 ppm; N_2 — 90–80 ppm [10]. On evidence derived from other data [3] a degree of desulphuration of the melt with initial oxygen content of 0.03 % after 30–40 min of steel LT is 65 and 78 %, respectively; after 40 min of steel LT with silicocalcium blowing — more than 85 %; total oxygen content — 10–30 ppm; dephosphorization — less than 10 ppm; increase of the nitrogen content — less than 5 ppm. A coefficient of sulfur distribution between slag and metal achieves 130 in ALF [4] and 700 in PLF [7]. Work in combination with ALF has permitted a more than 30 % increase of the ASMF lining due to the fact that only melting and decarburation down to 0.5 % C have been performed in the ASMF [5].

Therefore, steel LT in ALF or PLF allows increasing steel quality and ASMF efficiency as well as decreasing consumption of main auxiliary materials and power [10]. Improvement of these indices makes it possible to fully compensate the cost of steel LT.

These results are a good foundation for development of new processes of steel-making with regard to basic provisions of the high technologies under market conditions.

It is evident from the above data that PLF have a number of advantages as compared to ALF. Plasma heating in contrast to arc heating provides improved thermodynamic and kinetic conditions for metallurgical reactions of deoxidization and refining of metal from gas and non-metallic inclusions. It is distinguished for its efficiency, optimal conversion of the electric power into heating power, increased stability, controllability and purity of the plasma discharge. It ensures air-tightness of the working space, good controllability of the atmosphere and a wide range of technological gas pressures.

These advantages allow expanding power, technological and metallurgical potentialities of the unit for complex ladle treatment of steel (UCLTS), decreasing of specific consumption of electric energy, heating duration and wear of the ladle lining, increase an assimilation degree of the alloying elements, active utilization of the gas and slag phases, prevention of metal contamination with carbon, nitrogen and hydrogen, improvement of steel quality, ecology of the metallurgical process and sanitary-hygienic condi-

Table 2. Change of steel composition under alloying by different methods

Method of alloying	Variations, %				
	C	Si	Mn	Al	V
Alloy addition under tapping from ASMF	0.06	0.12	0.23	0.07	0.02
Preliminary alloying under tapping and final alloying under steel treatment in ladle	0.03	0.09	0.11	0.033	0.015
Alloying under steel LT	0.02	0.05	0.05	0.02	–

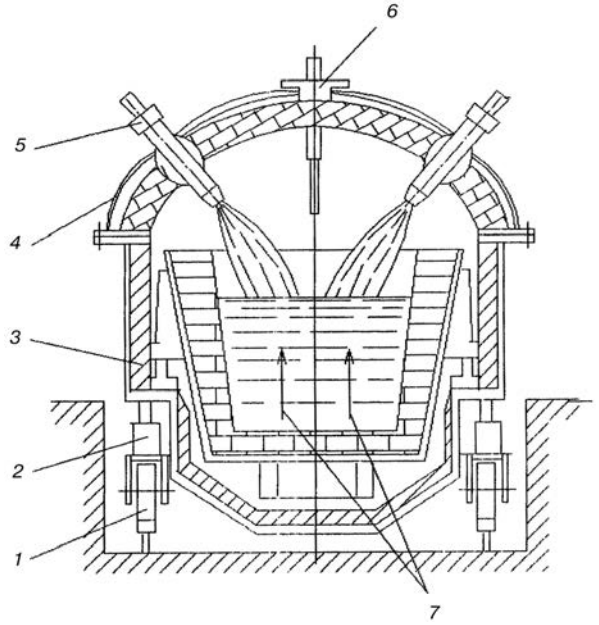

Plasma ladle-furnace: *1* — teeming ladle car; *2* — hydraulic cylinder; *3* — chamber; *4* — water-cooled cap; *5* — plasmatron; *6* — temperature probe; *7* — gas-blown melt

tions of labor. The use of PLF with all their merits allows essentially improving furnace and off-furnace metallurgical technology and producing steel, which is successfully certified according to the international standards.

The listed advantages of the use of plasma heating in metallurgy are confirmed by theoretical and practical developments of the E.O. Paton Electric Welding Institute of the NAS of Ukraine as well as by results of practical introduction of technology and equipment for plasma-arc melting, remelting and refining of metals and alloys in the water-cooled copper crucible, slag-lining and ceramic crucibles using plasmatrons of direct and alternating current of total power to 4.5 MW.

Basic operation parameters of direct and alternating current PLF (power conditions, arc current and voltage, useful efficiency, steel heating rate and others) are presented in [11–13]. Systematization of these data has allowed obtaining a universal parameter for determination of the power conditions for operation of the ladle-furnace of certain capacity, which is specific active power W_s provided by one or several DC or AC plasmatrons for steel heating with preset rate. Values of this parameter are within the range of 0.3–0.6 kW·h/(t·°C) and depend on the design of the unit, efficiency of plasmatrons, ladle temperature at the moment of metal pouring, the quality of the added alloying elements and others. Though the found values of W_s parameter vary within a wide range, the use of the parameter allows a sufficient accuracy in determination of the active power of the PLF plasmatrons at the initial stage of design.

The Paton Institute has contributed most of all into creation of the AC plasmatrons. Plasma-heating complexes (PHC) of 5–6 MW power developed at the Institute were installed into 3.5 t plasma furnace with ceramic lining («Krupp», FRG, 1986) and 100 t PLF («Nippon Steel», Japan, 1988), which were for the first time in the world put into operation. The PHC incorporates 3 plasmatrons of direct action with plasma electrodes, connected by a three-phase circuit, their power sources, equipment for control and regulation of electric and gas regimes. PHC plasmatrons ar equipped with plasma electrodes, thus ensuring their low wear degree and stable arcing within the wide range of technological regimes, in particular under excessive gas pressure in the melting cavity and under the rarefaction. Joint industrial trials of this plasma heating complex in the 100 t PLF of the «Nippon Steel» confirmed a possibility to compensate thermal losses and to heat the melt with 1 °C/min rate as specified by the Corporation. It also proved the correctness of the power calculations, engineering design and reliability of the equipment.

Peculiarities of PLF and plasma technology may be fully considered on the example of the steel LT process in the 30 t unit for complex ladle treatment of steel of the «Bummash» designed and put into operation by the Paton Institute in 1996–1998.

Under creation of AC PHC to equip the UCLTS-30 and bringing it to commercial level we employed the results of own theoretical and experimental studies as well as industrial trials at the «Nippon Steel». We also used the experience gained under creation of metallurgic AC plasmatrons with plasma electrodes and plasma-arc furnaces with water-cooled copper crucibles, slag-lining and ceramic crucibles and under making of high-quality steels and alloys in the above equipment [13].

Schematic diagram of the PLF (Figure) provides technical options for determination of temperature and chemical composition of the melt, temperature adjustment, treatment of steels with slag and their additional alloying in the inert atmosphere and that of argon-nitrogen mixtures or nitrogen. The ladle is installed in the chamber assembled on the teeming ladle car and covered with a cap. Three plasmatrons are evenly installed on the cap in a circle with slope at an angle 35–65° [14]. Air-tightness of the working space is created by compression of the chamber to the fixed cap by means of hydraulic cylinders. The PHC set includes also systems of gas, water and power supply, hydraulic unit and gas supply unit. Electric power is supplied to plasmatrons from a transformer through regulators of the arc current (controlled or non-controlled throttles). All PHC systems are controlled from the main control panel. The heating complex includes mechanisms, which allow moving plasmatrons along axis for regulating the lengths of arcs and varying their slope in the course of the operation. The PHC provides starting of plasmatrons in the arcing mode both in the middle point in plasma and in the surface of the metal or slag melt. It ensures high reliability of the start and stable arcing in space in the absence of metal or slag melt for any thickness of the slag layer on the metal surface or with solidified slag layer. Argon blowing of the melt is per-

formed through two porous plugs placed in the bottom of the ladle.

Power and technological potentialities of the process as well as reliability of the produced equipment were investigated in the course of melting in PLF. Walls and bottom of the ladle were lined with chamotte refractories and a slag zone — with periclase-carbon refractories. The chamber cap was gun-concreted with alumina-zirconium mass of thickness varying from 30 to 50 mm. Protection ceramic screen was not installed over the ladle in this series of melts. Depending on the technological requirements, duration of steel treatment varied from 30 to 80 min. Volt-ampere characteristics (VAC) of PLF are ascending, their curvature is $(0.5–0.7)\cdot10^{-2}$ V/A under operation in argon and $(0.7–1.0)\cdot10^{-2}$ V/A under operation in nitrogen. VAC of three-phase group of PLF plasmatrons when argon is used as plasma gas and arcing is in the preset regime, are well described by an empirical dependence

$$U_{a_{Ar}} = 1.1[(bI_a^m L_a) + l_e E_c + 10], \quad (1)$$

where b is the coefficient equal to 1.65–2.20; I_a is the arc current, A; m is the power index equal to 0.065–0.075; L_a is the arc length, cm; l_e is the penetration of the electrode into the nozzle, mm; E_c is the voltage gradient of the arc column part in the nozzle channel, V/mm.

When other gases or their mixtures with argon are used as plasma gases and under arcing in the atmosphere of gas mixtures the arc voltage U_a is calculated according to the formula

$$U_{a_{mix}} = U_{a_{Ar}}[10^2 (G)]^n, \quad (2)$$

where G is the volume fraction of gas in mixture with argon and n is the power index. Its values vary within 0.12–0.17 when using air or nitrogen, 0.05–0.08 when using helium and 0.32–0.35 when using hydrogen.

Rate of steel heating depends on the supplied power, consumption and composition of plasma gas, temperature condition of the ladle lining and slag regime. Under PHC power of 3.4–3.8 MW rate of steel heating was 1.0–1.5 °C/min, and increased up to 5.0–5.5 °C/min at 4.8–5.3 MW power. Analysis of the obtained results shows that under similar supplied power the steel heating rate in PLF is much higher than in ALF. Specific consumption of electric power for heating of steel, its refining and adjustment of chemical composition varies within 20–80 kW·h/t while specific active power does not exceed 0.9 kW·h/(t·°C) even if the initial temperature of ladle lining is 300–400 °C.

Plasma treatment of steel in the UCLTS provides better removal of gases, non-metallic inclusions and harmful admixtures as against electric arc heating. Quality of steels after plasma ladle treatment in argon and nitrogen or their mixture is on par with the quality of steels produced by the methods of special electrometallurgy and corresponds to the international standards.

Plasma heating complexes may be installed on other steel LT units and pony ladles of continuous casting machines, thus allowing refining and fine adjustment of the poured metal temperature. Use of plasma electrodes in PHC plasmatrons makes it possible to combine vacuum treatment and heating of steel in one unit.

Basic technological and operational indices of PLF (UCLTS-30)

Capacity of the ladle-furnace, t	25–30
Gas consumption under metal blowing with argon, nitrogen or their mixtures, m^3/h	11–40
Power of PHC, kW	2200–5500
Operational parameters of PHC plasmatron:	
arc current, kA	5.0–9.0
arc voltage, V	110–270
consumption of plasma gas (argon, nitrogen or their mixtures), nm^3/h	10–25
arc length, mm	250–500
Heating metal efficiency, %	50–60
Electrode material	graphite or tungsten
Steel heating rate, °C/min	1.5–5.3
Specific consumption of electric power, kW·h/t	20–80
Specific active power, kW·h/(t·°C)	0.3–0.9
Thickness of the applied slag layer, mm	up to 200
Refining from non-metallic inclusions	decrease of index from 3rd to 2nd
Minimal sulfur content in metal, %	0.003
Approximate area occupied by the equipment, m^2	600

New developments of plasma heat sources by the Paton Institute are of special importance for exposing potentialities of steel LT units and technologies. Increase of the PLF capacity (more than 100 t) and putting it into commercial operation were hindered until recently due to the lack of reliable and high-power plasmatrons with long operational life. Developed plasma-arc heaters (DPAH) with cheep graphite or self-sintering hollow electrodes [15, 16] created by the Paton Institute and tested at the Zestafon Ferroalloy Plant (Georgia) in pilot production and production conditions are distinguished for unlimited operational life, do not incorporate complicated water-cooled parts and permit developing practically unlimited power. DC- or AC-supplied DPAH (in some cases a combined power supply is possible) preserve all PHC advantages and do not require the use of bottom electrode. Power of one DPAH is enough to operate PLF with capacity up to 300 t, steel heating rate up to 5 °C/min and thickness of a slag layer on the melt surface from 50 to 500 mm. Peculiarity of DPAH lies in the fact that just as PHC it permits concentrating the focus of the steel heating power in the center of the ladle (providing high resistance of the slag zone lining) and achieving uniform heating of the melted steel pool with axial location of circles of equipotential curves of the metal temperature. It is worth noting that DPAH allows adding alloying elements, fine and powder charge and adjusting the composition of slag

or its replacement without switching off the heater. It also permits a wide-range regulation of power and steel heating rate. Considering the above it is recommended to use DPAH as heat sources in PLF with capacity of 100 t and higher.

CONCLUSIONS

1. The use of ALF or PLF together with ASMF allows decreasing electric power consumption 1.4–1.8 times, increasing ASMF efficiency by 30–80 % and lining resistance by more than 30 % as well as expanding the range of steel grades.

2. Steel LT in ALF and PLF promotes increased assimilation of alloying elements (by 10–30 %) and melt homogeneity in temperature and chemical composition with little variations of the latter.

3. Steel LT provides record-low gas content, increased purity as to non-metallic inclusions and deep desulphuration. Distribution coefficient of sulfur between slag and metal achieves 130 in ALF and 700 in PLF.

4. Accuracy of the temperature adjustment in the end of the steel LT process is +4–5 °C. Addition of 1 % of alloying elements decreases steel temperature in ALF by about 25 °C (not more than 8 % of alloying elements are added to the ladle).

5. Creation of PLF is one of the links in energy-saving high-technology systems of the modern steel-making industry.

6. Saving of electric power under steel melting according to the ASMF–PLF scheme is 50–100 kW·h/t as against steel melting only in ASMF.

7. Economic efficiency of using the steel LT process is $30–55 per 1 t of ready product.

8. A spheres of PLF application are resource- and energy-saving clean technological processes for production of high-quality steels and alloys.

9. Plasma steel LT was put into commercial operation in 100 t PLF at the «Nippon Steel» (Japan) in 1988 and in 30 t PLF at the «Bummash» (Russia) in 1996.

10. Now a new generation of DC and AC PHC of large capacity designed for using in plasma technological processes of ferroalloy production is under development and successful industrial trials.

1. Altgauzen, A.P. (1987) *Use of electric heating and increase of its efficiency*. Moscow: Energoatomizdat.
2. Samokhvalov, G.V., Chernysh, G.I. (1984) *Electric furnaces in ferrous metallurgy*. Moscow: Metallurgia.
3. Amblard, M., Legrand, H. (1989) *Rev. Met. (FR)*, **4**, 317–324.
4. Knyuppel, G. (1984) *Deoxidization and vacuum treatment of steel*. Moscow: Metallurgia.
5. Nosova, T.V. (1979) Steel refining in units of the ladle-furnace type. Series 6, Steel-making production. *Reviews*, Issue 3.
6. Yuzov, O.V., Chaplygin, V.A., Shleev, A.G. *et al*. (1982) Economical efficiency of the alloyed steel production in L.D. Plants using the ladle-furnace unit. In: *Management economy in metallurgy*. Moscow: Metallurgia.
7. Neuscheutz, D., Schubert, K.-H., Bebber, H.J. (1991) Metallurgical results from a 30 t AC plasma ladle-furnace. *Steel Research*, **9**, 390–394.
8. Eisenkolb, J., Linder, E., Menzel, J. *et al*. (1985) Wirtschaftlicher Einsatz von Legierungen und Zuschlagstoffen bei Anwendung pfannenmetallurgischer Verfahren. In: *Firmenschrift des VES ESW*, Freital, Sept.
9. Khauman, V., Kokh, F., Reknagel, V. (1984) Use of ladle metallurgy to produce steel for HP welded pipelines. *Chern. Metally*, **26**, 18–22.
10. Nikulin, A.A. (1988) Design and technological peculiarities of powerful electroslag furnaces abroad. Series 6, Steel-making production. *Reviews*, Issue 3.
11. Zhdanovsky, A.A., Zabarilo, O.S., Melnik, G.A. *et al*. (1994) Analysis of basic parameters of the power regime in industrial PLF. *Problemy Spets. Elektrometallurgii*, **1/2**, 53–60.
12. Bebber, H.J., Espendiller, V. (1991) Plasma torch cleans up the ladle furtance. *Steel Times*, **12**, 665–666.
13. Melnik, G.A., Zabarilo, O.S., Zhdanovsky, A.A. *et al*. (1991) Prospects in the use of plasma heating sources in units of the ladle treatment of steel. *Problemy Spets. Elektrometallurgii*, **2**, 60–65; **3**, 86–92.
14. Zhadkevich, M.L., Melnik, G.A., Zabarilo, O.S. *et al*. (1998) Creation and commercial launching of PLF. *Ibid*., **1**, 42–47.
15. Melnik, G.A., Zabarilo, O.S., Lezhava, K.I. *et al*. (2000) Plasma heating in ferroalloy production. *Ibid*., **2**, 45–57.
16. Lezhava, K.I., Aslanikashvili, V.V., Akhobadze, V.T. *et al*. (2000) Study of main technical and economic indices in production of manganese alloys using plasma heating. *Ibid*., **4**, 38–44.

MODEL OF INDUCTION HEATING FOR PLASMA-INDUCTION GROWING OF SINGLE-CRYSTALS

V.A. SHAPOVALOV*

The quality of metallic single-crystals is largely dependent on the temperature field, formed in plasma-induction heating that accompanies the processes of single-crystal growth. Considered in this connection is the problem of mathematical modelling of a single-crystal induction heating, to achieve optimal control of its temperature field formation. The problem of induction heating of a single-crystal is defined as a non-linear boundary problem of mathematical physics. Numerical-analytical solution of this problem has been derived and appropriate computer modelling has been performed.

Key words: *mathematical model, induction heating, metallic single-crystals, temperature field*

Problem definition. Structural perfection of single-crystals is largely responsible for their properties. Metallic single-crystals, unlike the semiconductor ones, have a considerable amount of structural defects (point, linear and volume). The number of defects, in the opinion of the authors of [1], depends on temperature stresses, arising when single-crystals are grown. In this connection, investigation of the thermal conditions of single-crystals growing is important for studying the laws of the dislocation structure formation.

With plasma-induction method of growing [2], the thermal field in the growing single-crystal forms under the influence of two heating sources, namely the induction and plasma-arc. Induction heating is manifested as resistance heating of the single-crystal body by high-frequency currents, flowing in a thin surface layer, and actually provides the stability of the single-crystal thermal field in time. Plasma-arc heating provides melting of the consumable material and single-crystal formation or growth. A zone, through which the heat comes from the plasma-arc heating source to the crystal, is the metal pool surface. In the case of formation of a profiled single-crystal, the plasma heating source moves over the surface being build-up, causing a periodical change of temperature in each point of the crystal. For a fixed point in (or on) the single-crystal body the process is of an oscillatory nature with a decreasing amplitude. Periodical temperature fluctuations, in view of the arising stresses, should influence the forming structure of the single-crystal. The influence of temperature variation on the structure can be different and depends, chiefly, on the total temperature of single-crystal heating by high-frequency currents.

The nature of temperature distribution in the crystal at induction heating depends not only on the inductor parameters, but also on the single-crystal dimensions. Temperature fields in induction heating can be studied by various methods: direct measurements, this being extremely complicated and expensive, or using mathematical modelling of thermal processes. In this paper a mathematical modelling method was selected for evaluation of temperature fields in the crystal at induction heating. This method allows studying the nature of temperature distribution, its dependence on inductor configuration and heating power. Determination of the actual temperature value, however, is still problematic, in connection with the assumed inaccuracy of description of the heat exchange conditions on the single-crystal boundary, when taking certain assumptions for calculation, that allow defining a linearized mathematical problem.

Development of a mathematical model of single-crystal induction heating. Let us assume, that the power of the electromagnetic flow is proportional to the square of the magnetic field intensity. At the change of current in the inductor, the magnetic field intensity changes simultaneously over the entire single-crystal surface. The induced current density changes in all the points of the heated ingot surface, accordingly, i.e. the density of the heat sources changes simultaneously. Then, the function of the heat source density can be presented as [3]

$$w\ (x,\ y,\ z,\ t) = q_0(t) w_0\ (x,\ y,\ z), \qquad (1)$$

where $q_0(t)$ is the specific surface power; $w_0(x, y, z)$ is the heat source density.

Let us find the dependence of the heat source density on the magnetic field intensity. Let us consider a plane electromagnetic wave, polarised in plane $z0y$, this being justified, as the geometrical dimensions of the heated single-crystal are such, that its length d is greater, than width b by almost an order of magnitude, while the inductor voltage changes sinusoidally [4].

Taking into account the above assumptions and on condition of a constant magnetic μ and dielectric ε permeability, with a little manipulation, allowing for equations of the magnetic field intensity and cur-

*The E.O. Paton Electric Welding Institute, Kyiv, Ukraine.

rent density, the specific power on the conducting medium surface can be given by the following expression:

$$p_0 = J_{me}^2 \rho\Delta/4 = \frac{10^{-4}}{4\pi}\sqrt{10^{-1} f_k \rho'} H_{me}^2, \quad (2)$$

where J_{me} is the current density; H_{me} is the magnetic field intensity; $\rho = \rho' \cdot 10^{-3}$ is the specific ohmic resistance; ρ' is its scaled value; f_k is the linear frequency; Δ is the depth of current penetration, that is defined as [3]

$$\Delta = \frac{1}{2\pi}\sqrt{\frac{\rho}{f_k \cdot 10^{-2}\mu}} = \frac{1}{20\pi}\sqrt{\frac{\rho'}{10 f_k}}.$$

Specific electrical resistance varies with temperature by the following law [5]:

$$\rho_T = \rho_{20}\,[1 + \alpha\,(T - 20\ ^\circ\mathrm{C})] = \rho_{20}\,[1 + \alpha\,(T + 253\ \mathrm{K})], \quad (3)$$

where $\alpha = \Delta\rho/(\rho\Delta T)$ is the resistance temperature coefficient. For tungsten, for instance, at T = 20 °C $\rho_{20} = 0.55 \cdot 10^{-3}$ Ohm·m and $\alpha_{20} = 0.41 \cdot 10^{-2}$ K^{-1}.

Depending on the selected linear frequency of the generator, heating of the single-crystal can be both surface heating, with different depth of current penetration, and through-thickness heating. In the real process the frequency is selected from the condition of a moderate force impact of the electromagnetic field on the molten zone (pool).

Thus, we can write, that

$$w_0 = p_0 \exp\,[(b/2 - x)/\Delta]. \quad (4)$$

As regards determination of the dependence of the specific electrical resistance on the single-crystal heating temperature, considering the explicit (exponential) dependence of ρ on T (3), the exponential dependence can be either approximated by a fractional rational function, or ρ can be considered to be constant in a certain temperature range, and then its value can be recalculated by equation (3).

In view of the above, we come to the next boundary problem, describing the process of induction heating of single-crystals of a rectangular cross-section.

Calculation of the single-crystal temperature field at induction heating. Let us find the solution of the boundary problem, describing the temperature field of a single-crystal of a rectangular cross-section of height h under the impact of a heat source of density w [6]:

$$\rho c_{v_0}\frac{\partial T}{\partial t} = \lambda_0\nabla^2 T + \frac{\partial\lambda}{\partial x}\frac{\partial T}{\partial x} + \frac{\partial\lambda}{\partial y}\frac{\partial T}{\partial y} + \frac{\partial\lambda}{\partial z}\frac{\partial T}{\partial z} + w = \lambda_0\nabla^2 T + w + N(T) \quad (5)$$

in region

$$D = \{x \in [-b/2;\ b/2],\ y \in [-d/2;\ d/2],\ z \in [0, h],\ t > 0\},$$

where $\lambda = \lambda(T)$ is the heat conductivity factor; $c_v = c_v(T)$ is the specific heat at a constant volume; ∇ is the Laplace operator; $N(T)$ is the non-linear part of the equation.

Boundary conditions are:

$$\frac{\partial T}{\partial x}\Big|_{x=0} = 0,\quad -\lambda_0 = \frac{\partial T}{\partial x}\Big|_{x=b/2} = \Delta p_x(T)\,|_{x=b/2}; \quad (6)$$

$$\frac{\partial T}{\partial y}\Big|_{y=0} = 0,\quad -\lambda_0 = \frac{\partial T}{\partial y}\Big|_{y=d/2} = \Delta p_y(T)\,|_{y=d/2}; \quad (7)$$

$$-\lambda\frac{\partial T}{\partial z}\Big|_{z=0} = \Delta p_{z_0}(T)\,|_{z=0}; \quad (8)$$

$$-\lambda\frac{\partial T}{\partial z}\Big|_{z=h} = \Delta p_{z_h}(T)\,|_{z=h}. \quad (9)$$

Initial conditions are $T(x, y, z, 0) = T(x, y, z)$.

Specific power of heat losses is given by the following equation:

$$\Delta p_k(T) = \varepsilon\sigma\,(T^4 - T_{c_k}^4) + \alpha_k\,(T - T_{c_k}) = \alpha_k T - D_{g_k} + \varepsilon\sigma T^4, \quad (10)$$

where $\alpha_1 = \alpha_x$, $\alpha_2 = \alpha_y$, $\alpha_3 = \alpha_{z_0}$ and $\alpha_4 = \alpha_{z_h}$ are the coefficients of heat exchange with the environment; ε is the emissivity; σ is Stefan–Boltzmann constant. Coefficient is given by

$$D_{g_k} = T_c\,(\alpha_k + \varepsilon\sigma T_{c_k}^3). \quad (11)$$

It is assumed, that in the latter expression the coefficients of the single-crystal heat exchange with the environment are constant, but their numerical values should be determined during modelling. This actually means, that when modelling the direct heat transfer problem, an inverse problem also has to be solved, namely determination of the coefficients of heat exchange between the single-crystal and the environment.

Dependence of the coefficients of heat conductivity and heat capacity of the material on temperature can be written as follows:

$$\lambda(T) = \lambda_0 + \lambda_1 T + \lambda_2 T^2 + \lambda_3 T^3; \quad (12)$$

$$c_v(T) = c_{v0} + c_{v1} T + c_{v2} T^2. \quad (13)$$

The magnitudes of these coefficients are determined from experimental data. The following dependencies were derived for tungsten:

$$\lambda(T) = 196.4 - 0.1357T + 0.463\,10^{-4}T^2 + 0.362 \cdot 10^{-9}T^3; \quad (14)$$

$$c_v(T) = 130 + 0.0136T + 0.404 \cdot 10^{-5}T^2. \quad (15)$$

Taking these dependencies into account, the non-linear part of the boundary problem (5)–(9) becomes

$$N(T) = \frac{\partial \lambda}{\partial x}\frac{\partial T}{\partial x} + \frac{\partial \lambda}{\partial y}\frac{\partial T}{\partial y} + \frac{\partial \lambda}{\partial z}\frac{\partial T}{\partial z} + \\ + \rho T(c_{v1} + c_{v2}T)\frac{\partial T}{\partial t}. \quad (16)$$

Solution of the defined boundary problem will be sought, using the iteration method. Let us first find the solution of the linearized problem

$$\rho c_{v0}\frac{\partial T^{(0)}}{\partial t} = \lambda_0\left(\frac{\partial^2 T^{(0)}}{\partial x^2} + \frac{\partial^2 T^{(0)}}{\partial y^2} + \frac{\partial^2 T^{(0)}}{\partial z^2}\right) + w. \quad (17)$$

Boundary conditions are:

$$\frac{\partial T^{(0)}}{\partial x}\Big|_{x=0} = 0,\ \frac{\partial T^{(0)}}{\partial x} + \frac{\alpha_x}{\lambda_0}T^{(0)}\Big|_{x=b/2} = \\ = D_x = D_g/\lambda_0; \quad (18)$$

$$\frac{\partial T^{(0)}}{\partial y}\Big|_{y=0} = 0,\ \frac{\partial T^{(0)}}{\partial y} + \frac{\alpha_x}{\lambda_0}T^{(0)}\Big|_{y=d/2} = \\ = D_y = D_g/\lambda_0; \quad (19)$$

$$\frac{\partial T^{(0)}}{\partial z} - \frac{\alpha_{z_0}}{\lambda_0}T^{(0)}\Big|_{z=0} = D_{z_0}/\lambda_0, \\ \frac{\partial T^{(0)}}{\partial z} + \frac{\alpha_{z_h}}{\lambda_0}T^{(0)}\Big|_{z=h} = D_{z_h}/\lambda_0. \quad (20)$$

Initial conditions are $T(x, y, z, 0) = T_0(x, y, z)$.

Let us apply to the boundary problem integral transformations by space variables x, y, z [7]. Eigen functions $Z_n(z_n z)$, $Y_m(\upsilon_m y)$, $X_k(\mu_k x)$ of the problem, corresponding to eigen values z_n, υ_m, μ_k, were obtained in the following form:

$$Z_n(z_n z) = \frac{1}{\| Z_n(z) \|}\left[\frac{\beta_{z0}}{z_n}\sin(z_n z) + \cos(z_n z)\right]; \quad (21)$$

$$Y_m(\upsilon_m y) = \frac{1}{\| Y_m(y) \|}\cos(\upsilon_m y), \\ X_k(\mu_k x) = \frac{1}{\| X_k(x) \|}\cos(\mu_k x). \quad (22)$$

Let us find eigen values z_n, υ_m, μ_k of the problem as a solution of the following equations with relation to variables s and r:

$$s\sin s - d/2\beta_y\cos s = 0, \\ r\sin r - b/2\beta_x\cos r = 0, \quad (23)$$

where $\beta = \{\beta_x, \beta_y, \beta_{z_0}, \beta_{z_h}\}$; $\beta_{x_i} = \alpha_{x_i}/\lambda_0$.

$$(\beta_{z_0} + \beta_{z_h})\upsilon\cos(\upsilon h) + \\ + (\beta_{z_0}\beta_{z_h} - \upsilon^2)\sin(\upsilon h) = 0;\ z_n = \upsilon_n. \quad (24)$$

Solving in the time domain the Cauchy problem, derived through these transformations, we find the single-crystal temperature field in the linear approximation:

$$T^{(0)} = \sum_{nmk} Z_n(z)Y_m(y)X_k(x) \times \\ \times \left\{TI_{nmk}\, e^{-\delta_{nmk}} + \overline{Q}^I_{nmk}\,(1 - e^{-\delta_{nmk}})\right\} + \\ + \left[Y_m(y)X_k(x)R^z_{nmk} + Z_n(z)[X_k(x)R^y_{nmk} + Y_m(y)R^x_{nmk}]\right] \times \\ \times (1 - e^{-\delta_{nmk}}), \quad (25)$$

where

$$R^z_{nmk} = \frac{Rz_n sy_m sx_k}{\gamma^2_{nmk}};\ R^y_{nmk} = \frac{Ry_m sz_n sx_k}{\gamma^2_{nmk}}; \\ R^x_{nmk} = \frac{Rx_k sz_n sy_m}{\gamma^2_{nmk}}; \quad (26)$$

$$\gamma^2_{nmk} = \mu^2_k + \upsilon^2_m + z^2_n;\ \delta_{nmk} = \gamma^2_{nmk}\frac{\rho c_v}{\lambda}; \quad (27)$$

$$\overline{Q}^I_{nmk} = \int_0^h Z_n(z)q^I(z)dz\int_0^{d/2} Y_m(y)e^{(y-d/2)/\Delta}dy \times \\ \times \int_0^{b/2} X_k(x)e^{(x-b/2)/\Delta}dx = \frac{zq_n yq_m xq_k}{\gamma^2_{nmk}}. \quad (28)$$

Values R_{z_n}, R_{y_m} and R_{x_k} are determined as a result of application of integral transformations to the boundary problem. Coefficients of sz_n form are integrals of $sz_n = \int_0^h Z_n(z)dz$ form.

The non-linear part of equation (5), allowing for boundary conditions (6)–(8), as a result of integral transformations, becomes

$$N_1(T)_{nmk} = \int_0^h\int_0^{d/2}\int_0^{b/2} Z_n(z)Y_m(y)X_k(x) \times \\ \times N[T^{(0)}(x, y, z, t)] + NR[T^{(0)}(x, y, z, t)]\,|_B, \quad (29)$$

where B is the boundary of domain D.

In order to determine the explicit form of this function, it is necessary to substitute into the non-linear part of equation (5) the solution, derived in a linear approximation, integrate it with respect to the respective space variables, as well as perform the required direct and inverse Laplace transformations (L_t^{-1}).

Let us write the general solution of the boundary problem (5)–(9), describing the temperature field distribution in the single-crystal, in the following form:

$$T^{(m)}(x, y, z, t) = T^{(0)}(x, y, z, t) + \frac{1}{\rho c_{v0}} \times \\ \times \sum_{nlk} Z_n(z)Y_l(y)X_k(x)L_t^{-1}\left\{\frac{1}{p + \delta_{nlk}}L_t[N_1(T^{(m-1)})]\right\}. \quad (30)$$

The results of modelling the derived problem solution are given below in the graphical form. Let us consider the extreme case, when the single-crystal has the greatest height. The schematics of three different

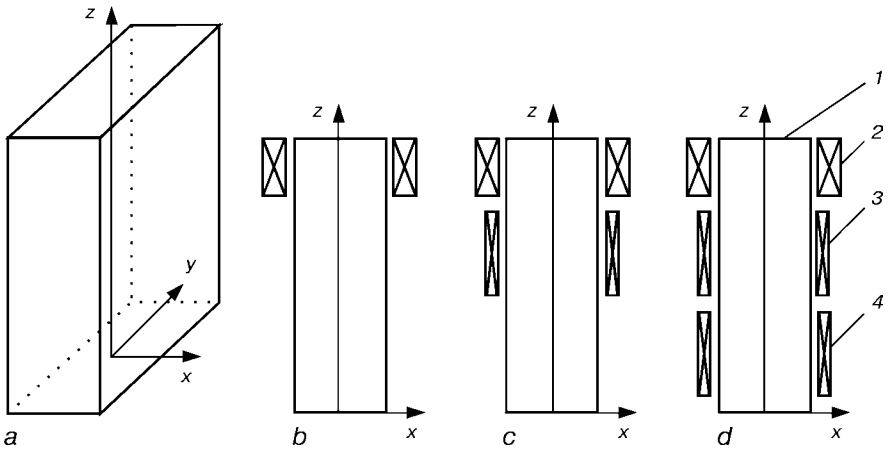

Figure 1. Schematic of single-crystals heating: *a* — relative position of the axes of co-ordinates and the single-crystal; *b, c, d* — heating by a single-, two- and three-section inductor, respectively; *1* — single-crystal; *2, 3, 4* — inductor sections

heating variants are given in Figure 1, and the temperature fields of the single-crystal — in Figure 2.

The form of temperature fields indicates, that the highest thermal stresses are applied to the single-crystal in heating by a schematic, shown in Figure 1, *a*, and the minimal ones — in heating with three sections (Figure 1, *c*). On the other hand, the crystal surface temperature in $x0y$ plane is non-uniform, i.e. this plane is not part of the isothermal surface. Applying various heating conditions to the mathematical model allows selection of such an inductor configuration that enables the heating process to be conducted with minimal temperature gradients.

CONCLUSIONS

1. The degree of the single-crystal structural perfection is greatly influenced by thermal stresses, not only during the single-crystal growth, but also during its cooling.

2. Mathematical definition of the problem of single-crystal induction heating has been presented as a non-linear boundary problem of heat transfer, that

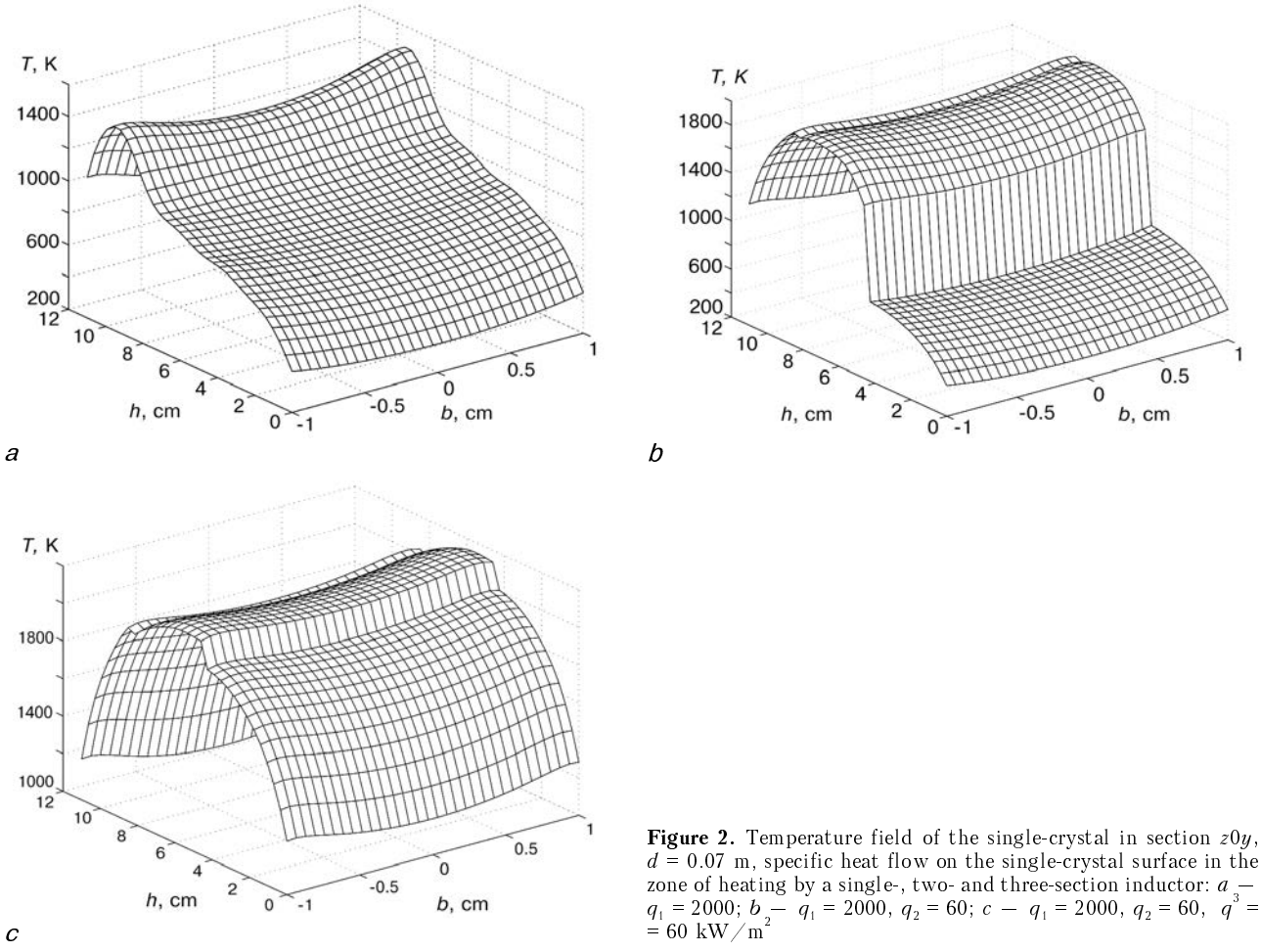

Figure 2. Temperature field of the single-crystal in section $z0y$, d = 0.07 m, specific heat flow on the single-crystal surface in the zone of heating by a single-, two- and three-section inductor: *a* — $q_1 = 2000$; *b* — $q_1 = 2000$, $q_2 = 60$; *c* — $q_1 = 2000$, $q_2 = 60$, $q^3 = 60$ kW/m^2

allows for the non-linear properties of thermophysical parameters of the material and the conditions of heat exchange on the crystal surface.

3. Numerical-analytical solution of the boundary problem has been derived, allowing analysis of the single-crystal temperature field, formed under the influence of induction heating and identification of the conditions of heat exchange with the environment.

1. Kervalishvili, P.D., Shchelkin, Yu.F. (1982) Thermal conditions as a factor, responsible for producing perfect single-crystals. *Fizika i Khimiya Obrab. Materialov*, **5**, 70–80.
2. Latash, Yu.V., Shapovalov, V.A., Kovalenko, A.A. *et al.* (1995) Producing large profiled single-crystals of refractory metals. *Vysokochistye Veshchestva*, **1**, 48–51.
3. Nemkov, V.S., Polevodov, B.S. (1980) *Mathematical modelling of high-frequency heating devices in a computer*. Leningrad: Mashinostroyeniye.
4. Slukhotsky, A.E., Nemkov, V.S., Pavlov, N.A. *et al.* (1981) *Induction heating units*. Leningrad: Energoizdat.
5. Kukhling, Kh. (1982) *Reference book on physics*. Moscow: Mir.
6. Pavlov, N.A. (1978) *Engineering heat calculations of induction heating*. Moscow: Energia.
7. Koshlyakov, N.S., Gliner, E.B., Smirnov, M.M. (1970) *Equations in partial derivatives of mathematical physics*. Moscow: Vysshaya Shkola.

RECYCLING HIGH-TEMPERATURE ALLOY WASTE BY VACUUM REMELTING METHODS

Yu.F. ANIKIN*, I.I. MAKSYUTA*, Yu.G. DOBKINA* and M.A. VERBILO*

Combined remelting of high-temperature alloy wastes, used in production of gas turbine engine blades, has been developed. Thermophysical conditions of melt solidification after remelting are established, that ensure formation of an equiaxial fine-grained structure in the charge material, thus promoting the increase of high-temperature ductility of the alloys with preservation of a high level of strength.

Key words: *high-temperature nickel alloys, vacuum-induction remelting, electron beam remelting, macro- and microstructure*

Recycling of metallurgical production wastes of such deficit materials, as high-temperature resistant nickel alloys, is becoming a strategic goal under the conditions of Ukraine, both for materials science and for special metallurgy. Therefore, Physico-Technical Institute of Metals and Alloys of the NAS of Ukraine developed the technology of recycling conditioned wastes (gates) of high-temperature ChS70-VI and ChS88U-VI alloys of Ni–Co–Mo–W system, applied in production of GTE cast blades.

A feature of the proposed processing modes for recycling high-temperature alloy wastes, is the fact that achievement of the optimal result is only possible at a multiple refining process. The first stage consists in melting for compacting and initial refining of the melt with production of a cylindrical ingot of 70 mm diameter, and in the second stage the refining remelting and production of cast items are performed after correction of the billet composition. The rationality of such a two-stage process is attributable to the impossibility of using the wastes that accumulate in the enterprises-manufacturers of gas-turbine engines, as charge materials without their preliminary refining treatment and composition correction.

This paper presents three sequences of the technological process, each of which uses either just vacuum-induction remelting (VIR) [1], or combinations of the induction and electron beam remelting (EBR): VIR → VIR; VIR → (VIR + EBR); VIR → (VIR + + EBR) → (VIR + EBR) [2–4].

The thermal impact on the melt during combined melting can be regarded as thermal-time treatment at vacuum-induction melting [5]. In the first case, however, it takes place in the local volume of the crucible at a moderate integral temperature of the melt that does not exceed 1600 °C. It results in a decrease of the lining interaction with the melt and considerable reduction of its contamination with non-metallic inclusions, this being confirmed by metallographic investigations.

Total duration of vacuum-arc remelting is equal to 28 min, and the specific power consumption is 2.0 kW·h/kg; duration of one-cycle combined remelting (VIR → (VIR + EBR) is 27 min, and specific power consumption is 2.5 kW·h/kg; that of combined two-cycle remelting VIR → (VIR + EBR) → → (VIR + EBR) is 26 min, and specific power consumption is 2.1 kW·h/kg.

As the power consumption and process duration are almost comparable, the influence of each of the technological remelting processes on the change of composition, degree of refining to remove gases and non-metallic inclusions, structural features and mechanical properties of the alloys, was studied in this work.

In evaluation of the composition of the alloys before and after remelting, attention should be given to the fact, that in the majority of cases their composition meets the specification requirements, the content of non-ferrous metal impurities and gases also being within the ranges, envisaged by the specification. Check analysis indicated the following content of impurity elements in the alloys, %: B ~ 0.001; Mg ~ 0.01; Sn < 0.0005; Sb < 0.001; Bi < 0.005; In < 0.001; Cb < 0.00005; O_2 < 0.0035; H_2 < 0.0003. Thus, the billets produced by waste remelting, as a rule, can be used for further processing without any essential correction of the composition.

Microstructure of 70 mm diameter ingots was studied on longitudinal and transverse sections [6]. In the

*Physico-Technical Institute of Metals and Alloys, Kyiv, Ukraine.

Table 1. Characteristics of structural components of alloys ChS88U-VI and ChS70-VI

Kind of remelting	Average amount of non-metallic inclusions per 1 mm^2, pcs		Average size of non-metallic inclusions, μm	Average size of carbide inclusions, μm	Average size of eutectic precipitates $a \times b$, μm	Average size of γ-phase, μm	Average quantity of γ-phase per 1 mm^2
	Casting edge	Casting middle					
				ChS88U-VI			
VIR→VIR	50	38	16	10–14	70×36	0.23–0.31	563
VIR→(VIR + EBR)	23	16	13	9–13	40×30	0.25–0.32	578
VIR→(VIR + EBR)→ →(VIR + EBR)	8	5	8	5–8	24×20	0.21–0.30	591
				ChS70-VI			
VIR→VIR	50	35	7–9	10–15	62.5×37.5	0.1–0.4	572
VIR→(VIR + EBR)	32	20	6–7	8–12	42.5×25.0	0.1–0.4	585
VIR→(VIR + EBR)→ →(VIR + EBR)	8	5	4–5	7–5	25.0×12.5	0.1–0.4	594

cast metal of all the remelting series two structural zones are observed in the direction, normal to the evaporation plane, namely a subsurface zone of long-axis columnar crystals, that is replaced by a zone of grains more uniform in size, when moving closer to the ingot center. Double combined remelting results in a maximal refinement of the dendrites. In all the remelting modes the ingot density is satisfactory, and no casting defects in the form of scattered shrinkage cavities or liquation striation are found. This is indicative of the composition uniformity along the entire length of the ingot that is confirmed by the data of spectral analysis of the specimens from the upper, medium and bottom parts of the billet.

Studying the content of non-metallic inclusions in recycled high-temperature alloys reveals an abrupt reduction of their amount after VIR → (VIR + + EBR), as well as a reduction of their size and a more favourable distribution through the cast specimen volume. Calculation of the quantity of non-metallic inclusions of various types (nitrides, carbonitrides) and analysis of their distribution were conducted at 400 magnification on transverse microsections in 25 fields for two specimens from each melt (without etching). The amount of phases was calculated for three zones: subsurface zone; zone at 1/2 radii distance; axial (central) zone. The data derived for each zone, were averaged. It is proven that a higher concentration of non-metallic inclusions in the subsurface zone is characteristic of all the melts. This is indicative of washing out of this type of inclusions, possibly, from the mould material at dynamic impact on the mould ceramic shell during the melt pouring. It should be noted, that the number of non-metallic inclusions and their size are reduced already after remelting by the sequence of VIR → (VIR + EBR). Considering, that 100 % is the total amount of non-metallic inclusions, fine inclusions make up ~ 50 %, medium-sized ~ 25 % and large ones ~ 25 % for specimens after all kinds of remelting (Table 1).

Ingot microstructure was studied on longitudinal and transverse sections that were selected from the upper, middle and bottom parts of the billets. In specimens of all the kinds of remelting the interdendritic areas are fringed with precipitates of round carbide phases of $M_{23}C_6$ type, and isolated precipitates of fine carbides of the same type and disperse precipitates of the type of Ti(CN) carbonitrides are observed in the dendrite axes. Finely-dispersed isolated precipitates of high-temperature carbide phases are represented through the grain bulk of MC type carbides (Te, Cr, Mo, W).

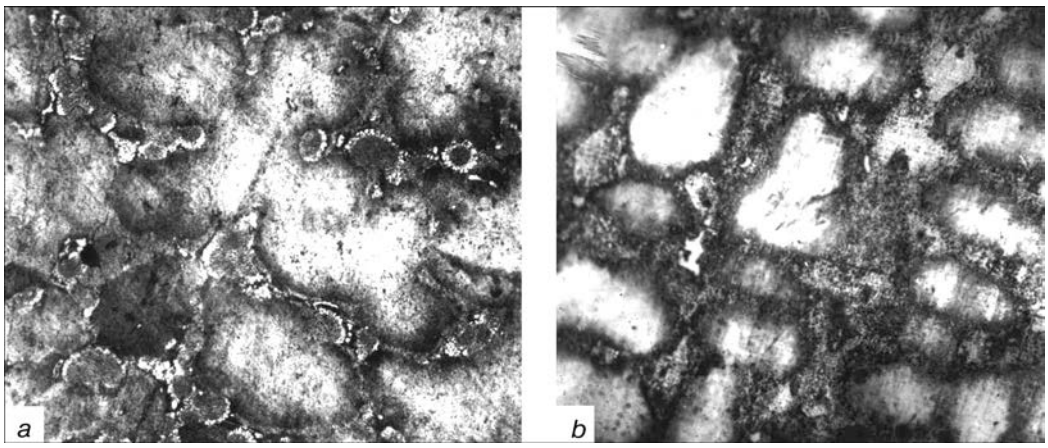

Microstructure of ChS88U-VI alloy after various kinds of remelting: *a* — VIR → VIR; *b* — VIR → (VIR + EBR) → (VIR + EBR) (×200)

Table 2. Mechanical properties of alloys ChS88U-VI and ChS70-VI after remelting of 100 % of the wastes

Kind of remelting	Short-time strength			Long-time strength		
	σ_t, MPa	δ, %	ψ, %	τ, h	δ, %	ψ, %
			ChS88U-VI			
VIR→VIR	961	5.8	6.2	105	8.2	15.6
VIR→(VIR + EBR)	914	4.8	5.2	151	8.2	19.7
VIR→(VIR + EBR)→ →(VIR + EBR)	895	4.0	7.7	144	8.3	19.7
TU 1-809-1040–96	≥ 882	≥ 4.0	≥ 5.0	У 100	≥ 8.0	≥ 10.0
			ChS70-VI			
VIR→VIR	964	6.4	22.5	103	9.0	13.5
VIR→(VIR + EBR)	979	5.2	21.3	124	8.3	12.0
VIR→(VIR + EBR)→ →(VIR + EBR)	871	7.2	18.4	328	10.0	14.0
TU 1-809-1040–96	≥ 833	≥ 3.0	≥ 4.0	≥ 100	≥ 8.0	≥ 10.0

Note. Heat treatment mode is homogenizing annealing: heating up to 1170 °C (ChS88U-VI) and 1160 °C (ChS70-VI), soaking for 3 h, cooling in air; ageing: heating up to 1050 °C, soaking for 4 h, cooling in air; heating up to 850 °C, soaking for 16 h, cooling in air.

Analysis of alloy microstructure after double remelting and especially after multi-cycle treatment reveals the tendency for improvement of morphological characteristics of the main structural elements, depending on the number of high-temperature treatment cycles. The size of carbide inclusions is reduced with the increase of the number of treatment cycles. The studied specimens, both in the cast condition and after heat-treatment, demonstrate a considerable thinning of the grain boundaries, absence of massive carbide groupings or eutectic clusters in the form of round multi-tier «petals» (see the Figure). Intergranular carbide frame is formed of disperse carbide precipitates.

Uniformity of medium-sized grains, spheroidization and reduction of the carbide precipitate dimensions, both in the middle of the grain and along its boundaries, reduction of the number of nitride and carbonitride non-metallic inclusions, almost complete absence of acute-angled phases of $M_{23}C_6$ and MC type — all these are favourable structural changes (Table 1). They are attributable, possibly, to further homogenizing of the melt and a higher degree of its refining under the impact of the electron beam and influence the increase of long-time strength and ductility of the alloys. Mechanical testing was conducted according to the existing standards for these alloys. Ductile properties were determined at the temperature of 600 °C, strength properties — at the load of 245 MPa and temperature of 900 °C (Table 2).

After all the remelting cycles the alloys did not manifest any morphological changes of γ′-phase. From remelting to remelting it has a cupola-like shape and is uniformly distributed over the section area. Distribution density remains unchanged, the phase volume fraction being equal to 43–50 %, this being the optimal value for this alloying complex.

Favourable structural transformations, found in the alloys after multiple remelting cycles, are, possibly, attributable to lower values of liquation coefficients of the alloying elements, i.e. degree of chemical inhomogeneity of the melt during high-temperature homogenizing under the influence of electromagnetic stirring and treatment by the electron beam.

Thus, the proposed improved technology of recycling the conditioned wastes of high-temperature nickel alloys allowed, in the case of application of multi-cycle vacuum remelting, production of cast recycled billets with the grade composition, structure and level of mechanical properties, complying with TU specification requirements.

1. Sims, Ch., Khagel, V. (1976) *High-temperature alloys*. Moscow: Metallurgia.
2. Ladokhin, S.V., Kornyushin, Yu.V. (1988) *Electron beam skull melting of metals and alloys*. Kyiv: Naukova Dumka.
3. Movchan, B.A., Tikhonovsky, A.L., Kurapov, Yu.A. (1973) *Electron beam melting and refining of metals and alloys*. Kyiv: Naukova Dumka.
4. Rykin, N.N., Zuev, I.V., Uglov, A.A. (1978) *Fundamentals of electron beam treatment of materials*. Moscow: Mashinostroyeniye.
5. Kochegura, N.M. (1998) Temperature-time homogenising treatment as a method to improve the properties of high-temperature nickel alloys. *Metalloznavsto ta Obrobka Metaliv*, **3**, 39–44.
6. Bokshtein, S.Z. (1973) *Structure and properties of metal alloys*. Moscow: Metallurgia.

SIMULATION OF WEAR RESISTANCE CHARACTERISTICS OF HIGH-MANGANESE STEEL TURNOUT FROGS IN SERVICE

M.I. GASIK*, I.A. SEMENOV*, O.P. YUSHKEVICH*, A.N. OVCHARUK* and Yu.S. PROJDAK*

Service conditions of cast frogs of high-manganese steel are considered. The rate of frog failure in service for the reasons of reaching limit level of contact fatigue defects and higher wear is determined. The paper analyses the joint influence of carbon and phosphorus on development of service defects in frogs, made of high-manganese steel. Equations of multiple regression are derived, that describe the interrelation between the content of carbon and phosphorus in 110G13L steel and the failure rate of frogs in service. Methods for improvement of the quality of 110G13L steel for railway frogs are determined.

Key words: *high-manganese steel, railway turnout frogs, mathematical simulation, contact fatigue defects, increased wear, optimal and rational chemical compositions of steel*

Unique properties of high-manganese steel 110G13L, in particular, good resistance to abrasive wear of the working surface in the deformed condition with rather high ductile and strength properties, led to its application for fabrication of parts, components of machines and mechanisms (for instance, excavating machine teeth, wear plates of crushers and mills, turnout cores and frogs), exposed to high dynamic and static loads under the conditions of abrasive wear. In operation 5 to 620 MPa pressure is applied to wear plates of various crushers and mills [1]. Dynamic pressure of 116–225.4 kN is applied to railway turnout frogs and cores when the train moves at the velocity of 70 km/h and axle load of 225.4 kN, the average value of tangential stresses reaching 1715–2254 mN/m^2 [2].

Depending on the service conditions of parts and products of 110G13L steel, the requirements, made of its composition, are different. A large number of works are devoted to study of the influence of 110G13L steel composition on its physico-mechanical properties. However, the issues of the joint influence of carbon and phosphorus on formation of various defects in service, leading to shorter service life of products of this steel, are insufficiently described in publications.

In this work the case of railway frogs is used to analyse the joint influence of carbon and phosphorus on service properties of heat-treated castings of high-manganese steel. Selection of frogs as an object of investigations is due to a number of reasons. First of all, the frogs are exposed to higher dynamic and static loads in service, than other products, made of steel 110G13L. Secondly, higher requirements are made of the performance of frogs, that are one of the main components of railway turnouts, as accident-free operation of railway transport and economic characteristics of the railway operation are largely dependent on their reliability and fatigue life.

Our statistical analysis of the data on removal of 520 frogs from service, when the frog service life in the main track was not less, than 2–2.5 years and not less, than 140–150 mln tons of cargo had been transported over them, showed, that 40 to 60 % of them had contact fatigue defects in the roll zone, leading to increased tangential stresses and disturbing the normal operation of turnouts, and 20 to 30 % had greater wear (more than 7 mm), that results in increase of dynamic pressure of the wheels on the frog. If the roll surface wear is higher, than 7 mm, the level of dynamic pressure increases by 188–480 kN, thus leading to intensive wear of the frogs up to their removal from service [2, 3]. In view of the above, statistical analysis was performed of the data on frogs removal from the track for the reason of having reached limit parameters of contact fatigue defects and greater wear.

Frogs of steel 110G13L, removed from service, had the following composition, %: C — 1.1–1.28; Mn — 12.4–12.8; Si — 0.49–0.56; P — 0.04–0.082,

*National Metallurgical Academy of Ukraine, Dnepropetrovsk, Ukraine.

Table 1. Carbon and phosphorus influence on the rate of frog failure because of contact fatigue defects

Carbon content, wt.%	Rate of frog removal from service (%) at phosphorus content in the metal, wt.%			
	0.04	0.06	0.075	0.085
1.125	7.04	7.40	8.81	9.50
1.175	5.29	5.90	7.76	8.81
1.225	4.24	4.59	5.29	8.11
1.275	2.47	3.53	4.22	7.04

corresponding to the requirements of GOST 7370–96 standard. In the frog metal the content of manganese and silicon varies only slightly and with a certain degree of assumption, it was taken to be constant, so that only the influence of carbon and phosphorus on development of contact fatigue defects was analysed.

The values of mathematical expectations of the content of carbon and phosphorus in the metal and the frog failure rate because of contact defect formation, corresponding to this composition, are given in Table 1.

Mathematical processing of the data, given in this Table, yielded the equation of multiple regression, describing the inter-relation between the content of carbon and phosphorus in the steel with the rate of frog failure because of development of contact fatigue defects.

Combined influence of carbon and phosphorus on development of contact fatigue defects, p_c, is given by the following equation:

$$p_c = 32.548 - 26.0\ [\%C] + 75.413\ [\%P]. \qquad (1)$$

The estimated mean root square deviation for the absolute term is 3.688, for the factor at [%C] — 3.180 and for the factor at [%P] — 10.490.

As follows from equation (1), with the increase of phosphorous content in the metal at a constant content of carbon, the rate of frog failure because of development of contact fatigue defects becomes higher. On the other hand, at the increase of carbon content in the frog metal and approximately constant content of phosphorous, the rate of frog failure because of this defect, becomes lower. Different nature of the influence of carbon and phosphorous on development of contact fatigue defects, is attributable to formation of deformation martensite (ε- or α-martensite) in service [4], having an incoherent boundary with austenite that is the main metallogrpahic structure of heat-treated castings of railway frogs. Formation of ε- and α-martensite in the high-manganese high-carbon austenite, having a high (40–80 mJ/m^2) stacking fault energy (SFE) and, therefore, low susceptibility to phase transformations [5] under dynamic loading, is attributed by authors of [4, 6] to a local lowering of carbon concentration, that may lead to SFE decreasing to values below 40 mJ/m^2. According to our data [7] with the increase of phosphorous content in the steel, carbon solubility in high-manganese austenite becomes lower. At [P] = 0.02 % interaction parameter $\varepsilon_C^P = 1.36$, and at [P] = 0.1 % $\varepsilon_C^P = 1.64$. Coefficient of carbon diffusion (D_{11}) decreases from $8.9 \cdot 10^{11}$ at [P] = 0.02 % to $8.0 \cdot 10^{-11}$ m^2/s at [P] = 0.1 %, and non-diagonal coefficient (D_{12}) becomes $-1.43 \cdot 10^{-2}$ m^2/s.

Thus, phosphorus reduces carbon solubility in iron, while carbon, in its turn, lowers the already low coefficient of phosphorus diffusion into steel [8]. As a result, phosphorus content in austenite microvolumes can rise up to high values, even exceeding its solubility limits in γ-iron. Phosphorus atoms drive carbon atoms away and form microvolumes, depleted or enriched in carbon, respectively. It is known, that phosphorus determines the degree of dendrite liquation development and the size of the austenite grain in interdendritic areas, the metal of which is the last to solidify. Therefore, with the increase of phosphorus content in 110G13L steel, there is a higher probability of non-uniform distribution of carbon and phosphorus, thus leading to formation of chemical microinhomogeneity. The above factors have an essential influence on the kinetic of phase transformations, proceeding in 110G13L steel. On the other hand, increase of carbon content in the steel, promotes stabilisation of austenite [9], thus ultimately resulting in slowing down of martensite formation processes.

Values of mathematical expectations of carbon and phosphorus content in the metal, and the rate of frog failure because of inadmissible wear, corresponding to this composition, are given in Table 2.

Mathematical processing of data from this Table yielded the equation of multiple regression, describing the combined influence of carbon and phosphorus on the rate of frog failure because of higher wear p_w, that has the following form:

$$p_w = 82.906 - 56.37\ [\%C] - 138.64\ [\%P]. \qquad (2)$$

The estimated mean root square deviation for absolute term is 10.901, for the factor at [%C] — 8.943 and for the factor at [%P] — 29.480.

Analysis of equation (2) shows, that with the increase of the content of carbon and phosphorus within the range of the grade composition, the rate of frog failure because of greater wear of the roll surface, becomes smaller. Carbon and phosphorus have a similar effect on frog wear resistance. Increase of wear resistance with the increase of carbon content in high-

Table 2. Carbon and phosphorus influence on the rate of frog failure because of higher wear

Carbon content, wt.%	Rate of frog removal from service (%) at phosphorus content in the metal, wt.%			
	0.04	0.06	0.075	0.085
1.125	16.93	13.13	7.60	4.14
1.175	11.23	9.67	6.04	3.45
1.225	6.21	5.70	4.83	3.45
1.275	2.76	2.10	1.72	1.04

manganese steel is accounted for by the fact, that carbon forms interstitial solid solutions at phosphorus concentrations of not more, than 0.09 % in heat-treated steel 110G13L. Increase of the content of interstitial element in the solid solution above its «free dissolution concentration» results in further distortion of the crystalline lattice. The term «free dissolution concentration» is understood to be the amount of interstitial elements, that is found in the solid solutions under quasi-equilibrium conditions, achieved by slow solidification or during long-term isothermal soaking above A_3 temperature and subsequent slow cooling at a rate of not more than 20–50 deg/h [10]. For instance, when carbon concentration in steel 110G13L is increased from 0.9 to 1.3 %, the tetragonality (c/a ratio) of fcc-lattice increases from 1.04 up to 1.06. This induces local stresses, rising up to 400 MPa, and results in increased number of dislocations, appearance of annealing and deformation twins, and in some cases leads to development of stacking faults [4, 10]. Formation of large numbers of dislocations, their clusters and stacking faults, results in dislocation fixation and increased resistance to their sliding at application of external forces [10], this leading to strengthening of the frog metal and ultimately slowing down the wear process (height reduction). Phosphorus atomic radius (r_P = = 0.130 nm) being larger, than that of carbon (r_C = = 0.101 nm), crystalline lattice distortion, caused by phosphorus dissolution, is greater, than at carbon dissolution. This, at other conditions being equal, is exactly what accounts for a stronger influence of phosphorus on improvement of high-manganese steel wear resistance.

Regression models (1) and (2) allow forecasting the service properties, determining the optimal and rational content of carbon and phosphorus in 110G13L steel, designed for production of castings of railway turnout frogs and cores.

Equations (1) and (2) were used to plot the diagram (see the Figure), that allows selection of the ratio of carbon and phosphorus content in the finished metal, providing a rational combination of service properties.

Simultaneous solution of equations (1) and (2) with respect to unknown [%C] and [%P] yields a system of equations, that describe the dependence of 110G13L steel composition on the specified service properties of the frogs and the cores:

$$[\%C] = 1.375 - 0.0176p_c = 0.0095p_w, \qquad (3)$$

$$[\%P] = 0.04 + 0.0072p_c - 0.00335p_w. \qquad (4)$$

The derived equations allow forecasting the optimal content of carbon and phosphorus, at which the wear and development of contact fatigue defects will be minimal. Selecting from Tables 1 and 2 the minimal characteristics of wear $p_{w\,min}$ = 1.04 and of contact fatigue defect development $p_{c\,min}$ = 2.47 and substituting them into equations (3) and (4), we determine the optimal content of carbon and phosphorus:

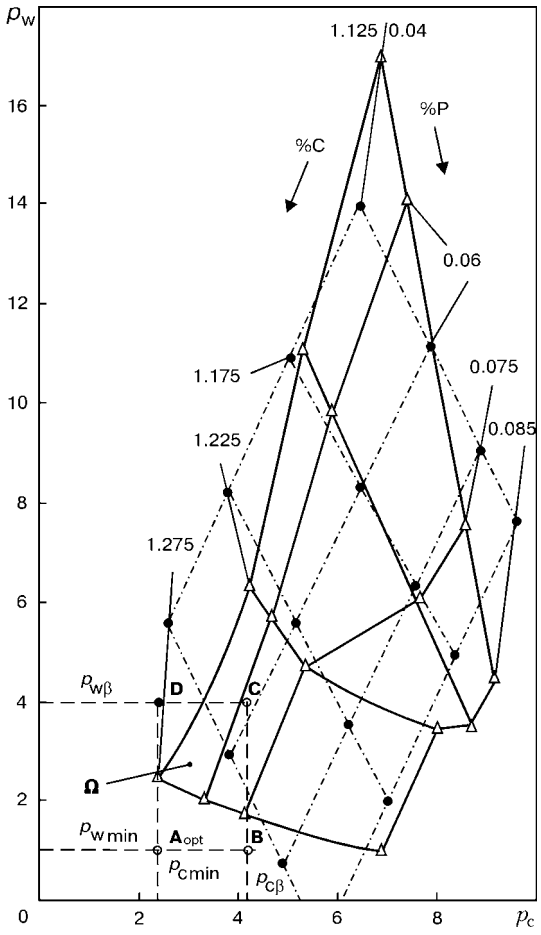

Diagram of frog failure rate because of contact fatigue defects and higher wear at different content of carbon and phosphorus in 110G13L steel: ● — experimental data; ○ — design data; Δ — peaks in rational value region

$$[\%C]_{opt} = 1.32, \quad [\%P]_{opt} = 0.054. \qquad (5)$$

Taking into account the calculation corrections, we get the optimal combination of the steel chemical components $[\%C]_{opt}$ = 1.29 and $[\%P]_{opt}$ = 0.0458, that determines A_{opt} point in the space of parameters p_w and p_c (Figure 1). Point A_{opt} has a statistically diffuse region Ω, evaluated through confidence probability β, which determines the rational limits of service parameters.

Let us write the interval estimate of minimal values of service properties $p_{w\,min}$ and $p_{c\,min}$ with confidence probability β (assigned by the experimenter and usually equal to 0.9–0.95), considering that the negative second addends in the expression for the considered problem are meaningless:

$$p_{w\,\beta} = p_{w\,min} + t_\beta\sigma/\sqrt{n}, \qquad (6)$$

$$p_{c\,\beta} = p_{c\,min} + t_\beta\sigma/\sqrt{n}, \qquad (7)$$

where $t\beta$ is the accuracy of interval estimate of $p_{w\,min}$ and $p_{c\,min}$ at confidence probability β (found from Student distribution table); n is the number of ele-

ments of the total population; σ is the mean root square deviation.

Expression (6) and (7) allow finding rational intervals of variation of service property values [$p_{w\,min}$, p_w] and [$p_{c\,min}$, p_c], that in the system of p_w and p_c co-ordinates form a rectangular region of the optimal service properties Ω (see the Figure) with peak co-ordinates: $A_{opt}(p_{c\,min}, p_{w\,min})$, $B(p_c, p_{w\,min})$, $C(p_{c\,min}, p_{w\,\beta})$ and $D(p_{c\,\beta}, p_{w\,\beta})$. Assigning the thus found various combinations of rational values of the frog service properties, that are the co-ordinates of points, belonging to the region of optimal values, Ω, it is possible to find from equations (3) and (4) the rational values of carbon and phosphorus content in the finished metal. For instance, at $p_w = 4.14$ and $p_{c\,min} = 2.47$ [%C] = 1.262, [%P] = 0.0354; at $p_{w\,min} = 1.04$ and $p_c = 4.22$ [%C] = 1.291, [%P] = 0.067.

The required content of carbon in the finished metal at phosphorus concentration specified during the steel production, can be found from the following equation:

$$[\%C] = 1.415 - 0.0104p_c - 0.0128p_w - [\%P], \quad (8)$$

derived from the system of equations (3) and (4).

Carbon and phosphorus concentration in the finished liquid high-manganese steel 110G13L can be controlled, by melting it by the technologies, developed and proposed by the Chair of Electrometallurgy of National Metallurgical Academy of Ukraine [7], envisaging out-of-furnace dephosphorization or decarbonization of the steel pool, using gaseous oxygen.

1. Andreev, S.E., Petrov, V.A., Zverevich, V.V. (1980) *Crushing, grinding and screening of mineral products*. Moscow: Nedra.
2. Simon, V.I. (1983) *Operation of turnouts*. Moscow: Transport.
3. Glyuzberg, B.E. (1984) Features of turnout wear. *Vestnik VNIIZhT*, **3**, 39–42.
4. Petrov, Yu.N. (1978) *Defects and diffusionless transformations in steel*. Kyiv: Naukova Dumka.
5. Gasik, M.I., Petrov, Yu.N., Yakubtsov, I.A. *et al*. (1988) Phosphorus influence on austenite stability in high-manganese steels. *Doklady AN Ukr. SSR, Ser. A*, **6**, 78–80.
6. Gasik, M.I., Petrov, Yu.N., Semenov, I.A. *et al*. (1987) Phosphorus influence on local structural instability and mechanical properties of steel 110G13L. *Problemy Spets. Elektrometallurgii*, **1**, 13–18.
7. Gasik, M.I., Petrov, Yu.N., Semenov, I.A. *et al*. (1990) *Metallurgy of high-manganese steel*. Kyiv: Tekhnika.
8. Kazarnovsky, D.S. (1966) *Influence of arsenic, phosphorus and carbon on steel properties*. Moscow: Metallurgia.
9. Lee, Y.-K., Choi, C.-S. (2000) Driving force for $\gamma \rightarrow \varepsilon$ martensitic transformation and stacking fault energy of γ in Fe–Mn binary system. *Metallurgical and Materials Transformation*, **2**, 355–360.
10. Karaman, I., Sehitoglu, H., Gall, K. *et al*. (2000) Deformation of single-crystal hadfield steel by twinning and slip. *Acte Mater*., Vol. 48, 1345–1359.

ENTHALPY OF LIQUID SLAGS OF THE $CaO–Al_2O_3–SiO_2$ SYSTEM AT DIFFERENT TEMPERATURES

L.P. MOJSOV*, B.P. BURYLEV* and D.M. LAPTEV**

Relative enthalpy of liquid slags of the $CaO–Al_2O_3–SiO_2$ system of different compositions and at different temperatures was calculated on the basis of the V.A. Kozheurov's theory of regular ionic melts and standard reference data. Isenthalpies of this system were obtained.

Key words: *relative enthalpy of slags, statistical-thermodynamic theory, thermodynamic values, basicity, isenthalpy*

Slags formed in electric arc welding and surfacing should meet different requirements. One of them is to minimize power consumption, which is determined by a relative enthalpy of liquid slags. The latter was calculated in this study for the ternary system $CaO–Al_2O_3–SiO_2$.

Express relative enthalpy of the i-th component at temperature T in solid state S in terms of $\Delta H_{iS}^T = H_{iS}^T - H_{iS}^{298\,K}$. Then the relative enthalpy of a mechanical mixture of k solid components will have the following form:

$$\Delta H_S^T = \sum_{i=1}^{k} x_i \Delta H_{iS}^T, \quad (1)$$

where x_i is the ionic or mole fraction of the component in a mixture (depending upon the statistical-thermodynamic theory used).

In heating a mechanical mixture, the first portions of a liquid slag appear at temperature Ts, and the last portions of solid phases disappear at a temperature below the melting points of individual components. Therefore, to produce a liquid slag at temperature T, lower than the melting point of the highest-volatility component, it is necessary to preliminarily transform components from the solid state into the liquid one. Variation in enthalpy in this transition can be considered equal to the tabulated enthalpy of melting, as the latter varies but slightly with the temperature.

*OJSC NIIMontazh, Krasnodar, Russia.
**Siberian State Industrial University, Novokuznetsk, Russia.

In this connection, the relative enthalpy of a liquid slag, in an assumption that slag is an ideal solution, is as follows:

$$\Delta H_{sl}^{T} = \sum_{i=1}^{k} x_i (\Delta H_{iS}^{T} + \Delta H_i^{melt}). \quad (2)$$

Here ΔH_i^{melt} is the tabulated enthalpy of melting of the i-th component.

To obtain the true relative enthalpy of a liquid slag, the enthalpy of formation of slag of pure components, normally called the enthalpy of mixing, ΔH_{mix}, should be added to the right part of expression (2). Then

$$\Delta H_{sl}^{T} = \sum_{i=1}^{k} x_i \left(\Delta H_{iS}^{T} + \Delta H_i^{melt}\right) + \Delta H_{mix}. \quad (3)$$

The enthalpy of mixing can be determined providing that the statistical-thermodynamic theory is available, which satisfactorily describes thermodynamic properties of a liquid slag. This condition is met by the V.A. Kozheurov's theory of ionic solutions with a common ion [1].

According to the Kozheurov's theory, enthalpy of mixing of slag (J/g-cation), consisting of k components, will be written as follows:

$$\Delta H_{mix} = \sum_{i=1}^{k-1} \sum_{j=i+1}^{k} x_i\, x_j\, Q_{ij} + (3x_{Si} - 1)^2 \sum_{i=1}^{k-1} x_i\, q_i, \quad (4)$$

where Q_{ij} is the energy of mutual exchange in the i–j system; x_i and x_j are the ionic fractions of cations introduced by components i and j; x_{Si} is the ionic fraction of silicon cations; q_i is the parameter that allows for polymerization of silicon-oxygen tetrahedrons in the i–SiO_2 system.

In this expression summand

$$(3x_{Si} - 1)^2 \sum_{i=1}^{k-1} x_i\, q_i$$

is allowed for only in the case of acid slags, i.e. at an ionic fraction of silicon equal to $x_{Si} > 1/3$. If $x_{Si} \le 1/3$ (basic slags), it decreases. Substituting the value of the enthalpy of mixing from expression (4) into equation (3) yields

$$\Delta H_{sl}^{T} = \sum_{i=1}^{k} x_i \left(\Delta H_{iS}^{T} + \Delta H_i^{melt}\right) + \sum_{i=1}^{k-1} \sum_{j=i+1}^{k} x_i\, x_j Q_{ij} + (3x_{Si} - 1)^2 \sum_{i=1}^{k-1} x_i\, q_i \quad . \quad (5)$$

To obtain a specific relative enthalpy of slag (J/g), divide expression (5) by mass of 1 g-cation of slag, equal to $\sum_{i=1}^{k-1} x_i M_i/\nu_i$ (ν_i is the number of g-cations introduced into slag by one mole of oxide; M_i is the molecular mass of oxide):

$$\Delta h_{sl}^{T} = \frac{\sum_{i=1}^{k} x_i \left(\Delta H_{iS}^{T} + \Delta H_i^{melt}\right)}{\sum_{i=1}^{k} x_i M_i/\nu_i} + \frac{\sum_{i=1}^{k-1} \sum_{j=i+1}^{k} x_i\, x_j Q_{ij} + (3x_{Si} - 1)^2 \sum_{i=1}^{k} x_i\, q_i}{\sum_{i=1}^{k} x_i\, M_i / \nu_i}. \quad (6)$$

In the majority of cases the slags can be regarded with a sufficient degree of accuracy as consisting of CaO, Al_2O_3 and SiO_2, other components being ignored. To describe thermodynamic properties of this three-component system, based on the theory of [1], it is necessary to know energy parameters of binary systems given in Table 1.

Relative enthalpies of the i-th component at temperature T (ΔH_{iS}^{T}), which are included into formula (6), are calculated by a traditional method from the following equation:

Table 1. Values of energy parameters in the Kozheurov's theory

System	Parameters	
	Q, J/mole	q, J/mole
$CaO–Al_2O_3$	−195000	0
$CaO–SiO_2$	−113000	+26400
$Al_2O_3–SiO_2$	−70000	0

Table 2. Heat capacities and enthalpies of phase transitions of CaO, Al_2O_3 and SiO_2

Material	T_{melt}, K	ΔH^{melt}, J/mole	Heat capacity, J/(mole·K)
CaO	2845	75000	$C_p = 41.86 + 20.26\cdot10^{-3}\,T - 4.52\cdot10^{5}\,T^{-2}$
Al_2O_3	2323	109000	$C_p = 109.36 + 18.37\cdot10^{-3}\,T - 30.43\cdot10^{5}\,T^{-2}$
α-quartz	848	1200	$C_p = 47.0 + 34.3\cdot10^{-3}\,T - 11.3\cdot10^{5}\,T^{-2}$
β-quartz	1548	7100	$C_p = 60.3 + 8.1\cdot10^{-3}\,T$
β-crystal	1986	13000	$C_p = 60.3 + 8.6\cdot10^{-3}\,T$

Table 3. Enthalpies (J/g) of the $CaO–Al_2O_3–SiO_2$ system at different temperatures, basicities and contents of aluminium oxide (III)

Al_2O_3, %	Basicity (%CaO/%SiO_2)										
	10/0	9/1	8/2	7/3	6/4	5/5	4/6	3/7	2/8	1/9	0/10
						T = 1773 K					
0	3182	2914	2684	2498	2337	2258	2337	2247	2266	2266	2215
5	2994	2761	2559	2390	2246	2185	2165	2178	2208	2215	2197
10	2629	2435	2241	2099	1987	1923	1908	1924	1955	1981	1983
15	2469	2297	2163	2029	1937	1879	1870	1887	1920	1954	1975
20	2343	2197	2075	1978	1900	1854	1841	1862	1900	1941	1975
25	2238	2117	2017	1933	1866	1837	1833	1854	1895	1937	1979
30	2155	2050	1971	1908	1862	1837	1833	1854	1895	1946	1987
35	2084	2004	1941	1895	1862	1845	1849	1870	1912	1962	2017
40	2033	1975	1929	1900	1874	1866	1874	1895	1937	1983	2042
45	2004	1962	1929	1908	1895	1895	1920	1933	1966	2017	2075
50	1996	1962	1941	1933	1929	1937	1954	1979	2017	2063	2117
						T = 1823 K					
0	3040	2773	2544	2350	2200	2123	2100	2115	2135	2135	2087
5	2852	2620	2419	2252	2109	2049	2031	2045	2056	2084	2063
10	2700	2505	2311	2168	2056	1991	1975	1991	2021	2047	2048
15	2540	2368	2234	2100	2008	1950	1937	1954	1987	2021	2038
20	2414	2268	2146	2046	1971	1920	1912	1929	1966	2006	2038
25	2305	2184	2084	2004	1937	1908	1899	1920	1958	2004	2045
30	2222	2121	2042	1979	1933	1904	1899	1920	1962	2008	2054
35	2155	2075	2013	1962	1929	1926	1916	1937	1975	2025	2079
40	2105	2042	1996	1962	1941	1933	1937	1962	2004	2050	2109
45	2075	2029	1996	1975	1962	1966	1975	2000	2033	2084	2142
50	2063	2033	2013	2000	1996	2004	2021	2046	2084	2130	2184
						T = 1873 K					
0	3110	2843	2615	2417	2267	2189	2165	2179	2198	2198	2148
5	2963	2689	2488	2320	2177	2116	2097	2110	2135	2147	2125
10	2770	2575	2380	2237	2123	2058	2031	2056	2086	2110	2111
15	2611	2435	2305	2167	2071	2017	2000	2017	2050	2084	2105
20	2485	2339	2213	2113	2038	1987	1979	1997	2029	2071	2105
25	2377	2255	2155	2071	2004	1975	1966	1987	2025	2067	2109
30	2298	2192	2109	2050	2000	1975	1964	1987	2029	2075	2117
35	2226	2146	2079	2033	2000	1983	1983	2004	2042	2092	2146
40	2176	2113	2067	2033	2008	2004	2008	2029	2071	2117	2176
45	2146	2100	2071	2046	2033	2033	2046	2067	2100	2151	2209
50	2142	2105	2084	2071	2067	2075	2088	2113	2151	2197	2251
						T = 1923 K					
0	3182	2914	2684	2493	2337	2258	2237	2247	2267	2266	2215
5	2994	2761	2559	2390	2246	2185	2165	2178	2208	2215	2192
10	2842	2645	2451	2307	2193	2127	2110	2125	2154	2164	2178
15	2682	2506	2372	2238	2142	2084	2071	2088	2121	2151	2171
20	2556	2410	2284	2184	2109	2059	2046	2063	2100	2138	2171
25	2448	2326	2226	2142	2075	2042	2033	2054	2092	2142	2176
30	2364	2264	2180	2117	2071	2042	2038	2059	2096	2142	2184
35	2297	2218	2151	2105	2071	2054	2054	2075	2113	2150	2213
40	2247	2184	2138	2105	2079	2071	2079	2100	2138	2184	2243
45	2218	2171	2138	2113	2105	2105	2113	2138	2167	2218	2276
50	2205	2176	2151	2138	2138	2142	2159	2184	2218	2264	2318

$$\Delta H_{iS}^{T} = \int_{298}^{T_\alpha} C_{pi}^{\alpha}\, dT + \Delta H^{\alpha-\beta} + \int_{T_\alpha}^{T_\beta} C_{pi}^{\beta}\, dT + \ldots + \Delta H^{\beta-\gamma} + \ldots \int_{T_\lambda}^{T} C_{pi}^{\lambda}\, dT, \quad (7)$$

where C_{pi}^{α} and C_{pi}^{β}–C_{Pi}^{λ} are the molar heat capacities of modifications α and β–λ; T_α and T_β–T_λ are the temperatures of the modification transitions; $\Delta H^{\alpha-\beta}$ and $\Delta H^{\beta-\gamma}$ are the enthalpies of modification transitions α→β and β→γ, respectively.

Thermochemical data [2, 3] required for calculation of relative enthalpies of pure CaO, Al_2O_3 and SiO_2 are given in Table 2.

Table 2 was used to derive temperature dependencies of a relative enthalpy of pure solid oxides upon the temperature (J/mole):

$$\Delta H_{CaO}^{T} = -14890 + 41.86\,T + 10.13\cdot10^{-3}\,T^2 + 4.52\cdot10^{5}\,T^{-1}, \quad (8)$$

$$\Delta H_{Al_2O_3}^{T} = -43600 + 109.36\,T + 9.19\cdot10^{-3}\,T^2 + 30.43\cdot10^{5}\,T^{-1}, \quad (9)$$

$$\Delta H_{SiO_2}^{T} = -12200 + 60.3\,T + 4.3\cdot10^{-3}\,T^2 \quad (10)$$

(above 1548 K).

Substituting dependencies (8) to (10) together with values of enthalpies of melting of components from Table 2, and energy parameters from Table 1, yields calculation formulae for specific relative enthalpies of slags of the CaO–Al_2O_3–SiO_2 system:

$$\Delta h_{sl}^{T} = \frac{x_1\,(60110 + 41.86\,T + 10.13\cdot10^{-3}\,T^2 + 4.52\cdot10^{5}\,T^{-1})}{56x_1 + 51x_2 + 60x_3} + \frac{x_2\,(32700 + 54.68\,T + 4.60\cdot10^{-3}\,T^2 + 15.22\cdot10^{5}\,T^{-1})}{56x_1 + 51x_2 + 60x_3} + \frac{x_3\,(800 + 60.3\,T + 4.3\cdot10^{-3}\,T^2)}{56x_1 + 51x_2 + 60x_3} - \frac{(195000x_2 + 113000x_3x_1 - 70000x_2x_3) + (3x_3 - 1)^2 26400x_1}{56x_1 + 51x_2 + 60x_3}. \quad (11)$$

Here numerical indices of ionic and mole fractions correspond to the following numbering of the components: CaO — 1, Al_2O_3 — 2 and SiO_2 — 3.

In study [4] similar calculations, but for the four-component system CaO–MgO–Al_2O_3–SiO_2, are compared with experimental data, and they are in satisfactory agreement for a wide range of temperatures of solid and liquid states of slags. Therefore, equation (1) was used as a base for the calculation of relative enthalpies of slags of the CaO–Al_2O_3–SiO_2 system at four temperatures, and the calculation results for each of the temperatures, constant concentrations of Al_2O_3 and different basicities of slags are given in

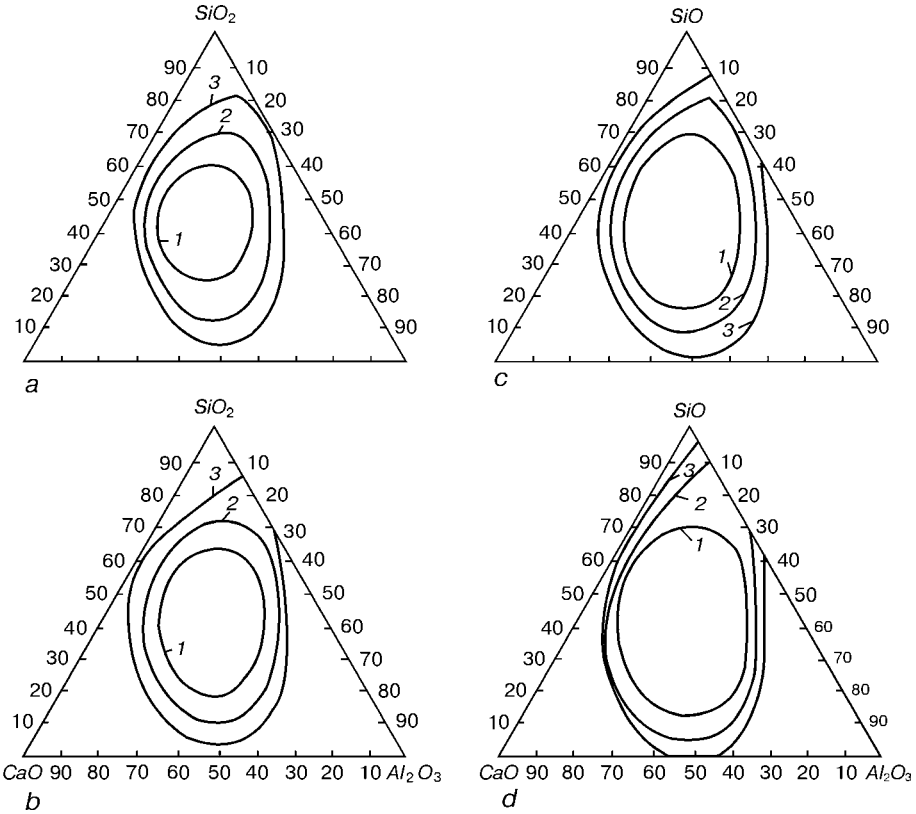

Dependence of specific relative enthalpy of slag upon the composition of the CaO–Al_2O_3–SiO_2 system at temperatures: *a* — 1773 K (*1* — 1883; *2* — 1925; *3* — 1966 J/g); *b* — 1823 K (*1* — 1966; *2* — 2008; *3* — 2050 J/g); *c* — 1873 K (*1* — 2050; *2* — 2092; *3* — 2134 J/g); *d* — 1923 K (*1* — 2134; *2* — 2176; *3* — 2218 J/g)

Table 3. Basicity ($\%CaO/\%SiO_2$) and weight percent of Al_2O_3 were selected as the main parameters which determine composition of a slag. Ionic fractions of calcium, aluminium and silicon were found from the composition in percent, followed by calculation of Δh_{sl}^T from formula (11).

Analysis of the Table shows that a specific relative enthalpy of the three-component slags at a constant content of Al_2O_3 with a decrease in basicity passes through a minimum at a basicity of 0.6–0.7. At an Al_2O_3 content of more than 30 %, the minimum shifts towards higher basicity, and at 50 % of Al_2O_3 it corresponds to a basicity of 1.5.

An increase in the Al_2O_3 content of slags of constant basicity, at the values of basicity higher than 9, is accompanied by a decrease in Δh_{sl}^T over the investigated range of compositions, whereas at basicities below 9 the $\Delta h_{sl}^T = f(\%Al_2O_3)$ dependence has a minimum. For slags with a basicity of 1.5 (6/4) and lower, this minimum is in a range of 25–30 % Al_2O_3.

Existence of two minima gives rise to a question concerning slags with the lowest value of a specific relative enthalpy. It follows from Table 3 that slags with a basicity of 0.6–1.0 at 25–30 % Al_2O_3 have the lowest value of Δh_{sl}^T. In the Figure the data of the Table are given in the form of isenthalpies of the $CaO–Al_2O_3–SiO_2$ system.

It should be noted in conclusion that the developed method for calculation of a specific relative enthalpy of slag, in the case of using modern statistical-thermodynamic theories of slags, provides good agreement with experiments, and allows calculation of the diagram of isenthalpies. At the same time, calorimetry measurements of a relative enthalpy of liquid slags of the $CaO–Al_2O_3–SiO_2$ system at different temperatures are required.

CONCLUSIONS

1. Equation for calculation of a relative enthalpy of liquid slags of the $CaO–Al_2O_3–SiO_2$ system was derived using reference data on enthalpies of phase transitions and heat capacities of individual oxides, and the V.A. Kozheurov's statistical-thermodynamic theory of regular ionic melts.

2. Calculations of enthalpy of liquid slags were made for a wide range of compositions and at different temperatures. Lines of equal enthalpies of slags were plotted. It is shown that enthalpies may have minimum values at different compositions. It was established that slags with a basicity of 0.6–1.0 at 25–30 % Al_2O_3 have the lowest values of a relative enthalpy.

1. Kozheurov, V.A. (1955) *Thermodynamics of metallurgical slags*. Sverdlovsk: Metallurgizdat.
2. (1965) *Thermodynamic properties of inorganic materials*. Handbook. Moscow: Atomizdat.
3. Belyankin, D.S., Toropov, N.A., Lapin, V.V. (1949) *Physical-chemical systems of silicate technology*. Moscow: Promstojizdat, .
4. Laptev, D.M., Mojsov, L.P., Burylev, B.P. (2001) *Temperature dependence of enthalpy of the CaO–MgO–Al_2O_3–SiO_2 system*. Dep. in VINITI No.1088 on 24.04.01. Krasnodar: OAO NIIMontazh.

PYROMETRY MEASUREMENTS IN EBCH MELTING

V.N. FEDOROV*, V.A. SHCHEKIN-KROTOV* and A.M. KASUMOV*

The possibility of using a pyrometer to determine a molten metal temperature through a window with a variable optical density is shown. The temperature measured is adjusted during the melting process by a liquidus temperature of the metal melted.

Key words: *electron beam melting, pyrometer, temperature, titanium, window, measurement*

Measurement of a temperature of molten metal in electron beam cold-hearth (EBCH) melting is an important technological operation, allowing regulation of both melting process and properties of a finished product. Unfortunately, traditional measurement methods, such as pyrometry, are rather difficult to use because of continuously varying optical transmission of glass and light attenuators in windows. In this case, in a formula of conversion of brightness temperature T_b, measured by a pyrometer, into actual temperature T [1]

$$\frac{1}{T} = \frac{1}{T_b} + A \qquad (1)$$

constant A becomes a variable, thus making it impossible to convert T_b into T.

Indeed, as shown by calculations, the A value can be given in the following form:

$$A = \frac{\lambda}{C_2} \ln \frac{\alpha Q}{\cos \varphi}, \qquad (2)$$

where $\lambda = 660$ nm is the effective wave length of the pyrometer; $C_2 = 1.4287 \cdot 10^{-2}$ m·deg is the constant; α is the optical transmission of glass and light attenuator in the window; Q is the emissivity factor of molten metal at the effective wave length and φ is the angle between the line of sight and perpendicular to the surface of a molten metal. This shows that in melting the A value should vary because of a decrease in α. This drawback can be eliminated using periodical adjustment of the A value, which can be readily achieved by measuring T_b of any process that has a known actual temperature T, followed by substitution of the values obtained into conversion formula (1).

In EBCH, solidification of metal in its discharge from the cold hearth into the mould can be selected as such a process. The discharge is accompanied by periodical (2–4 min) melting and solidification of metal in the discharge spout, which allows adjustment of the A value to be made at a frequency corresponding to its very small variations. In addition, selection of the process is advantageous also in the fact that stirring in the cold hearth provides metal with a high homogeneity of chemical composition, and T does not require any adjustment to fit the constitutional diagram.

Relative error of measurement of the actual temperature in EBCH, determined from conversion formula (1), is 4 %, which is 2 times as high as that in measurement without glasses and light attenuators [2].

The method described was employed for measuring temperature of the surface of molten metal in melting of ingots of alloy VT6 and commercial titanium VT1-0 with a diameter of 0.40 and 0.64 m, respectively. Schematic of location of measurement points and mean values of the temperature at them are shown in Figure 1 and in the Table.

Conditions of measurement of actual temperature of molten metal	Ingot No.	Temperature at measurement points, °C					
		1	2	3	4	5	6
Melting of alloy VT6 in a mould 0.42 m in diameter	108	1801	1763	1670	–	1756	–
	110	1769	1753	1670	–	1703	–
	121	1775	1770	1670	–	1741	–
	122	1791	1782	1670	–	1782	–
Melting of alloy VT1-0 in a mould 0.65 m in diameter	37	1805	1992	1668	1996	2010	1742

*AOZT «FIKO», Kyiv, Ukraine.

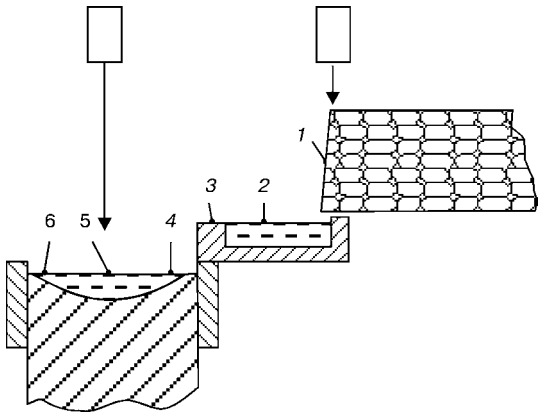

Figure 1. Schematic of location of points of measurement of temperature in the melting chamber: *1* — zone of melting of a consumable billet; *2* — cold hearth; *3* — discharge spout; *4–6* — mould

Increase in T with an increase in diameter of the mould is associated with variations of chemical composition of metal being remelted and electric current parameters of electron guns.

Effect on the melt by the beam causes an increase of 400–500 °C in the T values. Therefore, temperature of molten metal was measured at the absence of emission of electrons.

Variations in temperature T at the measurement points occur mainly simultaneously with variations in temperature of cooling water T_w (Figure 2).

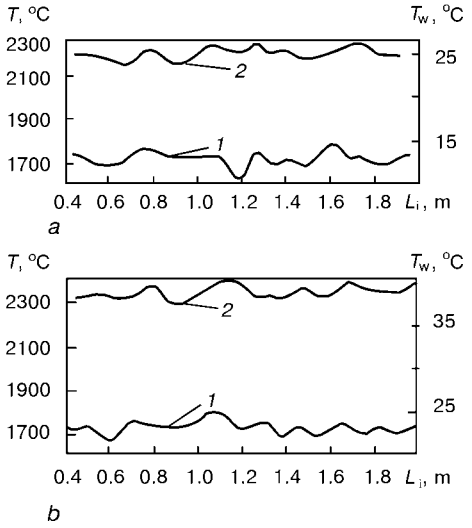

Figure 2. Variations in temperature of molten metal (*1*) and cooling water (*2*) depending upon length L_i of a drawn out ingot in mould 0.42 m in diameter (*a*) and in cold hearth (*b*)

Analysis of the obtained values of T shows that in a working range of temperatures the errors are distributed in accordance with the normal law, and a mean-root-square error is 32.5 deg, while the modulus of precision is 0.123 $deg^{-1/2}$.

1. Novikov, I.I., Gordov, A.N. (1983) *Methods and means of optical pyrometry*. Moscow: Nauka.
2. (1975) *Optical pyrometer OPPIR-017. Description and operating rules*. Khmelnitsk.

E.O. PATON ELECTRIC WELDING INSTITUTE
OF NATIONAL ACADEMY OF SCIENCES OF UKRAINE

The E.O. Paton Electric Welding Institute, a R&D centre established in 1934, is a multi-profile R&D complex which carries out the fundamental and applied research, develops technologies, materials, equipment and control systems, rational welded structures and items, methods and means for technical diagnostics and non-destructive testing in the following areas:

- *advanced technologies for materials welding and joining;*
- *strength, reliability and fatigue life of welded structures;*
- *technologies for surfacing, coating and surface treatment;*
- *processes of special electrometallurgy;*
- *advanced structural and functional materials.*

The PWI is a team of highly-qualified researchers among which there are 61 Doctors of Science (Eng.), and 252 Cand. of Sci. (Eng.). Departments and laboratories of the Institute are fitted with the advanced research and measurement-analytical equipment.

The PWI fulfills orders of local and foreign partners in the following areas:

- *R&D;*
- *scientific and technical consultations;*
- *scientific-technical and environmental examination of projects, structures and technologies;*
- *training and certification of the research and engineering-technical personnel and workers;*
- *design of special equipment and fixtures;*
- *engineering and technical assistance in transfer to the interested organisations of the advanced technologies, equipment, control and monitoring systems;*
- *standard and special tests of welded joints;*
- *certification of structures, technologies, materials and equipment in compliance with national and international standards;*
- *providing scientific-technical and reference information;*
- *exportimport operations.*

Scientists of the Institute achieved considerable success in the theoretical and experimental studies of the arc discharge physics, low-temperature plasma, high-power sharply-focused electron beams, energy conversion for different processes of welding, melting and solidification of metals, hydrodynamics of welding and electrometallurgical processes, processes of evaporation and condensation in vacuum, strength of welded structures under different conditions of service, as well as in development of special equipment and systems of automatic control. The results of these studies were implemented by the Institute in specific technologies, advanced materials and structure and unique equipment.

The Institute incorporates the design-technological bureau, engineering centres on advanced technologies, technological bureau and pilot production on explosion welding and treatment, as well as three pilot plants for welding equipment, welding consumables and advanced technologies, which are capable of developing, manufacturing and supplying experimental samples and batches of special equipment, welding consumables and filler materials, welded structures and items.

The PWI publishes the following journals in English and Russian languages:

- *«The Paton Welding Journal» (monthly), English*
- *«Advances in Electrometallurgy» (quarterly), English*
- *«Avtomaticheskaya Svarka» («Automatic Welding») (monthly), Russian*
- *«Tekhnicheskaya Diagnostika i NRK» («Technical Diagnostics and Non-Destructive Testing») (quarterly), Russian*

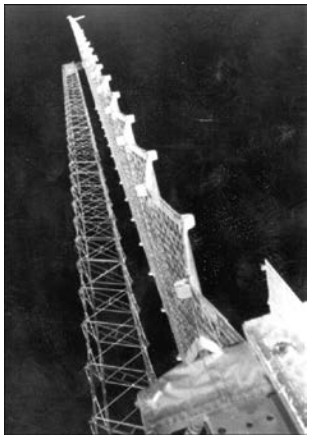

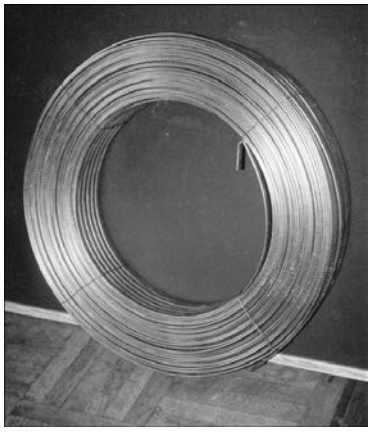

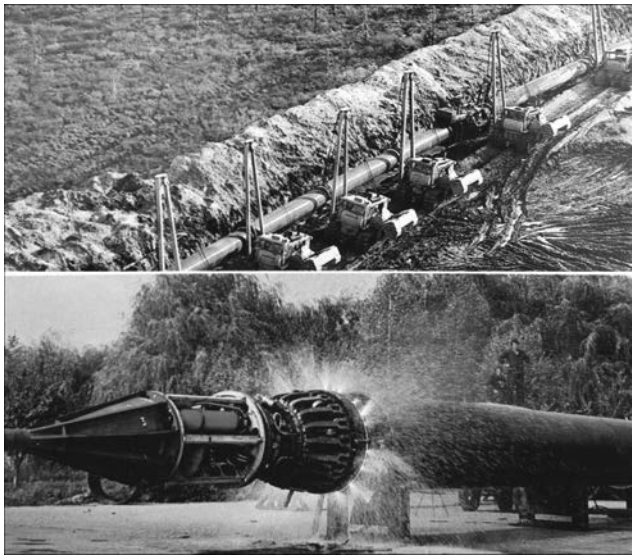

- *«Problemy Spetsialnoj Elektrometallurgii» («Problems in Special Electrometallurgy») (quarterly), Russian.*

The PWI has extensive international experience in accomplishing R&D projects for space exploration, development of new power systems, construction of main gas and oil pipelines, work in the underwater shelf, rocket and aircraft construction, production and processing of mineral resources, development of unique welded structures and constructions.

The PWI offers cooperation on the following fields:

- *multi-functional thin- and thick-film composite coatings;*
- *amorphous and superhard materials for strengthening and protection of surfaces of parts;*
- *advanced high-energy processes of surface treatment;*
- *advanced processes of recycling of ecologically hazardous wastes;*
- *use of advanced Al-, Ti-, Ni-base alloys in welded aircraft structures;*
- *technologies of welding, cutting and repair under water at large depths;*
- *wear-resistant electric arc and electroslag surfacing of parts of machines and mechanisms with the aim of extending their service life;*

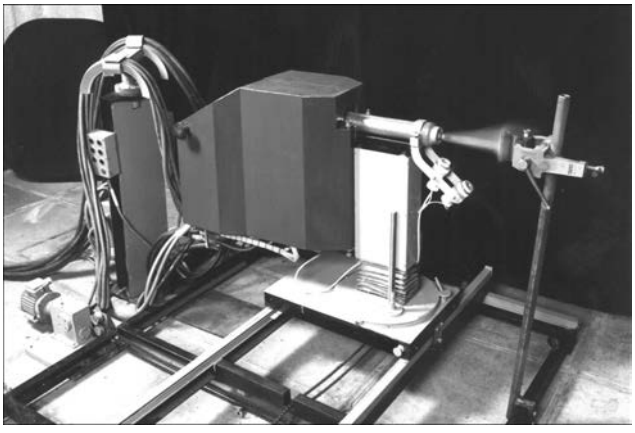

- *highly-effective technologies and welding consumables for welding titanium and its alloys, which allow making joints on 0.8 to 1.5 m thick metal;*
- *technology for producing fine-grained Ni- and Ti-base alloys, as well as pure alloys and oxygen-free copper by the method of electron beam melting in the intermediate crucible;*
- *highly-effective processes and advanced welding consumables for arc welding of commercial grades of copper and its alloys of 0.5 to 50 mm thickness;*
- *automatic submerged-arc welding;*
- *plasma-arc welding;*
- *welding in the atmosphere of different shielding gases (argon, helium, nitrogen), including by using activating fluxes (A-TIG process);*
- *welding and repair of large-sized copper parts with highly-efficient electrodes of ANTs-3 type;*
- *pulsed-arc non-consumable electrode welding of Al–Li and other high-strength light alloys of different alloying systems for fabrication of critical products. The technology provides an improvement of 10 to 15 % in the quality of welds and their strength;*
- *pulsed-arc consumable-electrode welding of sheet strucures (1 – 4 mm) for fabrication and repair of boats, launches, ship superstructures, equipment for the food and chemical industry, car-tanks, pipelines, etc. The technology is characterized by decreased distortions and reduced costs of welding;*
- *electroslag welding of components of aluminium busbars and billets of a large cross-section (50 to 210 mm thickness) under stationary and field conditions. The electrical resistance in the joining zone is not higher than that of the base metal and is characterised by a high stability;*
- *electroslag welding of critical thick-walled structures, such as frames of rolling mills, pressing equipment, etc.;*
- *electron beam and laser welding and surfacing of aluminium alloys for fabrication of large-sized shells and tanks, stringer panels, structures of heat-exchangers, household equipment and appliances, pistons with cooling cavities and strengthened grooves for rings. The technology provides a high quality and stability of mechanical properties of permanent joints of 0.5 to 350 mm thickness;*
- *joining of dissimilar metals and composite Al-base materials with fibrous (steel, silicon carbide, carbon, boron) and disperse (oxides, carbides, intermefallics) reinforcement. The technologies and materials are used in ship-building, motor industry, aerospace engineering, electrical engineering, in welding aluminium and its alloys with steels, copper and other metals;*
- *R&D in the area of high-rate electron beam evaporation of materials in vacuum, including by using a «hot source»;*
- *study of the intensive vapour flow condensation and fabrication of non-organic materials with prescribed structure, such as dispersion strengthened, microlayer, microporous materials;*
- *investigation of properties of new materials and searching for the ways of their practical application, first of all in the form of different coatings;*

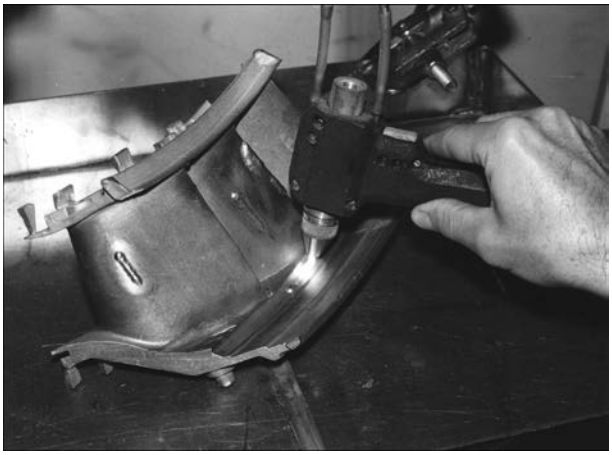

- *development of microlayer and gradient coatings for various-purpose gas turbine blades;*
- *development and manufacturing (if necessary, jointly with other manufacturers) of electron beam guns, as well as laboratory, pilot and commercial EB PVD equipment;*
- *professional training of researchers, engineers and technicians for operation in the field of EB PVD;*
- *technologies of electron beam welding of low- and high-alloyed steels up to 150 mm thick, including the technology of fading-out of circumferential welds, titanium, aluminium and their alloys of up to 250 mm thick;*
- *products for electronic, aerospace and medical engineering, made from titanium, aluminium, molybdenum, zirconium and their alloys from 0.05 to 1.00 mm thick;*
- *heat-exchangers from stainless steel, titanium, copper, aluminium from 0.3 to 5.0 mm thick, using tubes from 3 to 30 mm in diameter;*
- *high-voltage power sources and welding guns with power of 3, 30, 60 and 120 kW and accelerating voltage of 60 and 120 kV;*
- *systems of real-time seam-tracking and butt following at up to 100 kW beam power;*
- *completely fitted EBW units;*
- *methods for investigation and evaluation of the fatigue strength of welded joints in different structural materials. Probabilistic-statistical method of fatigue analysis of welded structures, allowing for the role of residual welding stresses. Method of fatigue analysis of welded joints under polyfrequency loading;*
- *technology and equipment for the ultrasonic impact peening of welded joints, providing increasing of fatigue strength of welded joints up to a level of the base material strength;*
- *computerized methods of strength analysis of welded joints with geometrical concentrators under various kinds of loading, determination of welding stresses and strains, assessment of the residual life of welded joints and structures;*
- *holographic methods and means for quality control and determination of the stress-strain states of welded joints and structures;*
- *methods and means for technical diagnostics of welded structures based on application of acoustic emission;*
- *energy-saving technologies and equipment for welding and repair of equipment in heat and power engineering;*
- *technologies for welding dissimilar materials and precision cutting of metal structures using the energy of explosion;*
- *technologies of welded joints treatment by explosion for elimination of residual welding stresses.*

For further information please contact:
E.O. Paton Electric Welding Institute
11, Bozhenko St., Kyiv, 03680, Ukraine
Phone: (38044) 220 87 87, 227 60 16
Fax: (38044) 268 04 86, 220 91 84
E-mail: office@paton.kiev.ua
http://www.paton.kiev.ua

TECHNOLOGY OF PRODUCING FUNCTIONAL MATERIALS AND COATINGS BY EB PVD

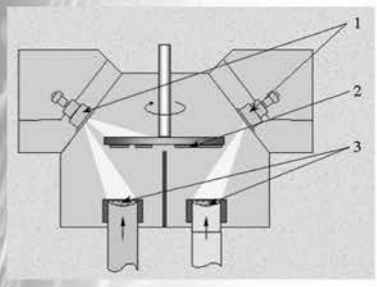

Schematic of EB PVD: *1* — EB guns; *2* — condensate; *3* — crucibles

✦ Efficiency of modern electron beam evaporators that incorporate 3–4 sources (crucibles), is 10 to 15 kg of vapour per hour. This allows producing at a high rate (up to 10 μm/min) thick coatings (10–150 μm), as well as making massive semi-finished products (10–20 kg) with the specified distribution of alloying elements. Technologies of evaporation of pure metals, including refractory metals, and their alloys, as well as oxides, borides, silicides and other compounds have been developed.

COATINGS AND MATERIALS PRODUCED BY EB PVD

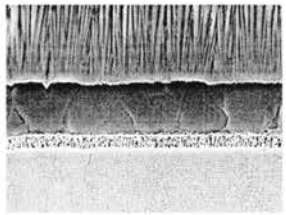

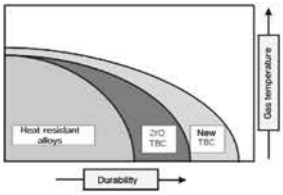

Thermal barrier coatings (TBC)

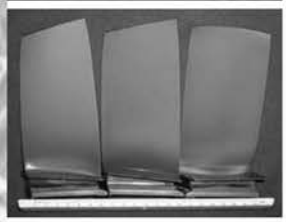

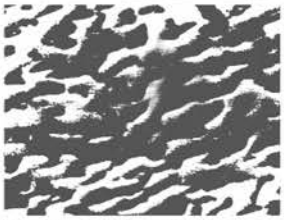

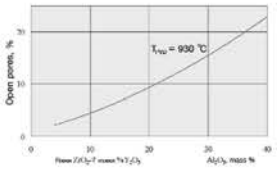

Gas turbine blades with porous ceramic coatings

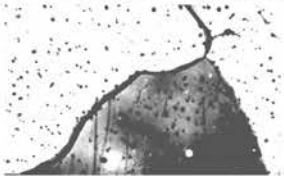

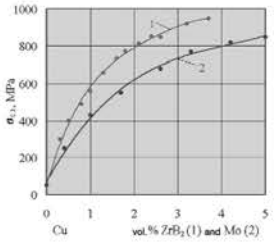

Dispersion-strengthened copper

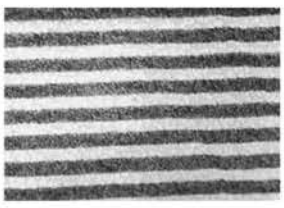

Model disc with refractory microlayers of TiAl/Ti (~ 10,000 layers)

E. O. Paton Electric Welding Institute of the NAS of Ukraine
11, Bozhenko st., 03680, Kiev, Ukraine
Fax: (38044) 268 04 86, tel.: (38044) 220 87 87, 227 60 16
E-mail: office@paton.kiev.ua http://paton.kiev.ua

INFORMATION FOR CONTRIBUTORS TO «ADVANCES IN ELECTROMETALLURGY»

«ADVANCES IN ELECTROMETALLURGY» is a scientific journal publishing fundamental and applied papers and short notes in the area of

- *electroslag welding and cladding*
- *electroslag remelting, casting, hot topping, heating*
- *plasma-arc melting and remelting*
- *vacuum-arc remelting*
- *induction melting*
- *electrometallurgy of steel and ferroalloys*
- *electron beam remelting*
- *electron beam evaporation and condensation of metallic materials in vacuum*
- *ladle steel treatment*
- *metal dispersion and producing condensates*
- *designing of electrometallurgical equipment*
- *technologies of producing ingots, high-quality castings from different materials*
- *technologies of producing titanium alloy ingots*
- *deposition of coatings, including those of composite materials*
- *energy- and resources-saving technologies*
- *physical and chemical fundamentals of steel production*
- *theories of metallurgical processes*
- *investigations in gas-slag-metal system*
- *systems of automation of remelting processes*
- *mathematical modelling of processes*

The journal accepts also advertisements and announcements of conferences and publications on related topics.

«ADVANCES IN ELECTROMETALLURGY» is published quarterly. Subscription requests should be sent to the Editorial Office.

Manuscripts should be submitted in duplicate in English, and supplemented with a text file and figures on a diskette. An electronic copy may be submitted by e-mail.

The rules for submission of electronic copies are as follows:

- an electronic copy should be submitted on a diskette or by e-mail simultaneously with sending a hard copy of the manuscript;
- acceptable text formats: MultiEdit (txt), MS Word 97 (rtf, doc);
- acceptable graphic formats for figures: EPS, TIFF, CDR. Figures created using software for mathematical and statistical calculations should be converted to one of these formats.

Manuscripts should be sent to

Alexander T. Zelnichenko
Executive Director of Project
«Advances in Electrometallurgy»,
11, Bozhenko Str.,
03680, Kyiv, Ukraine
PWI, International Association «Welding»
Tel.: (38044) 227 67 57, Fax: 268 04 86
E-mail: journal@paton.kiev.ua
E-mail: tomik@mac.relc.com

Manuscripts should be supplemented with

- official letter signed by a chief manager of the institution where the work was performed. This rule does not apply to papers submitted by international groups of authors;
- publication permission: conclusion of a commission authorized to permit open publication of the paper (only for authors from Ukraine).

Title Page:

- title of the paper and name(s) of the author(s);
- name of affiliated institution, full address, telephone and fax numbers, e-mail addresses (if available) for each author.

Abstract: up to 100 words, must be presented in English. Before the abstract text one should indicate in the same language: the paper title, surnames and initials of all authors.

Key words: their amount must not exceed eight word units. In the specific cases it is acceptible to use two- or three-word terms. These words must be placed under the abstract and written in the same language.

Text should be printed double-spaced on white paper (A4 format) with a 12-point font. Titles of the paper and sections should be typed with bold capitals.

Tables should be submitted on separate pages in the format of appropriate text processors, or in the text format (with columns separated by periods, commas, semicolons, or tabulation characters). Use of pseudographic characters is not allowed.

List of references should be double-spaced, with references numbered in order of their appearance in the text.

Captions for figures and tables should be printed in the manuscript double-spaced after the list of references.

Pictures will be scanned for digital reproduction. Only high-quality pictures can be accepted. Inscriptions and symbols should be printed inside. Negatives, slides and transparencies are accepted.

Figures: each figure should be printed on a separate page of the manuscript and have a size not exceeding 160 × 200 mm. For text in figures, use 10-point fonts. All figures are to be numbered in order of their appearance in the text, with sections denoted as (a), (b), etc. Placing figure numbers and captions inside figures is not allowed. On the back side, write with a pencil the paper title, author(s) name(s) and figure number, and mark the top side with an arrow.

Photographs should be submited as original prints. Color printing is possible if its cost is covered by the authors or their sponsors. For information about the rules and costs, contact the Executive Director.

No author's fee is provided for.

Publication in «Advances in Electrometallurgy» is free of charge.